

https://dspace.org/

The extraction of rare earth elements from various resources using the sulfation roastingleaching process

Maluleke, Kgomotso Charlotte

2022

https://hdl.handle.net/10539/34191

Downloaded from a DSpace repository. https://dspace.org/



UNIVERSITY OF THE
WITWATERSRAND,
JOHANNESBURG

THE EXTRACTION OF RARE EARTH ELEMENTS FROM VARIOUS RESOURCES USING THE SULFATION ROASTING-LEACHING PROCESS.

Kgomotso Charlotte Maluleke (824549)

A dissertation submitted to the Faculty of Engineering and the Built Environment, University of the Witwatersrand, Johannesburg, South Africa, in fulfilment of the requirements for the degree of Master of Science in Engineering.

Johannesburg,
October 2021

Declaration

I declare that this dissertation is my own unaided work which is being submitted for the degree of Master of Science in Engineering to the University of the Witwatersrand, Johannesburg, South Africa.

It has not been submitted before for any degree or examination to any other University.



……

Kgomotso Charlotte Maluleke

14th day of October 2021

Abstract

Rare Earth elements (REEs) are commonly extracted from mineral concentrates using conventional hydrometallurgical processes such as alkaline and/or acid baking. These processes are known to be highly efficient in extracting the REEs but tend to be highly unselective because they also extract gangue metals such as Fe, Mn and Th. Co-extraction of gangue metals contaminates the product stream and therefore requires multiple purification stages to produce a cleaner sellable product. The non-selectivity of these processes is also associated with high reagent consumptions and the production of large waste streams that are difficult and expensive to discard. The aim of the study was to investigate the technical feasibility of using sulfation roasting and leaching processes for the selective conversion and extraction of LREE (La, Ce, Nd and Pr) from South African REE-bearing resources, i.e. Zandkopsdrift (ZKD) ore and PyEarth ™ slag. This was achieved by conducting fluidized sulfation roasting tests where the effect of operational parameters; temperature, reaction time and stoichiometric ratio of SO_2 to O_2, on the conversion efficiency of Light REEs (LREEs) in the ZKD ore and the PyEarth ™ slag were investigated.

The sulfation roasting and leaching process was proven to be technically feasible for the conversion and extraction of LREEs from both the ZKD ore and PyEarth ™ slag. The study further indicated that the sulfation roasting and leaching process was a function of temperature, time, and gas composition. The highest LREE extractions for the ZKD ore, i.e. 88% La, 87% Pr, 86% Nd, 61% Ce, were obtained for samples roasted at 700°C for 8 hours in an O_2-enriched gas atmosphere. Fe was the least extracted metal at all the roasting conditions investigated for the ZKD ore. Sulfation roasting of the PyEarth™ slag was associated with significantly high Fe extractions, highest of 72%, compared to the highest LREE extractions of 24% Nd, 21% Pr, 21% La, and 21% Ce obtained at 700°C for 8 hours in an O_2-enriched gas atmosphere. These results indicated that selectivity was attained for the ZKD ore as compared to the PyEarth ™ slag for the conditions that were investigated. It is therefore recommended that more conditions are investigated for the PyEarth ™ slag to make a more accurate conclusion in terms of the applicability and selectivity of the sulfation roasting and leaching process for slag feed materials.

Acknowledgements

First and foremost, I'd like to thank the Almighty God for seeing me through this personal quest. I do not understand the mystery of grace – only that it meets us where we are but does not leave us where it found us. I would like to express my very great appreciation to my Parents, brother Monamoledi and sister Lebogang for all the support and love throughout this journey. I would also like express my deepest appreciation to Zizipho and Mmapitso for being my biggest cheerleaders, accountability partners and support system throughout this Masters journey.

I would also like to express my great appreciation to my supervisors Professor Sehliselo Ndlovu, Dr Xolisa Goso and Dr Elias Matinde for their patient guidance, encouragement, and useful critiques of this body of work. It was definitely Gods hand at work having me be guided by the best in my budding career. Special mention to Dr Goso and his staff from the Technology Demonstration Group at Mintek for the technical input and knowledge sharing towards this work. A special thank you to Metro Majola for the technical and operational support during the sulfation roasting studies. I would also like to thank my colleagues from the Metal Extraction and Recovery Research group under Professor Ndlovu for their invaluable input and guidance throughout the different stages of the work. I would also like to thank the staff from the School of Chemical and Metallurgical Engineering in the various roles they played towards the success of this research project.

While many contributed to the work in some way or the other I'd like to extend a special thank you to Dr Charles Sekgetho Mokwatlo for the guidance during my write-up, as well as Mosili Pebane for the geological input throughout the study. I'd like to make a mention to Sun-El Musician and Simmy for always clearing my head, healing my heart, and lifting my spirits as I was burning the midnight oil.

Publications and Conference Proceedings

Maluleke, K. C., Goso, X. C., Ndlovu, S., Matinde, E., & McCullough, S. (2020). Preliminary investigation into the extraction of light rare earth elements from different resources using the sulphation roasting process. *Journal of the Southern African Institute of Mining and Metallurgy*, *120*(5), 319-325.

Sections of the work during the study were presented at the following conference proceedings

Maluleke, K. C., Goso, X. C., Ndlovu, S., Matinde, E., & McCullough, S. (2018). Sulphation roasting process for the extraction of rare earth elements. *Proceedings of the 4th Young Professionals Conference, Sandton, South Africa. South African Institute of mining and Metallurgy, 51-61.*

Maluleke, K. C., Goso, X. C., Ndlovu, S., & Matinde, E. (2020). Sulphation roasting and leaching for the selective extraction of Light REEs from various South African Resources. *Proceedings of the 3rd Conference on European Rare Earth Resources, Greece (Virtual Conference).*

Table of Contents

DECLARATION ..... **i**

ABSTRACT ..... **ii**

ACKNOWLEDGEMENTS ..... **iii**

PUBLICATIONS ..... **iv**

LIST OF FIGURES ..... **viii**

LIST OF TABLES ..... **xii**

LIST OF SYMBOLS ..... **xiv**

LIST OF ABBREVIATIONS ..... **xv**

1. INTRODUCTION **1**

1.1. BACKGROUND 1

1.2. RESEARCH MOTIVATION 3

1.3. PROBLEM STATEMENT 4

1.4. RESEARCH OBJECTIVES 4

1.4.1. Research Aim 4

1.4.2. Objectives 5

1.5. LAYOUT OF DISSERTATION 5

2. LITERATURE REVIEW **7**

2.1. LREEs 8

2.1.1. LREE Applications and Uses 8

2.1.2. REE Abundance 9

2.1.3. REE Mineralogy 10

2.1.4. South African Rare Earth Deposits 12

2.2. REE CONVENTIONAL PROCESS FLOWSHEET 13

2.2.1. Mining and Physical Beneficiation Processes 14

2.2.2. Chemical Beneficiation 15

2.3. HIGH TEMPERATURE MONAZITE PROCESSES 17

2.3.1. Carbochlorination Processes 17

2.3.2. Soda Roast-Acid Leach Process 18
2.3.3. Calcium Chloride-Calcium Carbonate Roasting 19
2.3.4. Smelting of South African REE Resources: PyEarth ™ Process 20
2.4. SULFATION ROASTING 21
2.4.1. Sulfation Roasting Chemistry 21
2.4.2. Sulfation Roasting Thermodynamics 22
2.4.3. Review of Acid-Based Sulfation Roasting of REE-Bearing Resources 26
2.4.4. Critical Evaluation of the Acid-Based Sulfation Roasting for REE Extraction 28
2.5. FLUIDIZATION BACKGROUND 30
2.5.1. Principles of Fluidization 30
2.5.2. Fluidization Stages 32
2.5.3. Geldart Classification 33
2.5.4. Entrainment 34
2.6. SUMMARY OF LITERATURE 36
3. METHODOLOGY 38
3.1. INTRODUCTION 38
3.2. MATERIALS 38
3.3. EXPERIMENTAL PLAN 39
3.4. PRELIMINARY SULFATION ROASTING 41
3.4.1. Thermochemical Calculations 41
3.4.2. Preliminary Sulfation Roasting 42
3.5. FLUIDIZED SULFATION ROASTING STUDIES 45
3.5.1. Sample Preparation 45
3.5.2. HEAD SAMPLE CHARACTERIZATION 45
3.5.3. ROTAMETER CALIBRATIONS 46
3.5.4. FLUIDIZATION STUDIES 50
3.5.5. SULFATION ROASTING STUDIES 53
4. PRELIMINARY SULFATION ROASTING RESULTS 60
4.1. INTRODUCTION 60
4.2. THERMOCHEMICAL CALCULATIONS 60
4.2.1. One Metal – SO_2 – O_2 Calculations 60
4.2.2. Two Metal-SO_2 – O_2 Calculations 62
4.3. MASS CHANGE EVALUATION 65
4.4. MINERALOGICAL CHARACTERIZATION 67
4.5. METAL SULFATE STABILITY TESTS 68

4.6. LEACHING OF ROAST PRODUCTS 69
4.7. SUMMARY 71
5. FLUIDIZED SULFATION ROASTING STUDIES 72
5.1. INTRODUCTION 72
5.2. MINERALOGICAL CHARACTERIZATION – FEED MATERIALS 72
5.3. FLUIDIZATION PARAMETERS 75
5.3.1. Particle Size and the Geldart Classification 75
5.3.2. Minimum Fluidization Velocity 78
5.4. FLUIDIZED SULFATION ROASTING RESULTS 78
5.4.1. Mineralogical Characterization of Roast Samples 78
5.4.2. ZKD Ore Sulfation 86
5.4.3. PyEarth ™ Slag Sulfation 94
5.5. SUMMARY 97
6. CONCLUSIONS 98
7. RECOMMENDATIONS 101
REFERENCES 102
APPENDICES 109
APPENDIX A: EQUIPMENT USED FOR SAMPLE PREPARATION 109
APPENDIX B: ROTAMETER MEASUREMENT PRINCIPLE 111
APPENDIX C: EXPERIMENTAL SETUP FOR FLUIDIZED SULFATION ROASTING STUDIES 113
APPENDIX D: SAFETY, HEALTH AND ENVIRONMENTAL 114
APPENDIX E: PREDOMINANCE PHASE DIAGRAMS 116
APPENDIX F: PRELIMINARY SULFATION ROASTING-LEACHING MASS BALANCES 119
APPENDIX G: FLUIDIZATION PARAMETERS 120
APPENDIX H: SULFATION ROASTING BED SAMPLES XRD ANALYSIS 123
APPENDIX I: POURBIAX DIAGRAMS 127
APPENDIX J: MASS BALANCES 129

LIST OF FIGURES

Figure 2.1. The REEs on the periodic table (Generalic, 2020). 8
Figure 2.2. Crustal abundance of the lanthanide elements (Jordens et al., 2013). 10
Figure 2.3. Process flowsheet for the extraction of REEs from monazite concentrates (Habashi, 2013; Sadri et al., 2017). 14
Figure 2.4. Typical flowsheet for the sulfation roasting of metal oxides or metal sulfates. (Guntner and Hammerschmidt, 2011). 21
Figure 2.5. The standard Gibbs free energy for the sulfation reactions of different oxides in the temperature range 500°C - 1000°C (HSC v.8) (Teixeira et al., 2018). 24
Figure 2.6. Thermal Stability of selected REE sulfates and major gangue metals present in REE resources. (Teixeira et al., 2018). 25
Figure 2.7. Flowsheet of the acid-based sulfation-roasting-leaching process (Borra et al., 2015). 27
Figure 2.8. The different stages of fluidisation (Chhabra and Gurappa, 2019). 32
Figure 2.9. Geldart's classification of powders according to their fluidization behaviour under ambient conditions (Geldart, 1973). 34
Figure 2.10. Zones in the fluidized bed freeboard (Folayan et al., 2015). 35
Figure 3.1. Experimental Plan. 40
Figure 3.2. PREDOM Module window on FactSage 7.2 ©. 42
Figure 3.3. Schematic representation of the sulfation roasting experimental setup (Sithole et al., 2017). 43
Figure 3.4. Picture of the ¼'' NPTF rotameters used for the sulfation roasting experiments. 47
Figure 3.5. Schematic of the soap bubble meter setup. 48
Figure 3.6. Calibration curve for oxygen and nitrogen gas rotameters. 50
Figure 3.7. Calibration curve for the sulfur dioxide rotameter. 50
Figure 3.8. Visual representation of the cold test setup consisting of (a) rotameters for control of gas flow, (b) gas inlet and (c) the material lying on the porous bed. 52
Figure 3.9. Schematic of sulfation roasting experimental setup. 55
Figure 3.10. A picture of the sulfation roasting experiments furnace and reactor setup. 56
Figure 3.11. A picture of the shaking bath and Erlenmeyer flasks containing the leach slurries. 58
Figure 4.1. Predominance diagram for Ce–O–S system at temperatures between 630°C and 800°C. 61

Figure 4.2. Predominance diagram for Pr–O–S system at temperatures between 630°C and 800°C. 62
Figure 4.3. Predominance diagram for Ce-Fe–O–S system at 600°C. 64
Figure 4.4. Predominance diagram for Ce-Fe–O–S system at 750°C. 64
Figure 4.5. Predominance diagram for Ce-Fe–O–S system at 800°C. 65
Figure 4.6. Graphical representation of mass changes for the sulfation of synthetic CeO_2 at different sulfation temperatures. 66
Figure 4.7. Graphical representation of the effect of sulfation temperature and time on Ce leaching efficiency. 70
Figure 5.1. Backscattered electron images and EDS analyses for the ZKD ore head+ sample. 74
Figure 5.2. Backscattered electron images and EDS analyses for the PyEarth ™ slag sample. 75
Figure 5.3. Cumulative frequency distributions of the PyEarth ™ slag and ZKD ore feed materials prior to roasting. 76
Figure 5.4. Geldart Classification- ZKD Ore (Red) and PyEarth slag (Blue). 77
Figure 5.5. SEM-EDS results showing the mode of occurrence of the REE-bearing phases in the roasted ZKD ore samples. Diagram A-F represent group samples obtained at 700°C..... 82
Figure 5.6. SEM-EDS results showing the mode of occurrence of the REE-bearing phases in the roasted PyEarth ™slag samples. Diagram A-C represent group samples roasted at 700° C in an O_2-depleted atmosphere for 1, 4, and 8 hours, respectively. 85
Figure 5.7. SEM-EDS results showing the mode of occurrence of the REE-bearing phases in the roasted PyEarth ™slag samples. Diagram D-E represent group samples roasted at 700° C in an O_2-enriched atmosphere. 86
Figure 5.8. The effect of sulfation temperature on the LREE and Fe extraction efficiencies from the roasted ZKD ore. 88
Figure 5.9. Eh-pH diagram of the system Fe-O-H (1). Fe = 10^{-10}, 298.15K, 10^5 Pa (Takeno, 2005). 89
Figure 5.10. The effect of roasting time on the LREE and Fe extraction efficiency of the ZKD ore (600°C). 91
Figure 5.11. The effect of roasting time on the LREE and Fe extraction efficiency of the ZKD ore (700°C). 91
Figure 5.12. The effect of roasting time on the LREE and Fe extraction efficiency of the ZKD ore (800°C). 92

Figure 5.13. Metal extraction as a function of roasting time for sulfation roasting of the ZKD ore in an O_2-rich atmosphere at 700°C. 93
Figure 5.14. Metal extraction as a function of roasting time for sulfation roasting of the ZKD ore in an O_2-depleted atmosphere at 700°C. 94
Figure 5.15. Metal extraction as a function of roasting time for sulfation roasting of the PyEarth ™ in an O_2-enriched atmosphere at 700°C. 95
Figure 5.16. Metal extraction as a function of roasting time for sulfation roasting of the PyEarth™ slag in an O_2-depleted atmosphere at 700°C. 96
Figure 0.1. Picture of the jaw crusher used in the test work. 109
Figure 0.2. Picture of the Sieb Technik Mill and a sample bowl with the ZKD ore. 110
Figure 0.3. A picture of the riffle splitter used for sampling the materials. 110
Figure 0.4. A picture of the vibrating sieve shaker and woven wire sieves used for the sizing of the samples. 111
Figure 0.5. Rotameter measurement principle (Yokogawa, n.d). 112
Figure 0.6. Extraction system utilised during the sulfation roasting experiments. 113
Figure 0.7. Data logger used to monitor the sample bed temperature through the K-type thermocouple 113
Figure 0.8. Predominance diagram for La–O–S system at 600°C. 116
Figure 0.9. Predominance diagram for La–O–S system at 700°C. 117
Figure 0.10. Predominance diagram for La–O–S system at 800°C. 117
Figure 0.11. Predominance diagram for Nd–O–S system at 600°C. 117
Figure 0.12. Predominance diagram for Nd–O–S system at 700°C. 118
Figure 0.13. Predominance diagram for Nd–O–S system at 800°C. 118
Figure 0.14. X-ray diffraction pattern for the ZKD ore sulfated in a O_2 depleted atmosphere at 600°C. 123
Figure 0.15. X-ray diffraction pattern for the ZKD ore sulfated in a O_2 depleted atmosphere at 700°C. 123
Figure 0.16. X-ray diffraction pattern for the ZKD ore sulfated in a O_2 depleted at 800°C. 124
Figure 0.17. X-ray diffraction pattern for the ZKD ore sulfated in a O_2-rich atmosphere at 600°C. 124
Figure 0.18. X-ray diffraction pattern for the ZKD ore sulfated in a O_2-rich atmosphere at 700°C. 124
Figure 0.19. X-ray diffraction pattern for the ZKD ore sulfated in a O_2-rich atmosphere at 800°C. 125

Figure 0.20. X-ray diffraction pattern for the PyEarth ™ slag samples after sulfation roasting. 126
Figure 0.21. Eh-pH diagram of the system La-O-H (1). Fe = 10−10, 298.15K, 105 Pa (Takeno., 2005). 127
Figure 0.22. Eh-pH diagram of the system Ce-O-H (1). Fe = 10−10, 298.15K, 105 Pa (Takeno., 2005). 127
Figure 0.23. Figure 0.20. Eh-pH diagram of the system Nd-O-H (1). Fe = 10−10, 298.15K, 105 Pa (Takeno., 2005). 128
Figure 0.24. Figure 0.20. Eh-pH diagram of the system Pr-O-H (1). Fe = 10−10, 298.15K, 105 Pa (Takeno., 2005). 128

LIST OF TABLES

Table 2.1. Applications of the LREEs (Charalampides et al., 2015; Balaram, 2019). 9

Table 2.2. Important rare earth minerals (Krishnamurthy and Gupta, 2004; Castor and Hendrick, 2006). 11

Table 3.1. Bulk chemical composition of the Zandkopsdrift head sample. 39

Table 3.2. Bulk chemical composition of the PyEarth ™ slag head sample. 39

Table 3.3. Bulk density calculated for the feed materials. 39

Table 3.4. PREDOM module inputs for the calculation of predominance phase diagrams. ...41

Table 3.5. Summary of the preliminary sulfation roasting tests. 44

Table 3.6. Summary of rotameter gas settings for sulfation roasting experiments. 54

Table 3.7. Sulfation roasting experiment test plan. 57

Table 3.8. Summary of the ZKD ore leaching studies. 59

Table 4.1. Summary of the phase chemical compositions of the sulfated CeO2. 67

Table 4.2. X-Ray Diffraction results of various cerium sulfate materials at different temperatures (extracted from Poston et al., 2003). 68

Table 4.3. Summary of the mass changes for the stability tests and the sulfation of the REE-bearing ore. 69

Table 4.4. Stability of metal sulfates of interest 69

Table 5.1. Phases identified in the ZKD ore head sample and their formulae. 73

Table 5.2. Phases identified in the PyEarth ™ slag sample and their formulae. 73

Table 5.3. Feed material d50. 77

Table 5.4. Summary of the Gerldart Classification. 77

Table 5.5. Minimum fluidization velocity. 78

Table 5.6. Bulk mineralogical composition of the ZKD ore roasted at 600°C. 79

Table 5.7. Bulk mineralogical composition of the ZKD ore roasted at 700°C. 80

Table 5.8. Bulk mineralogical composition of the ZKD ore roasted at 800°C. 80

Table 5.9. Phases identified in the PyEarth ™ slag sample after sulfation roasting and their formulae. 83

Table 0.1. Mass Balance for Preliminary Sulfation Roasting studies.....119
Table 0.2. Mass Balance for the Stability Tests.....119
Table 0.3. Terminal Velocity of the head samples. 120
Table 0.4. Experimental data for the ZKD ore elutriation calculation. 121
Table 0.5. Experimental data for the PyEarth ™ slag elutriation calculation. 121
Table 0.6. Elutriation Constants.....123
Table 0.7. Summary sulfation roasting consitions for the PyEarth ™ slag. 125
Table 0.8. Detailed XRD analysis for the sulfation of the PyEarth slag. 125
Table 0.9. Mass Balance for The ZKD Ore Sulfation Roasting Studies (Ce and La). 129
Table 0.10. Mass Balance for The ZKD Ore Sulfation Roasting Studies (Nd and Pr). 130
Table 0.11. Mass Balance for The ZKD Ore Sulfation Roasting Studies (Fe).....131
Table 0.12. Mass Balance for The PyEarth ™ Slag Sulfation Roasting Studies (Fe). 131
Table 0.13. Mass Balance for The PyEarth ™ Slag Sulfation Roasting Studies (Ce and La). 132
Table 0.14. Mass Balance for The PyEarth ™ Slag Sulfation Roasting Studies (Fe). 132
Table 0.15. pH readings for the fluidized sulfation roasting bed samples leaching tests. 133
Table 0.16. Mass Balance over the fluidized bed setup.....134

LIST OF SYMBOLS

A_B	Cross section area of bed, cm^2
mf	Subscript for "at minimum fluidization conditions"
H	Depth of bed, cm
ε	Bed voidage
ρ_p	Density of particles, g/cm^3
ρ_f	Fluid density, g/cm^3
ρ_g	Gas density, g/cm^3
g	Acceleration due to gravity, g/cm^3
ΔP	Pressure drop across depth L, Pa
L	Depth of bed, cm
μ	Fluid viscosity, g/cm.s
U	Superficial fluid velocity through the bed, cm/s
$\emptyset_s$	Particle sphericity
d_p	Sauter mean particle size, cm
W_{io}	Initial weight of mass fraction i
W_i	Final weight of mass fraction i
W	Total weight of sample before fluidization
A	Area of reactor, m^2
t	Time, s
k_i^*	Elutriation constant, $kg/m^2.s$
p_{SO_2}	Partial pressure of sulfur dioxide, atm.
p_{O_2}	Partial pressure of oxygen, atm.
U_{mf}	Minimum fluidization velocity, cm/s
Q	Gas flowrate at inception of fluidization, cm^3
r	Radius of reactor, cm
u_t	Terminal velocity, cm/s

LIST OF ABBREVIATIONS

LREE	Light rare earth element
MREE	Medium rare earth element
HREE	Heavy rare earth elements
TREO	Total rare earth oxide
REE	Rare earth element
PSD	Particle size distribution
ZKD	Zandkopsdrift
SEM	Scanning Electron Microscope
EDS	Energy Dispersive Spectroscopy
ICP-OES	Inductively Coupled Plasma Optical Emission Spectroscopy

1. INTRODUCTION

1.1. BACKGROUND

Rare earth elements (REEs) are a group of 17 chemically similar metals, consisting of 15 lanthanides and two associated metals yttrium (Y) and scandium (Sc). REEs have gained popularity due to their unique chemical, catalytic, magnetic, optical, electrical, and metallurgical properties that allow them to be utilised in a wide range of applications (Castor and Hedrick, 2006). These metals are considered as valuable additions in a wide range of high technology, high value-added and fast-growing sectors such as the permanent magnets, phosphors, battery alloys, fluid catalytic cracking, ceramics, and glass additives, polishing powders, auto catalysts and metallurgy. They are also used in emerging sectors such as the renewable energy sector, electronics and in hydrogen storage alloys (UNCTAD, 2014; De Lima and Leal Filho, 2015).

Unlike what their name suggests REEs are moderately abundant in the earth's crust. The total rare earth crustal abundance, 220 ppm, is higher than that of carbon which is known to be 200 ppm. Some of the lanthanides are significantly more abundant than commonly exploited elements, such as cobalt, lead, platinum group elements and mercury (Krishnamurthy and Gupta, 2015; Jordens et al., 2013; Habashi, 2013). REEs do not exist in nature in their metallic form, instead they are contained as compounds in minerals. There are over 200 minerals that have been identified to be REE-bearing, with the commonly exploited ones being bastnaesite (fluoro-carbonate), monazite (phosphate) and xenotime (phosphate). Bastnaesite and monazite are exploited for Light REE (LREE) bearing minerals while xenotime is exploited for Heavy REEs (HREE) (Krishnamurthy and Gupta, 2015; Humphries, 2013).

China is currently the dominant REE producer with approximately 90% of REE mining activities taking place in the country. China also contains the largest REE resource, estimated to be approximately 48 million tons of rare earth oxide (REO). Although China is the REE hub, its recent reduction in export quotas has resulted in an increasing demand for REEs from non-Chinese sources (Koltun and Tharumarajah, 2014). Countries such as the United States of America, Brazil, Australia, Greenland, Canada, and South Africa are known to be hosts to REE-bearing deposits which can serve as potential contributors to the global REE supply. South Africa contains over 1 million metric tons of REOs that are found in the

Steenkampskraal, Phalaborwa carbonatite and the Zandkopsdrift deposits (Krishnamurthy and Gupta, 2015).

The Zandkopsdrift (ZKD) rare earth deposit is located close to the Atlantic coast in the Northern Cape Province (Takagi, 2012). This deposit is one of the largest known rare earth deposits, containing approximately 950 kilo tonnes total rare earth oxides (TREOs). This ore is dominated by Fe and Mn oxides and oxyhydroxides such as goethite and manganomelane minerals. Approximately 97% of the rare earths in these deposits are contained in monazite, chemically weathered or altered monazite, REE-bearing aluminium phosphates of the crandallite group (florencite, gorxceite, crandallite), and xenotime minerals (Fronteir Rare Earths, 2015; Bisaka et al., 2017).

REEs are commonly extracted from their host minerals using conventional process flowsheets consisting of both physical beneficiation and chemical decomposition processes that are predominantly hydrometallurgy-based. These processes are associated with high REE extractions but tend to co-extract gangue constituents such as Fe, Mn, and Th, therefore making the processes relatively non-selective (Amer et al., 2013). Deposits such as the ZKD ore are considered to be Fe-rich due to their high Fe content. These materials pose challenges for REE extraction using the conventional process flowsheet. The ore deposit tends to display poorer liberation using physical beneficiation processes as it contains altered monazite that is often finer-grained than monazite. Leaching of this material is also known to result in solubilisation of Fe minerals which require removal using excessive amounts of reagents such as lime. The increased acid consumption and discarding of the formed Fe precipitates tend to make conventional process flowsheets economically not viable (Bisaka et al., 2017).

REE-bearing ores associated with high Fe content such as the Zandkopsdrift ore are often pre-treated using high temperature processes such as smelting, roasting and direct reduction prior to the leaching stages. These processes are utilised for the separation of Fe from the REE-bearing phases. The processes achieve this through the conversion of Fe oxides into a form that facilitates its separation from the valuable metals (Faris et al., 2017). The PyEarth ™ process is one such process which is utilised for the pre-treatment of Fe-rich, REE-bearing carbonatite deposits, i.e. ZKD ore, from South Africa. The process utilises direct smelting of the ore for the selective removal of Fe into a saleable Fe-rich alloy while concentrating the REOs in the slag phase called the PyEarth ™ slag. The REE-bearing slag is further processed using acid leaching techniques to get the REEs into solution. High temperature processes are known to be

energy intensive and are associated with large reagent, i.e. reductants and fluxing reagents, consumption. These processes also produce large amounts of slag. These challenges tend to make their application on an industrial scale economically not viable (Bisaka et al., 2017; Faris et al., 2017).

A gas-based sulfation roasting process is proposed in this study as an alternative process for the selective conversion and extraction of LREEs from various South African resources. Sulfation roasting is a pyrometallurgy-based process that is utilised for the conversion of metal oxides and/or sulfides into metal sulfates that are soluble in water or dilute acid solutions. The sulfation roasting process is successfully utilised for the extraction of base metals, copper and cobalt, from Fe-rich sulphide materials (Guntner and Hammerschmidt, 2011). The process is attractive as it utilises operational temperatures that are below the melting points of the metals and therefore, avoids fusion. The process is also attractive as it allows for selective conversion and extraction of targeted metals through the manipulation of operational parameters such as roasting temperature and gas composition (Ma, 2019; Thomas and Cole, 2016). Reported literature on the application of the sulfation roasting process on South African REE-bearing resources was not found during this study.

1.2. RESEARCH MOTIVATION

REEs are extracted from their host minerals using the conventional process flowsheet consisting of physical beneficiation and chemical decomposition processes that are predominantly hydrometallurgy-based. These processes are known to be highly efficient in extracting the REEs but tend to be highly non-selective because they also extract gangue metals such as Fe, Mn and Th. Co-extraction of gangue metals contaminates the REE product stream which generally requires multiple purification stages prior to the production of a high purity sellable product stream. The non-selectivity of the conventional processes is also associated with high reagent consumptions and the production of large waste streams that are difficult and expensive to discard. The sulfation roasting and leaching process was proposed in the study as an alternative extraction process to address the selectivity problem associated with current conventional processes. Sulfation roasting processes have been successfully investigated and industrially applied for the selective extraction of base metals from high Fe sulfide materials. The sulfation roasting process involves the roasting of the feed material in the presence of SO_3 gas to convert the target metal compounds to metal sulfates. The process is carried out at

conditions where the impurity metal sulfates are thermodynamically unstable and therefore, allowing the process to be selective. Like the base metal sulfates, the REE sulfates are readily soluble in water. Although this is the case, literature on the application of the sulfation roasting and leaching process on South African resources was not found during this study.

1.3. PROBLEM STATEMENT

The recent decrease in China's export quotas as well as the increasing popularity of the rare earth metals has resulted in a rapid increase in their demand. This surge in the market has resulted in an interest for non-Chinese sources to participate in the global REE market. This therefore means that countries such as South Africa could contribute to the global REE supply. South Africa contains over 1 million tonnes of REOs that are currently not being exploited. These metals are commonly extracted from their minerals using the conventional process flowsheet which consists of physical beneficiation and hydrometallurgy-based chemical decomposition processes. These processes are highly efficient in the extraction of REEs, but they also tend to be highly unselective as they co-extract gangue metal components such as Fe. This makes the process flowsheets very complicated, tedious, and expensive. The sulfation roasting process was proposed in the study for the selective conversion and extraction of LREEs from South African resources. The process is attractive as it allows for selective conversion of targeted metals through the manipulation of operational parameters such as temperature. The process is also carried out at lower temperatures than the melting temperatures of the metals, therefore avoiding fusion. Although the process has been successfully utilised for processing of other materials, base metals from Fe-rich sulfide ores, literature on the application of the sulfation roasting process on South African REE-bearing ores was not accessible during the study.

1.4. RESEARCH OBJECTIVES

1.4.1. Research Aim

The aim of the study is to investigate the technical feasibility of the sulfation roasting and leaching process for the selective conversion and extraction of LREEs from South African REE-bearing materials.

1.4.2. Objectives

The specific objectives are:

- To determine the suitable thermal conditions for the sulfation roasting of LREEs, through calculation of predominant phase diagrams using FactSage 7.2 © software.
- To investigate the suitable operational conditions of the sulfation roasting process through preliminary tests using synthetic REOs compounds.
- To determine fluidization parameters and behaviour of the different head samples.
- To investigate the effect of operational parameters; temperature, reaction time and stoichiometric ratio of SO_2 to O_2, on the conversion efficiency of LREEs in the ZKD ore and the PyEarth ™ slag by conducting fluidized sulfation roasting tests.
- To investigate the sulfation efficiency through mineralogical analysis of the head and roast bed samples.

1.5. LAYOUT OF DISSERTATION

Based on the background information described in Chapter 1, the investigation on the extraction of LREEs from South African REE-bearing resources using the sulfation roasting-leaching process was conducted as follows:

Chapter 2 consists of a literature review of the conventional hydrometallurgical REE extraction processes, high temperature/ pyrometallurgy beneficiation processes and the sulfation roasting-leaching process. The last section of the chapter is focused on reviewing the fluidization theory.

Chapter 3 describes the detail of the experimental setup and methodology of the preliminary sulfation roasting studies, the fluidization sulfation roasting tests as well as the leaching experiments. The techniques utilised for the analysis of the sulfation roasting and leaching products are also discussed in this chapter.

Chapter 4 and 5 discusses the results obtained from the sulfation roasting and leaching experiments as well as the product analysis. The chemical and mineralogical analysis results are included. The effect of reaction time, temperature, and gas composition on the selectivity of the sulfation roasting process are presented in this chapter.

The study was concluded in chapter 6 and the recommendations for future work were summarized in Chapter 7.

2. LITERATURE REVIEW

The literature review is divided into 5 main sections which cover the scope of the current research investigation:

- The first section discusses background information on the LREEs, their abundance, mineralogy, and applications.
- The second section reviews the current process flowsheet for the mining, beneficiation, extraction, and separation of LREEs from monazite mineral resources.
- Research developments on high temperature treatment processes of REE ores are investigated in the third section of the chapter.
- The sulfation roasting process is discussed in the fourth section of the chapter. The process has been applied to various materials but literature of the application of this process on South African REE-bearing resources has not been reported.
- The sulfation roasting process is commonly conducted using the fluidized bed setup and therefore it was important to understand fluidization theory for the purposes of this study. This is discussed in the last section of this chapter.

2.1. LREEs

REEs are a group of seventeen chemically similar metals, consisting of 15 lanthanides and two associated metals yttrium (Y) and scandium (Sc). These metals are commonly subdivided into Light REEs (LREEs) and Heavy REEs (HREEs) on basis of their atomic weight (Schulz et al., 2018), as illustrated in Figure 2.1. LREEs also known as the cerium sub-group elements contain lanthanides from, lanthanum (La) to gadolinium (Gd) while the Heavy REEs or the yttrium sub-group elements describes elements from terbium (Tb) to lutetium (Lu) and yttrium (King., 2013). Other resources further sub-divide the lanthanides into Medium REEs, therefore resulting in the LREE group consisting of lanthanum (La), cerium (Ce), praseodymium (Pr), neodymium (Nd) (Hower et al., 2016). REEs are widely viewed as critical metals as a result of their increasing importance in modern and green technologies (Goodenough et al., 2018). The LREEs are the focus in the study because they are the most prevalent metals in the South African REE resources utilised in the study.

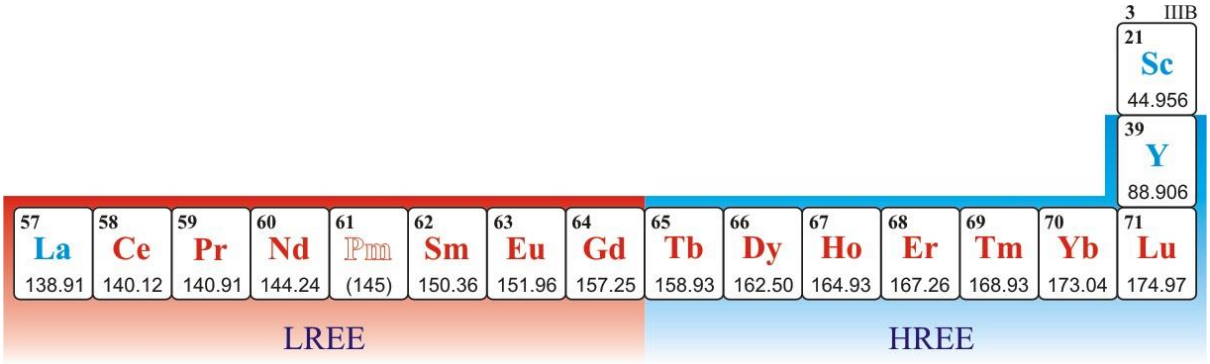


Figure 2.1. The REEs on the periodic table (Generalic, 2020).

2.1.1. LREE Applications and Uses

REEs have been coined "The Vitamins of Modern Industry" as they form part of the important ingredients in all high-technology gadgets. These metals have found application in a wide range of industries due to their unique physical, chemical, magnetic, and luminescent properties. The use of these metals in different applications results in technological advantages such as high performance at reduced energy consumptions, greater efficiency, miniaturization, speed, durability, and thermal stability (Balaram, 2019).

REEs are consumed in a wide range of markets. These include traditional/mature, new high-growth markets and green technology applications summarized in Table 2.1. The traditional/mature market includes the making of catalysts, glassmaking, lighting and

metallurgy, accounts for 59% of the total world REE consumption. While the newer, high-growth markets which include applications in battery alloys, ceramics and permanent magnets, accounts for 41% of the total world REE consumption (Charalampides et al., 2015). The recent REE demand is in the production of energy efficient gadgets (green technology) which are faster, lighter, smaller, and more efficient (Balaram, 2019).

Although most REEs are in demand, LREEs are the most consumed REEs due to their versatility which make them useful in most applications. They are also the most produced REEs because they are the most abundant REEs and because of their lower prices as compared to MREEs and HREEs. Lanthanum and cerium constitute about 80% of the REEs used in mature markets, while dysprosium, neodymium and praseodymium make up 85% of the REEs consumed in new market applications (Charalampides et al., 2015). As such, the REE demand is expected to increase, reaching 315,000 tons in 2030 (Pozo-Gonzalo, 2021).

Table 2.1. Applications of the LREEs (Charalampides et al., 2015; Balaram, 2019).

Metal	Applications
Lanthanum	Nickel metal hybride (NiMH) rechargeable batteries, Petroleum cracking catalysts, Hydrogen storage, metal alloys, lighter flints
Cerium	Catalytic converters, mechano-chemical glass polishing powders, glass additive, metal alloys, phosphors, corrosion protection, Carbon Arc Lamps, cigarette lighter flints.
Praseodymium	High intensity permanent magnets, misch metals, colourant in glass and enamels, optical fibres
Neodymium	Neodymium iron boron (NdFeB) magnets, lasers, colourant in glass and ceramics, electronics, hybrid engines.

2.1.2. REE Abundance

Unlike what their name suggests REEs are moderately abundant in the earth's crust. Cerium, which is the most abundant lanthanide has almost the same crustal abundance as commonly studied metals, such as copper, gold, platinum, and gold. Lanthanides with lower atomic numbers (LREEs) are more abundant in the earth's crust than those with higher atomic numbers; MREEs, and HREEs, shown in Figure 2.2 (Charalampides et al., 2015; Castor and

Hedrick, 2006; Jordens et al., 2013). LREEs are more abundant than the heavier REEs because of their larger ionic radii which makes them more incompatible and more strongly concentrated in the continental crust (Krishnamurthy and Gupta, 2004). The lanthanides obey the Oddo-Harkins rule; where the even numbered elements are more abundant than their odd numbered neighbours (Malaysia and Negara, 2011).

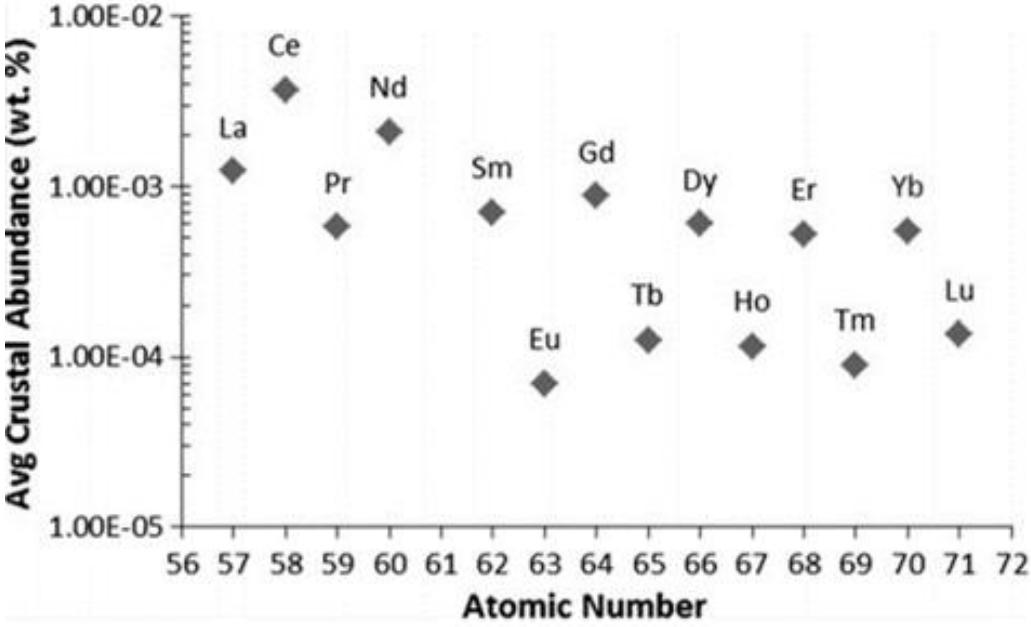


Figure 2.2. Crustal abundance of the lanthanide elements (Jordens et al., 2013).

2.1.3. REE Mineralogy

REEs do not occur naturally in their metallic form but instead occur as compounds in minerals. The metals are scattered dilutely in the earth's crust and occur as mixtures in many rock formations such as basalts, granites, gneisses, shales, and silicate rocks (Krishnamurthy and Gupta, 2004). The REE-bearing minerals may be differentiated into multiple groups based on their REE content. They can be identified as either cerium or yttrium minerals based on the distribution of the lanthanides in the mineral, i.e. whether it's rich in LREEs or HREEs (Jordens et al., 2013). REEs may also be contained in complex minerals, where the REE distribution can include all the lanthanides, or in selective minerals that have REE distributions which include the lanthanides in different portions (Krishnamurthy and Gupta, 2004).

To date, over 200 minerals have been identified to contain REEs, however, 95% of the world's REE resources are associated with only three minerals namely, bastnaesite, monazite and xenotime. Bastnaesite and monazite are LREE-bearing minerals while xenotime is mainly

exploited for Heavy REEs (Krishnamurthy and Gupta, 2004). Some of the REE-bearing minerals are listed in Table 2.2.

Table 2.2. Important rare earth minerals (Krishnamurthy and Gupta, 2004; Castor and Hendrick, 2006).

Mineral	Formula	Rare earth oxide content, wt. %
Aeschynite	$(Ce,Ca,Th)(Ti,Nb)_2O_6$	36
Bastnaesite	$(Ce,La,Pr)(CO_3)F$	76
Euxenite	$(Y,Ce,Ca,U,Th)(Ti,Nb,Ta)_2O_6$	<40
Fergusonite	$(Y,Sr,Ce,U)(Nb,Ta,Ti)O_4$	47
Gadolinite	$(Y,Ce)_2FeBe_2Si_2O_{10}$	52
Laporite	$(Na,Ca,Ce,Sr)_2(Ti,Ta,Nb)_2O_6$	36
Monazite	$(Ce,La\ldots)PO_4$	71
Mosandrite	$(Ca,Na,Ln)_{12}(Ti,Zr)_2Si_7O_{31}H_6F_4$	<65
Parasite	$Ca(Ce,La\ldots)_2(CO_3)F_2$	64
Synchisite	$CaLn(CO_3)_2F$	$(Y,Er)_2O_3$ 21.1–28.7 Ce_2O_3 3.7–4.3
Samarskite	$(Y,Er,U,Ce,Th)_4(Nb,Ta)_6O_2$	12
Thalenite	$Y_3Si_3O_{10}(OH)$	63
Xenotime	YPO_4	61
Yttrocerite	$(Ca,Y,Ce,Er)F_2$-$3H_2O$	<24

2.1.3.1. Bastnaesite [(Ce, La) (CO_3)F]

Bastnaesite is a primary fluoro-carbonate mineral containing approximately 70% REO. Bastnaesite is concentrated in LREEs and is currently the most exploited REE-bearing mineral, contributing 70% of the REEs produced globally (Lucas et al., 2014). Bastnaesite is found in vein deposits, metamorphic zones, and igneous carbonatites deposits (Krishnamurthy and Gupta, 2004).

2.1.3.2. Monazite [(Ce, La, Th) PO4]

Monazite is a LREE earth phosphate mineral made up of approximately 70% REOs which are primarily Ce, La, Pr and Nd. The mineral also contains considerable amounts of Th (4-12 wt. %) and small amounts of uranium (U) (Jordens et al., 2013). This mineral is recovered as a by-product in the mining of titanium placers in Australia, Brazil, China, India, Malaysia, South Africa, Sri Lanka, Thailand, and the United Sates (Jackson and Christiansen, 1993; Xie et al., 2014). Monazite is the 2nd largest REE resource with 20% of the REEs produced globally being

extracted from the mineral (Lucas et al., 2014). Carbonatite deposits such as the South African Zandkopsdrift deposit contain REEs predominantly in monazite mineral phases.

2.1.3.3. Xenotime [YPO_4]

Xenotime is an yttrium phosphate mineral, containing approximately 67% REOs, with the most abundant element being yttrium. The lighter REEs make up approximately 15% of xenotime and the heavier metals making up 85% (Jackson and Christiansen, 1993). This mineral occurs in granites of Minas Garaes in Brazil, pegmatite veins at hitter, as well as in crystalline metamorphic rocks (Jha et al., 2016). Xenotime co-occurs with monazite in placer deposits, but these deposits are very few. Despite the mineral being scarce it is an important source of HREEs and ion-adsorbed clays. Xenotime is recovered as a minor ore mineral during heavy sand recovery operations, primarily from monazite in Brazil, India, South Africa, and Australia.

2.1.4. South African Rare Earth Deposits

South Africa hosts more than 1 million metric tons of TREOs that are currently not being exploited (Gupta and Krishnamurthy, 2005). These REOs are contained in three major deposits namely the Steenkampskraal, Zandkopsdrift and the Phalaborwa carbonatite deposit.

2.1.4.1. Steenkampskraal Deposit

The Steenkampskraal deposit is contained in a monazite-apatite-quartz vein of Proterozoic granite located in the Western Cape Province. The vein contains up to 75% monazite and is accompanied by apatite, magnetite, and sulfides (Castor and Hedrick, 2006). The Steenkampskraal deposit is estimated to contain 26.2 kg/t of critical rare earths (which make up 30% of the deposit), making it the highest material grade amongst new REE projects currently under development globally (Jepson, 2012). The attraction to the Steenkampskraal mine is that the majority of the rare earths are contained in tailings, left above ground, from previous thorium production operations. While this is the case, there are environmental concerns about exploitation of this deposit due to the high levels of radioactive thorium (Jepson, 2012).

2.1.4.2. Zandkopsdrift (ZKD) Deposit

The Zandkopsdrift (ZKD) carbonatite deposit is located close to the Atlantic coast in the Northern Cape Province of South Africa. This deposit contains approximately 950 kilo tonnes

TREOs. The ZKD carbonatite deposit is characterized by a fine-grained REE-bearing phosphate with iron oxides. The main REE minerals in the ore deposit are monazite, xenotime and florencite. The REE-bearing phosphates and iron oxides occur as very fine grains (<10 μm) in the ore. The ZKD ore deposit is associated with low levels of radioactive metals (thorium and uranium), therefore reducing the safety hazards associated with processing and discarding radioactive waste materials (Takagi, 2012; Fronteir Rare Earths, 2020).

2.1.4.3. Phalaborwa Carbonatite Deposit

The Phalaborwa carbonatite contains significant amounts of copper and apatite production and has been evaluated as a potential REE source. The apatite concentrates which are can be potentially produced as by-products are estimated to contain 0.4% to 0.9% REOs (Castor and Hedrick, 2006). The Phalaborwa apatite contains Eu, Sm and Nd in significantly high proportions. This deposit is very attractive as it contains no radioactive thorium (Gupta and Krishnamurthy, 2005).

2.2. REE CONVENTIONAL PROCESS FLOWSHEET

The process flowsheets for the extraction of REEs vary widely and are dependent on the mineralogy of the deposits that are being processed. The type of deposit will also determine the economics of the operations and the utilised process routes. Processing and extraction of REEs from mineral concentrates generally consists of mining and physical beneficiation of ores to produce REE concentrates. REEs are recovered from concentrates using chemical beneficiation, purification and separation processes that are hydrometallurgy-based (Krishnamurthy and Gupta, 2004). The conventional process flowsheet utilised for LREE extraction from monazite containing ores, the mineral of interest in the study, is summarized in Figure 2.3**.**

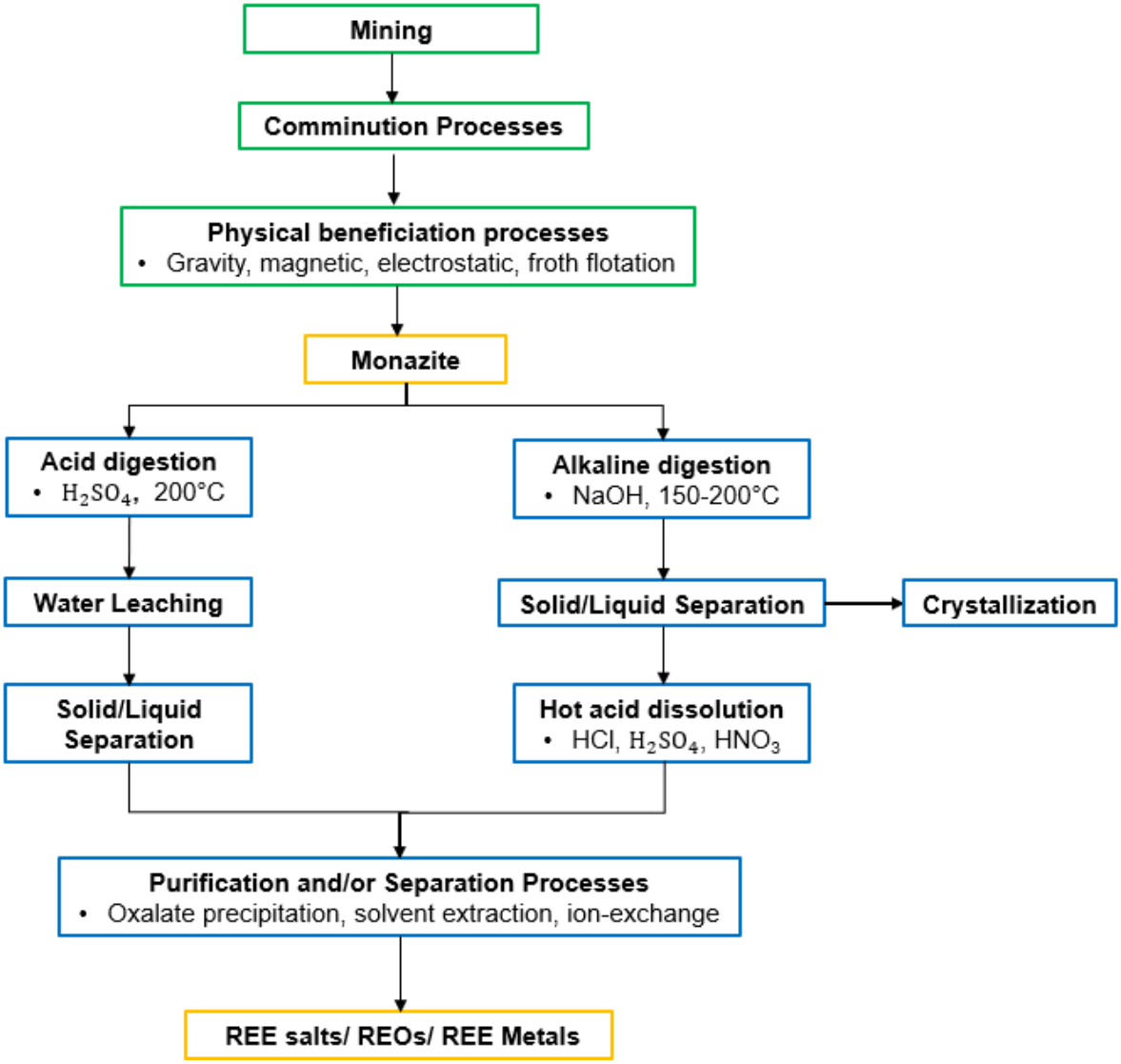


Figure 2.3. Process flowsheet for the extraction of REEs from monazite concentrates (Habashi, 2013; Sadri et al., 2017).

2.2.1. Mining and Physical Beneficiation Processes

Mining is the first stage of the process flowsheet for the extraction of REEs, which involves the removal of mineralized rock containing REE minerals from the ground (Haque et al., 2014). The mining stage is followed by comminution stages, such as crushing and milling, which are conducted for size reduction of the ore in preparation for physical beneficiation. Physical beneficiation processes are used to liberate the mineral ore from the host material, resulting in an increase in the REOs, without altering the chemical composition of the ore. These processes utilize the differences in physical properties such as gravity, magnetic susceptibility, and

surface ionization potential to enable methods such as gravity separation, flotation, electrostatic and magnetic separation to be utilized (Aplan, 1988).

2.2.2. Chemical Beneficiation

Chemical beneficiation stages consist of digestion, extraction, and separation/purification processes to produce REE compounds which are either an end-product or intermediate product for subsequent production of individual REEs or REE compounds (Zhang and Edwards, 2013). These processes are predominantly hydrometallurgy-based and are conducted on REE mineral concentrates produced from physical beneficiation processes. The decomposition and extraction processes use one or more reagents to decompose the REE minerals and to leach the REEs into solution.

2.2.2.1. Sulfuric Acid Digestion Process

Low temperature sulfuric acid decomposition/ baking processes are commonly utilised for the decomposition of low-grade monazite concentrates (Demol et al., 2019). The digestion of the monazite typically consists of heating up a monazite paste made up of 93% H_2SO_4 and monazite concentrate to temperatures of 200°C in a closed reactor or rotary kiln for 2-4 hours at an acid to concentrate ratio of 2:1. An acid-to-concentrate ratio lower than the prescribed results in incomplete reaction, while higher ratios interfere with the subsequent operations. Temperatures lower than 200ºC are known to result in slow reaction kinetics, while temperatures higher than 300ºC result in the formation of insoluble thorium pyrophosphate. The acid decomposition reaction is exothermic and can be represented by the reactions shown in equations (2.1) to (2.4) (Habashi, 2013).

$$2REPO_4 + 3H_2SO_4 \rightarrow (RE)_2(SO_4)_3 + 6H^+ + 2{PO_4}^{3-} \quad (2.1)$$

$$Th_3(PO_4)_4 + 6H_2SO_4 \rightarrow 3Th(SO_4)_2 + 12H^+ + 4{PO_4}^{3-} \quad (2.2)$$

$$ThSiO_4 + 2H_2SO_4 \rightarrow Th(SO_4)_2 + SiO_2 + 2H_2O \quad (2.3)$$

$$Ce_3(PO_4)_4 + 6H_2SO_4 \rightarrow 3Ce(SO_4)_2 + 12H^+ + 4{PO_4}^{3-} \quad (2.4)$$

The digestion process results in a grey mass mainly consisting of REE and Th salts. The digestion step is followed by a water leaching stage to get the REEs and Th in solution.

However, some of the impurities and unreacted monazite consisting of REE-phosphates and insoluble compounds produced during the digestion process remain as a precipitate in solution (Sadri et al., 2017). The leaching step is described by equations (2.5) to (2.7) (Kim and Osseo-Asare, 2012).

$$(RE)_2(SO_4)_3.nH_2O \rightarrow 2RE^{3+} + 3{SO_4}^{2-} + nH_2O \quad (2.5)$$

$$Th(SO_4)_2 \rightarrow Th^{4+} + 2{SO_4}^{2-} \quad (2.6)$$

$$Ce(SO_4)_2 \rightarrow Ce^{4+} + 2{SO_4}^{2-} \quad (2.7)$$

Low temperature acid baking is not preferred for monazite decomposition because the process results in the loss of the phosphate ion which has potential economic value (Berry et al., 2017). The process also results in the co-extraction of metal products such as Th and U, which are also converted to water-soluble sulfates during the baking process, thus making the process non-selective. Sulfuric acid baking is also problematic as it produces a high strength pasty mass that dries out in the baking equipment. Therefore, mass transfer inside of this equipment becomes a technical issue. Other challenges associated with acid baking include the evaporation of sulfuric acid as well as the selection of proper construction materials for the kilns due to the severe corrosive conditions inside of these equipment's (Verbaan et al., 2015; Amer et al., 2013).

2.2.2.2. Caustic Soda Decomposition Process

The alkaline decomposition of monazite concentrates is conducted using 50-75% NaOH solution at an operational temperature between 120℃ and 150℃. The caustic process differs from the acid process as it produces water soluble trisodium phosphates while the lanthanides, Th and U form insoluble hydroxides. The trisodium phosphate is washed from the bake residue along with the excess sodium hydroxide, while the insoluble REE hydroxides are left in the leach residue (Berry et al., 2017). The reactions that describe the decomposition process are shown in equation (2.8) to (2.10) (Habashi, 2013).

$$REPO_4 + 3NaOH \rightarrow RE(OH)_3 + Na_3PO_4 \quad (2.8)$$

$$Th_3(PO_4)_4 + 12NaOH \rightarrow 3Th(OH)_4 + 4Na_3PO_4 \quad (2.9)$$

$$UO_2HPO_4 + 2NaOH \rightarrow UO_2(OH)_2 + Na_2HPO_4 \quad (2.10)$$

The hydroxides are dissolved in hot acid, i.e. hydrochloric acid or nitric acid, while the phosphates are recovered as a by-product, i.e. trisodium phosphate (Na_3PO_4), which can be sold to the fertilizer industry (Kim and Osseo-Asare, 2012). The dissolution of rare earth hydroxides using HCl solutions is described by equation (2.11) to (2.12) (Qi, 2018):

$$RE(OH)_3 + 3HCl \rightarrow RECl_3 + 3H_2O \quad (2.11)$$

$$Th(OH)_4 + 4HCl \rightarrow ThCl_4 + 4H_2O \quad (2.12)$$

This process is preferred for monazite decomposition because of the simultaneous removal of phosphates during leaching, thus simplifying the Th concentrate purification step. This process also has the advantage of alkali regeneration after the cracking process (Sadri et al., 2017). Although conventional hydrometallurgy-based flowsheets are associated with high REE recoveries, the process techniques utilised are not suitable for the processing of Fe-rich REE ores. Bulk leaching of Fe-rich REE materials results in solubilisation of the Fe minerals and therefore increases acid consumption. The removal of Fe from leached solutions requires excessive amounts of reagents such as lime. Furthermore, the discarding of Fe precipitates increases the cost of the process beyond economic viability (Bisaka et al., 2017).

2.3. HIGH TEMPERATURE MONAZITE PROCESSES

The application of high temperature/ pyrometallurgical processes for the extraction of REEs from their host minerals has been investigated by several authors. Pyrometallurgical techniques such as smelting, and roasting are utilised as pre-treatment stages prior to leaching of these materials. This section is focused on reviewing high temperature processes for the extraction of REEs from monazite-containing concentrates.

2.3.1. Carbochlorination Processes

Chlorine gas (Cl_2), in the presence of carbon (C), is used in the carbochlorination process of monazite concentrates. The carbochlorination process is carried out at temperatures between 600°C and 1200°C for the decomposition of the REE–mineral concentrates and to produce REE chlorides. The process is associated with co-extraction of gangue constituents as these metals also form chlorides during the process (Zhang and Edwards, 2013). The major reactions

involved in the chlorination of monazite are described by equation (2.13) and (2.14) (Zhang and Edwards, 2013).

$$^1/_3\,REPO_4 + C + Cl_2 \rightarrow {}^1/_3\,RECl_3 + {}^1/_3\,POCl_3 + CO \quad (2.13)$$

$$^1/_3\,REPO_4 + {}^1/_2\,C + Cl_2 \rightarrow {}^1/_3\,RECl_3 + {}^1/_3\,POCl_3 + {}^1/_2\,CO_2 \quad (2.14)$$

The side reactions typically involved in the carbochlorination process are described by equation (2.15) to (2.17) (Zhang and Edwards, 2013).

$$^1/_2\,Fe_2O_3 + C + Cl_2 \rightarrow {}^2/_3\,FeCl_3 + CO \quad (2.15)$$

$$^1/_3\,Fe_2O_3 + {}^1/_2\,C + Cl_2 \rightarrow {}^2/_3\,FeCl_3 + {}^1/_2\,CO_2 \quad (2.16)$$

$$BaSO_4 + C + Cl_2 \rightarrow BaCl_2 + CO_2 + SO_2 \quad (2.17)$$

Although the carbochlorination process is known to have better economics and higher efficiencies as compared to the hydrometallurgical-based processes, this process is not selective and still requires subsequent extraction and separation processes to produce a cleaner product stream (Zhang and Edwards, 2013). The carbochlorination process for the extraction of REEs from monazite concentrates is currently not used on an industrial scale due to the presence of radioactive Th which contaminates both the REE-chloride product and the non-REE volatile product stream (Zhang et al., 2004).

2.3.2. Soda Roast-Acid Leach Process

The metallurgical processing of monazite is associated with the formation of various phosphides which cause pulverization of REE complexes. This creates a need for the phosphorus to be removed from the ore. The removal of phosphorus is challenging as it is very hard to decompose even at high temperatures due to its high thermal stabilities (Qun et al., 2001). The soda roast process followed by water leaching for phosphorus removal was suggested by Kumari et al. (2015). The thermal decomposition studies were conducted on a Korean monazite using sodium carbonate (Na_2CO_3) and/or NaOH at various temperatures, reagent ratios and reaction times. The phosphate decomposition using Na_2CO_3 was found to be significantly high (~95% phosphate removal) at the roasting temperature of 850°C. Complete phosphorus removal was observed at temperatures of 900°C and higher for tests conducted at

1:1 wt. ratio for 120 minutes. The process was also associated with REE recoveries in excess of 90%. The REE phosphate decomposition using Na_2CO_3 is described by equation (17) (Kumari et al., 2015).

$$2REPO_4 + 3Na_2CO_3 \rightarrow RE_2O_3 + 2Na_3PO_4 + 3CO_2 \quad (2.18)$$

Soda roasting experiments using NaOH were conducted on the monazite concentrate. The effect of NaOH concentration, roasting temperature, and reaction time on dephosphorization were studied and the results showed that there was a 99% phosphate removal at 400°C. The REE phosphate decomposition using NaOH is described by equation (2.19) (Kumari et al., 2015).

$$REPO_4 + NaOH \rightarrow RE(OH)_3 + Na_3PO_4 \quad (2.19)$$

The last stage in the study involved the washing of the roasted products in water, drying and leaching in dilute HCl solutions. The leaching tests were conducted at 80°C using 6 M HCl for 2 hours. The pulp density was maintained at 30 grams per litre. The leaching process is described by the reactions shown in equation (2.20) (Kumari et al., 2015).

$$RE_2O_3 + 6HCl \rightarrow 2RECl_3 + 3H_2O \quad (2.20)$$

2.3.3. Calcium Chloride-Calcium Carbonate Roasting

The calcium chloride - calcium carbonate roasting process was investigated by Merrit. (1990) for the decomposition of monazite for the simplification of subsequent separation stages where the REEs are separated from Th. The roasting process was carried out by decomposing the monazite by reacting it with calcium chloride and calcium carbonate in both reducing and sulfudizing environments at temperatures between 1250 K (976,85°C) and 1460 K (1186,85°C). The product stream after roasting consists of oxysulphides, oxychlorides, a Th-rich oxide solid solution and a calcium chlorophosphite (chlorapatite) (Merrit, 1990). The REEs are extracted from monazite by sodium hydroxide decomposition. These metals are separated from the phosphate first and then from the thorium.

The REEs are removed from the product by leaching in a 3% HCl solution followed by filtering for the separation of the gangue minerals and Th-rich oxide residue from the leach solution. The residue was found to be resistant to acid attack and therefore was suitable for disposal by burial. This method was found to be better than the conventional caustic leaching as more rapid

monazite decomposition was achieved without the need for grinding. The separation of Th-waste from the solution containing the REEs was also simplified. This process is limited because it did not improve the Th separation and the phosphate product was unable to be recovered for fertilizer (Merrit, 1990).

2.3.4. Smelting of South African REE Resources: PyEarth ™ Process

The PyEarth ™ is a novel process developed by Mintek for the efficient extraction of rare earths from iron-rich, rare earth bearing carbonatite ores from Southern Africa. The process utilises direct smelting of the ore for selective removal of Fe as a saleable Fe-rich alloy while concentrating the REOs in the slag phase. The smelting of Fe-rich, REE-bearing ores from Southern Africa using the PyEarth ™ process is based on thermodynamics; the temperature range utilised in the tests is such that the Fe oxides (Fe_2O_3, Fe_3O_4, FeO in FeO(OH)) are easily reduced to Fe by carbon and the REEs remain as oxides (Bisaka et al., 2017).

The Fe-rich, REE-bearing carbonatite ore utilised in the experiments was found to contain REEs predominantly in monazite and minor bastnaesite and REE-apatite, that were finely disseminated in a geothite-hematite matrix. The smelting stage consists of processing the Fe-rich, REE-bearing ore with anthracite in a direct current (DC) arc furnace to produce a concentrated rare-earth containing slag and a Fe-Mn alloy by-product. The REEs in the slag phase are contained in needle-shaped Ca silicate phases and the perovskite phases. The smelting is followed by leaching of the slag in a hydrochloric acid (HCl) medium, followed by neutralisation for the removal of Fe, Al and Th. The last stage in the process is the precipitation of rare earths using lime (Bisaka et al, 2016). The smelting stage resulted in the upgrading of the slag phase by more than a factor of 5 (13.8 wt. % TREO in the slag versus 2.5 wt. % in the ore), whilst the REE recovery was above 95%. The leaching efficiencies of the total rare earth elements (TREE) was found to range between 94% and 97%. Although this is the case, there was co-extraction of other impurities (such as Al, Ti, Mn, Fe, Th and U) from the slag (Bisaka et al., 2016).

The smelting of run-of-mine presents challenges on the operation of the blast furnace. The smelting of Fe-rich, REE-bearing ores is associated with high coke, high flux consumptions while the furnace through-put is low due to the large volumes of slag produced. The furnace refractories also experience a severe erosion due to the high fluoride content present in the slag,

therefore smelting of run-of-mine using the blast furnace is not currently practiced (Ding et al., 2013).

2.4. SULFATION ROASTING

Sulfation roasting is a salt roast process utilised for the conversion of metal sulfides or oxides into metal sulfates which can be dissolved using water or dilute acids. Sulfation is achieved by heating the feed material, i.e. ROM and/or concentrate, with sulfur trioxide (SO_3), a stoichiometric mixture of SO_2 and O_2, a sulfate such as sulfuric acid (H_2SO_4), Na_2SO_4, $(NH_4)_2SO_4$ or bisulfates such as $KHSO_4$ as the reductant (Habashi, 2017). The sulfation roasting process consists of two stages: the sulfation roasting stage and the leaching stage. The REEs are extracted from solution through solvent extraction and/or electrowinning processes as shown in Figure 2.4. Sulfation is conducted in fluidized bed reactors, multiple hearth furnaces, or rotary kilns (Habashi, 2003).

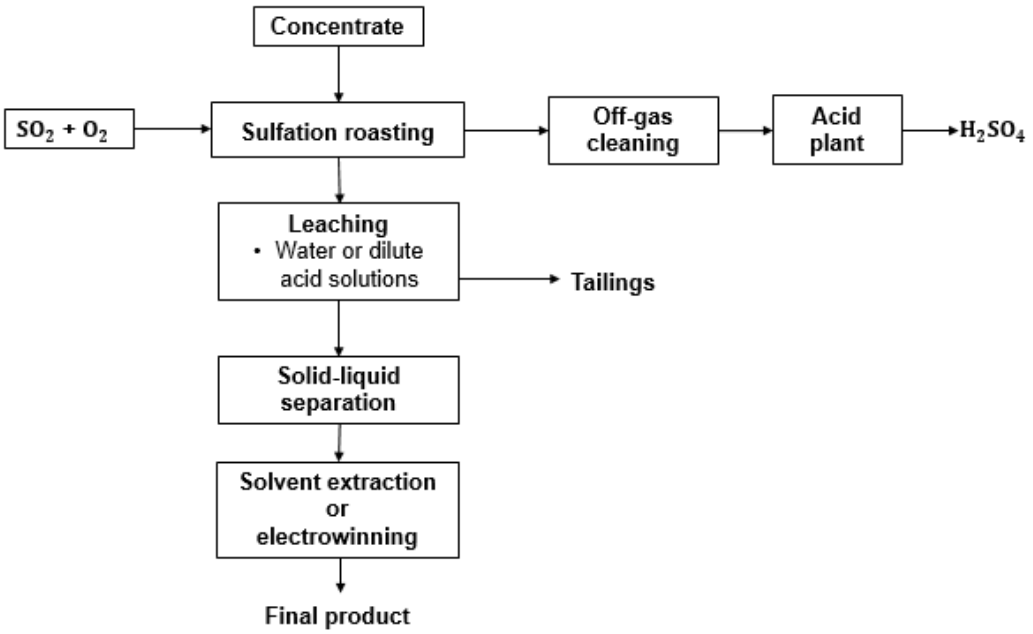


Figure 2.4. Typical flowsheet for the sulfation roasting of metal oxides or metal sulfates. (Guntner and Hammerschmidt, 2011).

2.4.1. Sulfation Roasting Chemistry

This section discusses the chemistry for the sulfation roasting of metal oxides using sulfur trioxide (SO_3) as the reductant. Sulfur trioxide is made up of a stoichiometric mixture of sulfur dioxide (SO_2) and oxygen (O_2). The formation of SO_3 is described by equation (2.21) (Shamsuddin, 2016).

$$SO_2 + {}^1/_2\, O_2 \rightarrow SO_3 \quad (2.21)$$

The sulfation of metal oxides to form water-soluble sulfates and basic sulfates is described by equation (2.22) to (2.24) (Guntner and Hammerschmidt, 2011; Shamsuddin, 2016).

$$MeO + SO_3 \rightarrow MeSO_4 \quad (2.22)$$

$$2MeO + 2SO_2 + O_2 \rightarrow 2MeSO_4 \quad (2.23)$$

$$2MeO + SO_3 \rightarrow MeO.MeSO_4 \quad (2.24)$$

The decomposition of sulfates to basic (oxy) sulfates is describe by equation (2.25) to (2.27) (Shamsuddin, 2016).

$$2MeSO_4 \rightarrow MeO.MeSO_4 + SO_3 \quad (2.25)$$

$$MeO.MeSO_4 \rightarrow 2MeO + SO_3 \quad (2.26)$$

$$MeSO_4 \rightarrow MeO.ySO_3 + (1-y)SO_3 \quad (2.27)$$

The roasting process is known to produce a mixed product stream. Metal oxides can form sub- and/or higher oxides instead of metal sulfates during the process. The formation of higher oxides is described by equation (2.28) and (2.29) (Shamsuddin, 2016).

$$2MeO \rightarrow Me_2O + {}^1/_2\, O_2 \quad (2.28)$$

$$2MeO + {}^1/_2\, O_2 \rightarrow Me_2O_3 \quad (2.29)$$

The roasting process has considerable side reactions taking place and these are dependent on the composition of the feed. The produced roast product depends on the chemical and mineralogical composition of the feed, temperature, and partial pressures of SO_2 and O_2 as well as process parameters such as particle size, mixing, reaction time, and roasting methods (Shamsuddin, 2016).

2.4.2. Sulfation Roasting Thermodynamics

Thermodynamic data described through diagrams such as stability diagrams, free energy diagrams and predominance phase diagrams is important in designing as well as exploiting the

selectivity of the sulfation roasting process. This section discusses the usefulness of these diagrams.

2.4.2.1. Standard Gibbs Free Energy

The standard Gibbs free energy for the sulfation reactions of different REOs and common 'gangue' metals associated with REEs is shown in Figure 2.5. This diagram is useful in determining the ease of reduction of these metal oxides in a sulfur trioxide atmosphere. The stability of the sulfation reactions decreases with increasing Gibbs free energy. Therefore, the sulfates formed by the reactions at the top of the diagram are less stable than the ones that appear at the bottom, i.e. the most stable sulfate being Ca and the least is Al. There are significant differences between the thermal stability of Fe and rare earth sulfates, particularly for Ce and La. The standard Gibbs free energy of formation of Fe sulfates and Al sulfates becomes positive at temperatures above 800°C, while that of the REEs remains negative. This shows that the decomposition of Fe and Al sulfate to their oxide derivatives (reverse reaction) occurs at higher temperatures, while the REE sulfates remain stable. The diagram also shows that La sulfates are the most stable amongst the REEs, while those of Nd are the least stable (Teixeira et al., 2018).

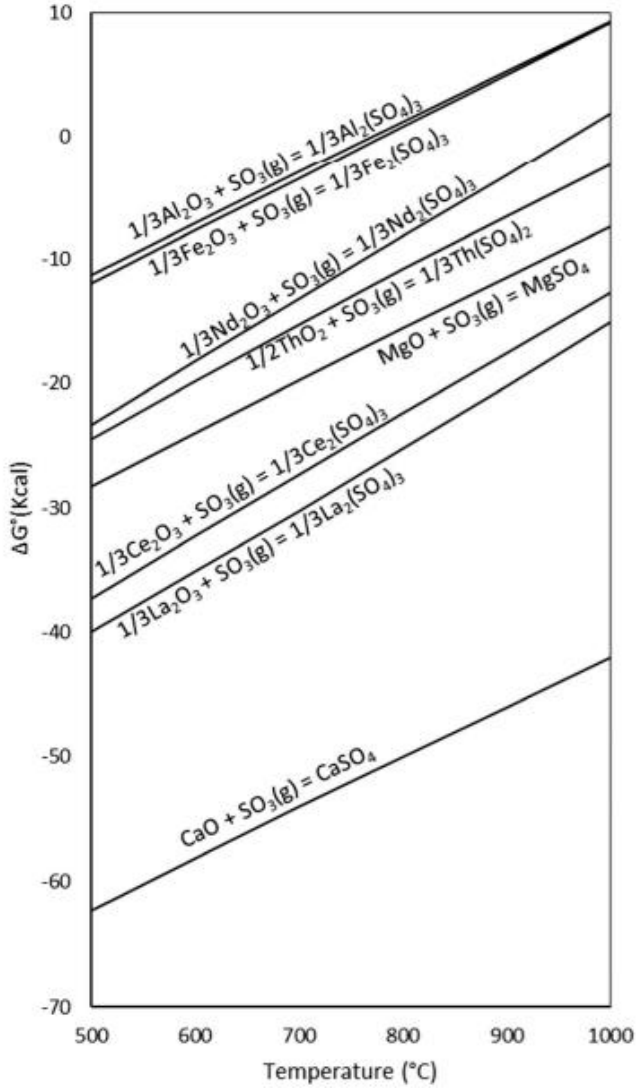


Figure 2.5. The standard Gibbs free energy for the sulfation reactions of different oxides in the temperature range 500°C - 1000°C (HSC v.8) (Teixeira et al., 2018).

2.4.2.2. Thermal Stability Diagrams

The thermal stability of different metal sulfates may be discussed using thermal stability diagrams. Figure 2.6. shows the thermal stability of REE sulfates that are assumed to form according to equation (2.30), where REE represents the rare earth element and the Delta symbol (Δ) indicates the heat being added to the system (Teixeira et al., 2018).

$$REE_2(SO_4)_3 \xrightarrow{\Delta} \Delta REE_2O_3 + 3SO_3 \quad (2.30)$$

The thermal stability diagram shows that there is a significant temperature difference between the decomposition of Fe sulfate and anhydrous REE sulfates, which is about 150°C for Nd and even higher for La. These diagrams can be utilised to determine suitable roasting temperatures

for selective sulfation of REEs, while keeping major gangue constituents such as Fe in their sparingly soluble oxide phase. Figure 2.6 shows that temperatures above 750°C and below 900°C are suitable for the selective sulfation of La, Ce and Nd, while allowing for the decomposition of Fe sulfates into Fe oxides (Teixeira et al., 2018).

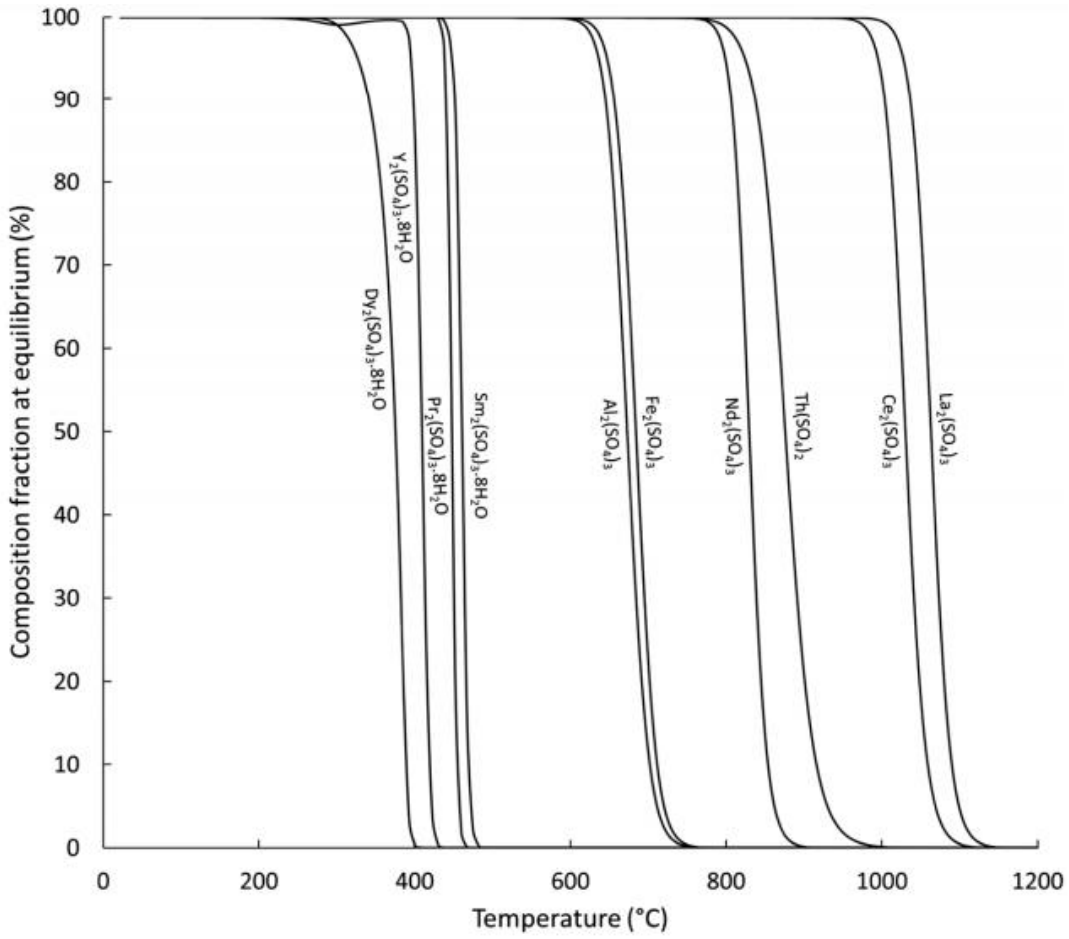


Figure 2.6. Thermal Stability of selected REE sulfates and major gangue metals present in REE resources. (Teixeira et al., 2018).

2.4.2.3. Predominance Phase Diagrams

Predominance phase diagrams are utilised to display the phase relations in metal-gas systems and to predict the roasting conditions to produce specific phases. Predominance phase diagrams are two-dimensional diagrams, where the axis and coordinate are partial pressures of any two gases (Shamsuddin, 2016; Sohn and Goel, 1979; Kellog and Basu, 1960). The equilibrium relations that exist in a system may be determined from first principles using the Gibbs Phase Rule, for the calculation of PADS, which is expressed as:

$$P + F = C + 2 \quad (2.31)$$

Where F is the degrees of freedom (variance of the system), C is the minimum number of chemical components in the system, P is the number of phases and 2 being an integer related to the number of intensive parameters such as temperature and pressure that are being considered (Alcock, 1976).

The products produced in a roasting process are determined through the consideration of the roasting reactions thermodynamics. Roasting is a solid-gas reaction; thus, the gas composition plays a significant role in the determination of the final stable phases (Alcock, 1976). In the case of roasting a REE-bearing material predominantly rich in Fe, a 2-metal (Ce, Fe) predominance phase diagram in the presence of a sulfur dioxide (SO_2) and oxygen (O_2) atmosphere can be calculated to predict the stable phases present at a specific roasting temperature. These diagrams and their applications are further discussed in Chapter 4 of this study.

2.4.3. Review of Acid-Based Sulfation Roasting of REE-Bearing Resources

Sulfation of REE-bearing materials using sulfuric acid is usually conducted alongside a roasting/heating stage. This process is usually conducted at temperatures in excess of 300°C and is therefore, considered to be a high temperature process. Sulfation and roasting processes are usually utilised for complex REE-bearing materials that contain significant amounts of gangue constituents such as Fe, Mn, Al, and Th. The high temperatures are used to decompose Fe sulfates into Fe oxides as well as to decrease Th extraction due to the formation of insoluble ThP_2O_7 (Zhang et al., 2016).

2.4.3.1. Sulfation-Roasting-Leaching of Bauxite Residues

Borra et al. (2015) investigated the sulfation-roasting-leaching process for the selective extraction of REEs from a Greek bauxite residue. The residue, which is generated as a waste product during the production of alumina using the Bayer process, contains significant amounts of REEs alongside major gangue constituents such as Fe, Al and Ca. Processing of bauxite residues using direct leaching processes produces relatively low REE yields. Improving the low yield requires an increase in acid concentration, which is problematic as it results in the increase of Fe dissolution which creates challenges in downstream extraction processes (Borra et al., 2015). The sulfation stage results in adequate formation of metal sulfates, while the roasting stage is utilised to decompose the unstable metal sulfates, mainly Fe sulfates, into their

respective metal oxides. The soluble REE-sulfates remain stable under these conditions and are further separated from the oxides during water leaching. The sulfation-roasting-leaching process flowsheet used in the study is shown in Figure 2.7**.**

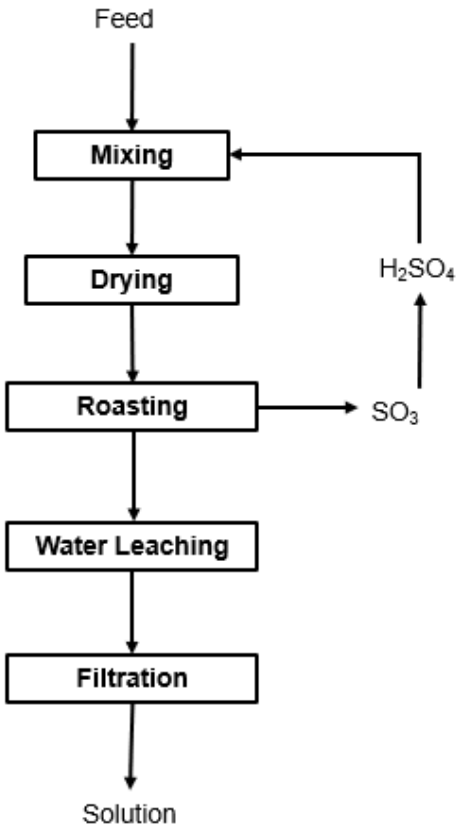


Figure 2.7. Flowsheet of the acid-based sulfation-roasting-leaching process (Borra et al., 2015).

The bauxite residue investigated by Borra et al. (2015) was rich in Fe oxide and alumina, and contained about 0.1 wt. % of REE content. The effect of roasting temperature, roasting time, and acid concentration on the REE extraction efficiency and impurity rejection during leaching were investigated. A decrease in roasting temperature was found to increase the dissolution of the REEs, Fe and Al. The effect of acid addition resulted in higher REE extractions. Under optimum conditions approximately 60% of Sc and more than 90% of the other REEs were extracted into solution, while very small amounts of Fe (<1% of total Fe) were solubilized. The leached residue was rich in Fe_2O_3, Al_2O_3, SiO_2 and $CaSO_4.0.5H_2O$ (Borra et al., 2015).

2.4.3.2. Selective Extraction of REEs from Monazite Ores with High Fe Content

Teixeira et al. (2019) conducted a thermodynamic analysis for monazite systems where the fundamentals of a selective process route for rare earth extraction from monazite ores with high

Fe content were discussed. The proposed process consisted of sulfation by means of a concentrated sulfuric acid and roasting using a muffle furnace at temperatures between 200°C to 800°C. Lastly, the roasted samples were leached in water under a controlled pH conditions (Teixeira et al., 2019).

Thermodynamic analysis using free energy diagrams and thermal stability diagrams for the REEs showed that REE-bearing monazite ores may be selectively treated for the separation of Fe and Th from the REEs if the material is sulfated and roasted at 700°C. The process was found to promote high REE extraction, between 70 and 80%, low Fe and Th extraction, below 1%, with low acid consumption, between 0.21 and 0.34 kg of acid for 1 kg of ore. The study showed that the key stage for selective extraction to be achieved is roasting, whereby the Fe sulfates decompose into Fe oxide and releases SO_3 gas. Fe sulfate decomposition was achieved at 700°C, a condition where maximum REE extraction was achieved. An increase in temperatures higher than 750°C was associated with an increased amount of insoluble rare earth compounds which in turn decreased the amount of recoverable REEs during the leaching stage and therefore rendered the processes ineffective for rare earth extraction (Teixeira et al., 2019).

2.4.4. Critical Evaluation of the Acid-Based Sulfation Roasting for REE Extraction

Sulfuric acid (H_2SO_4) baking also known as sulfation roasting, acid baking or acid digestion process has been investigated for the extraction of REEs from low-grade monazite mineral resources. Sulfation roasting processes are conducted at temperatures between 300°C and 800°C using sulfuric acid as the roasting reagent. High roasting temperatures have been adopted mainly for the rejection of impurities such as Fe, Th, Ca, and PO_4 which are contained in phases that are insoluble during the leaching stage (Liu et al., 2014; Zhang et al., 2015). The high operational temperatures are advantageous because they result in shortened processing times. Other advantages of the acid roasting process include the reduction of separation stages, reduced damage to equipment, improved REE recoveries, strong process continuity and adaptability to different REE concentrate grades (Zhang et al., 2015).

Although high temperature acid baking processes addressed several concerns brought by low temperature acid baking; the elevated temperatures have created other operational and environmental concerns. These are related to the increased amount of toxic off-gases such as SO_2 that require treatment (Zhang et al., 2015). The decomposition and volatilisation of H_2SO_4

is an important aspect of the acid-based sulfation roasting process. Equilibrium concentrations for the decomposition of pure H_2SO_4 acid based on thermodynamic data have been calculated by Schwartz et al. (2000) and Soltani et al. (2018). The calculations showed that both direct evaporation and decomposition to SO_3 and H_2O is expected to occur at temperatures above ~200°C according to reactions described by equation (2.32) and (2.33).

$$H_2SO_4 \rightarrow H_2SO_{4(g)} \quad (2.32)$$

$$H_2SO_4 \rightarrow SO_{3(g)} + H_2O_{(g)} \quad (2.33)$$

Soltani et al. (2018) observed direct evaporation of H_2SO_4 acid according to equation (2.32) at ~330°C, while the decomposition via equation (2.33) was the predominant process from both sources at temperatures above 350°C. A further increase in the roasting process temperature was shown to be associated with the occurrence of a second process involving the decomposition of SO_3 to SO_2 and O_2 according to equation (2.34). This reaction is more predominant than the one described by equation (2.33) as operational temperatures reach ~700°C (Soltani et al., 2018; Schwartz et al., 2000). Therefore, higher acid roasting temperatures increase the overall acid requirement due to the increased rate of acid loss to the gas phase (Demol et al., 2019).

$$SO_{3(g)} \leftrightarrow SO_{2(g)} + {}^{1}/_{2}\, O_{2(g)} \quad (2.34)$$

The other observation of the acid based roasting process is that higher acid to concentrate ratios have been found to improve REE extraction. A study conducted by Blickwedel. (1949) showed that lowering acid concentrations to below 93% rapidly decrease the reaction rates. Acid to concentrate ratios in the range of 1:1 to 2.5:1 (w/w) are typically utilised for high grade monazite concentrate sulfation. These amounts are equivalent to 2-3 times the stoichiometric requirement (Zelikman et al., 1966). These amounts are exceedingly higher for low-grade monazite materials due to accountability of the side reactions taking place during the roasting process.

Gas-based sulfation roasting is proposed in this study as an alternative technique for the selective extraction of REEs from various South African resources. Gas-based sulfation roasting also commonly known as sulfation roasting or sulfatizing roasting has been investigated successfully for the extraction of base metals from sulfidic ores as well as for the

extraction of manganese from different ore resources. Like the high temperature acid roasting process, this technique is commonly utilised for low-grade resources that commonly contain major gangue constituents such as Fe, Ca, and Th (Güntner and Hammerschmidt, 2012; You et al., 2015). SO_2 gas and O_2 and/ or air are utilised during the sulfation of oxide ores. The main advantage of the gas-based process is the lowered reagent consumption as compared to the high-temperature acid baking process. The reacting gas is only introduced into the system once the system has reached the required temperature. Literature on the application of the gas-based sulfation roasting process for REE extraction from various resources was not obtained during this study.

2.5. FLUIDIZATION BACKGROUND

The sulfation roasting process is commonly extracted using fluidized bed reactors as they provide superior heat transfer, the heat transfer rate can be five to ten times greater than that of a packed-bed reactor. Fluidized beds provide easy fluid-like movement of particles which is advantageous as these particles can transport heat much more efficiently than gas alone. Fluidized beds are also preferred as they can be used to process materials with a wide particle distribution (Cocco et al., 2014).

2.5.1. Principles of Fluidization

Fluidized bed reactors are well-stirred reactors that are characterized by excellent gas-solid contact, uniform temperature, and composition across the bed (Morris, 2001). A fluidized bed is a packed bed through which a gas fluid flows at a velocity that is high enough for the bed to be loosened resulting in the particle fluid mixture behaving like a fluid (Moodley, 2011).

The fluidization phenomenon can be understood by considering what happens when fluid is passed through a tube reactor with a porous plate supporting the solid particles. The particles become fluidized when an upward-flowing gas imposes a drag force that is high enough to overcome the downward force of gravity. The drag force is the frictional force imposed by the gas on the particle. The particle imposes an equal and opposite drag force on the gas (Cocco et al., 2014). As the particles become more fluidized, the drag forces tend to affect the local gas velocity around them, this effect is more significant on irregularly shaped particles. As the fluid velocity is increased the pressure drop also increases. At a specific fluid velocity, the point is reached when the upward drag force exerted by the fluid on the particles is equal to the weight

of the particles in the bed, equation (2.35) and (2.36). At this point the particles are lifted by the fluid, separation of the particles increases, and the bed becomes fluidized (Rhodes, 2008).

$$\left(\begin{array}{c}\text{Weight of solid}\\ \text{particles}\end{array}\right) = \left(\begin{array}{c}\text{Drag force on the particles}\\ \text{from upwards moving gas}\end{array}\right) \tag{2.35}$$

Or

$$A_B \Delta P = H_{mf}(1-\varepsilon_{mf})(\rho_p - \rho_f)g \tag{2.36}$$

A_B	Cross section area of bed, cm^2
mf	subscript for "at minimum fluidization conditions"
H	depth of bed, cm
ε	bed voidage,
ρ_p	density of particles, g/cm^3
ρ_f	fluid density, g/cm^3
g	acceleration due to gravity, g/cm^3

The minimum fluidization velocity, U_{mf}, which is also known as the inception of fluidization is described by the equation giving the pressure drop in a gas flowing through a packed bed as described in equation (2.37).

$$\frac{\Delta P}{h} = 150\frac{(1-\varepsilon_{mf})^2}{{\varepsilon_{mf}}^3}\frac{\mu U_{mf}}{(\emptyset_s d_p)^2} + 1.75\frac{(1-\varepsilon_{mf})}{{\varepsilon_{mf}}^3}\frac{\rho_f {U_{mf}}^2}{\emptyset_s d_p} \tag{2.37}$$

ΔP	Pressure drop across depth L, Pa
L	depth of bed, cm
ε	bed voidage,
μ	fluid viscosity, g/cm.s
U	superficial fluid velocity through the bed, cm/s
$\emptyset_s$	particle sphericity
d_p	sauter mean particle size, cm
ρ_f	fluid density, g/cm^3

The U_{mf}, assuming small spherical particles, Re_{mf} <20, can also be calculated using equation 2.37 (Kunii and Levenspiel, 1991)

$$U_{mf} = \frac{(\emptyset_s d_p)^2(\rho_p - \rho_f)\varepsilon^3 g}{150\mu(1-\varepsilon)} \quad (2.37)$$

While for larger particles, Re_{mf}>20, the U_{mf} is described by equation 2.38

$$U_{mf} = \left[\frac{(\emptyset_s d_p)^2(\rho_p - \rho_f)\varepsilon^3 g}{1.75\rho_f}\right]^{0.5} \quad (2.38)$$

Particle sphericity (Φ_s) is defined as the ratio of the surface area of the sphere to the surface area of a particle with the same volume. The value is between 0 and 1 and can be calculated using equation 2.39.

$$\emptyset_s = \frac{\text{surface of sphere}}{\text{surface of particle}} \quad (2.39)$$

2.5.2. Fluidization Stages

Figure 2.8 illustrates the different stages of fluidization. The fixed/packed bed (A) and the fluidized bed (B) stages were already discussed in the previous section. This section will discuss the other stages of fluidization.

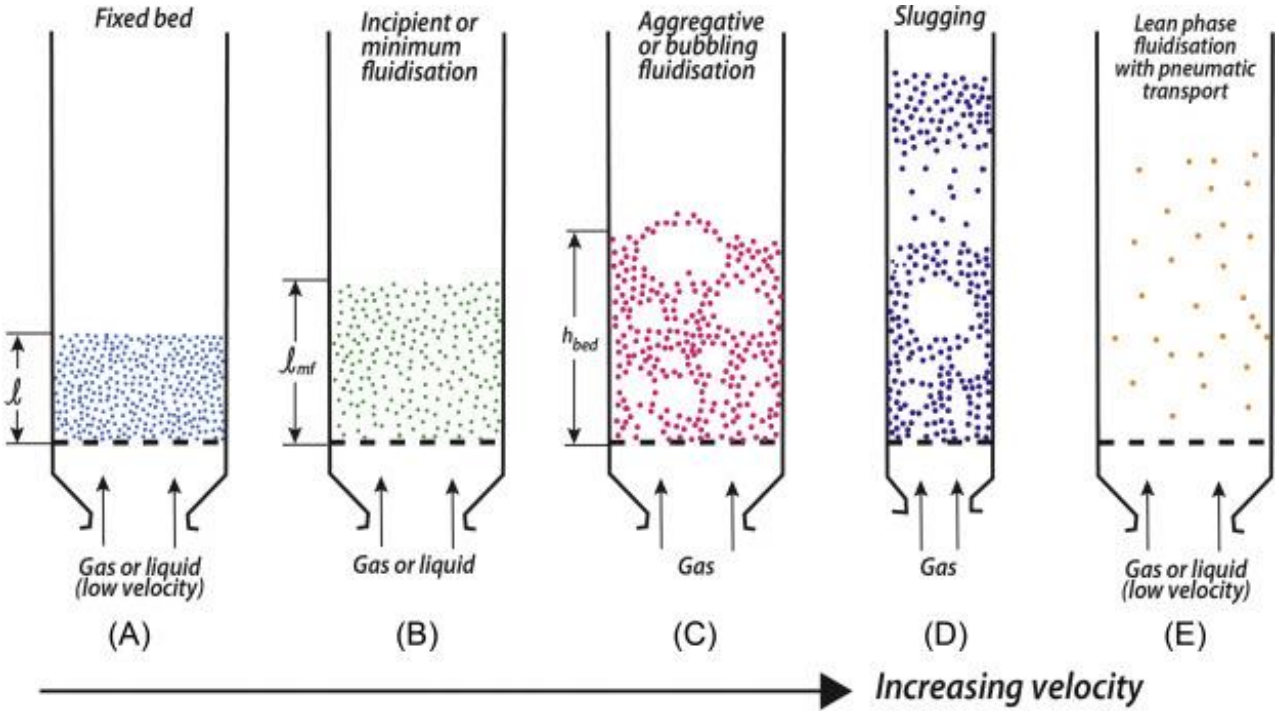


Figure 2.8. The different stages of fluidisation (Chhabra and Gurappa, 2019).

When the fluid velocity is increased above the minimum fluidizing velocity U_{mf} the bed transitions from a bubbling bed to a turbulent fluidized bed where the gas voids are no longer regularly shaped bubbles, but rather have elongated shapes. The number of particles being entrained increases and results in the top of the bed being less defined. This fluidization regime is usually called aggressive or bubbling fluidization as shown in Figure 2.8 (C) (Cocco et al., 2014).

Further increase in the fluid velocity can induce slugging which is caused by coalesce and growth of the bubbles. The bubbles can grow to reach a size where they occupy the entire cross-sectional area of the tube. The large bubbles push the solid particles ahead of it as shown in Figure 2.8 (D). The slugging regime is undesirable because it increases entrainment and elutriation and lowers the vessel's performance (Moodley, 2011).

A further increase in the fluid velocity can result in the bubbles occupying more space and can result in particles being carried out of the bed by the bursting bubbles, therefore making the top of the bed indistinct. This takes place when the fluid velocity exceeds the terminal velocity of the solids. This regime is known as lean phase fluidization with pneumatic transport. This phenomenon is shown in as shown in Figure 2.8 (E) (Moodley, 2011; Pell, 2012).

2.5.3. Geldart Classification

Geldart (1973) proposed the graph shown in Figure 2.9 to classify the fluidization behaviours of solid particles when fluidized under ambient conditions. Powders are classified into the following four groups based on their density and particle size (Cocco et al., 2014):

- Geldart Group A – Particles are aeratable and fluidize well (smooth fluidization).
- Geldart Group B – Particles exhibit sand-like behaviour (bubbles form at onset of fluidization.
- Geldart Group C – Particles are cohesive and experience significant channelling during fluidization.
- Geldart Group D – Particles are spoutable (bubbles formed are enormous therefore the bed tends to exhibit sluggish behaviour.

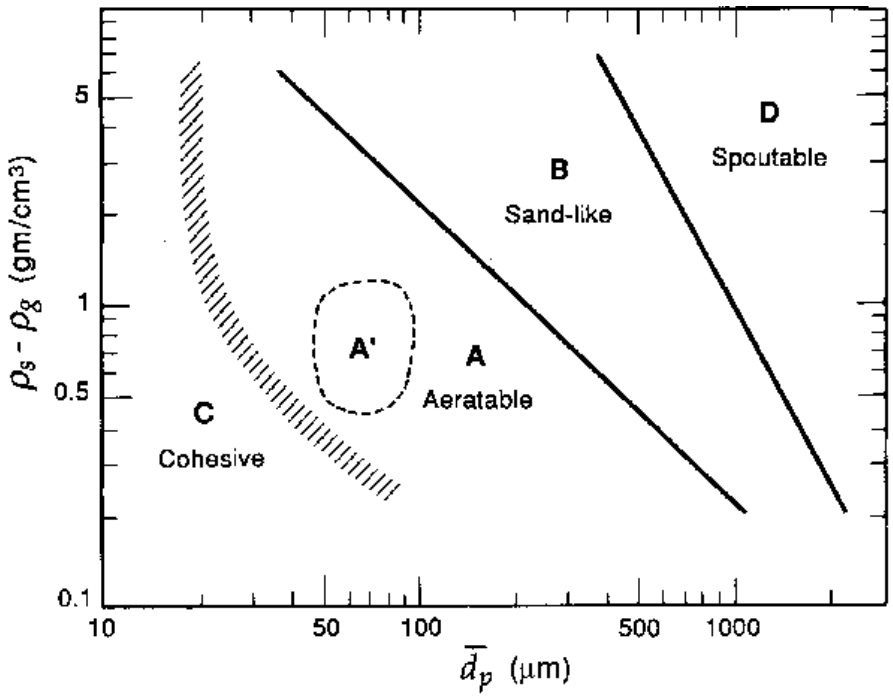


Figure 2.9. Geldart's classification of powders according to their fluidization behaviour under ambient conditions (Geldart, 1973).

2.5.4. Entrainment

Entrainment is described as the carryover of particles from the fluidized bed and their removal from the vessel in the fluidizing gas (Pell, 2012; Rhodes, 2008). The rate of entrainment and the size distribution of entrained particles is dependent on particle size and density, properties of the gas, velocity of the gas, gas flow regime-radial velocity profile and fluctuations and reactor diameter. The mechanisms by which particles are ejected into the gas stream from the fluidized bed are dependent on the bed characteristics, particularly the bubble size and the velocity at the surface, and the gas velocity profile immediately above the bed surface is distorted by the bursting bubbles. Due to these factors, entrainment predictions from first principles are not possible and therefore, empirical approaches must be adopted. The empirical approach defines coarse particles as particles whose terminal velocities are greater than the superficial gas velocity (U_T>U) and fine particles as those with less terminal velocity than superficial gas velocity (U_T<U). This approach also considers the regions above the fluidized bed surface to be composed of several zones shown in Figure 2.10 (Rhodes, 2008):

- Freeboard: Region between the bed surface and gas outlet
- Splash zone: Region above bed surface where coarse particles fall back down

- Disengagement zone: Region above the splash zone, where the upward flux and suspension concentration of fine particle decrease with increasing height.
- Dilute-phase transport zone: Region above disengagement zone in which all particles are carried upwards; particle flux and suspension concentration are constant with height.

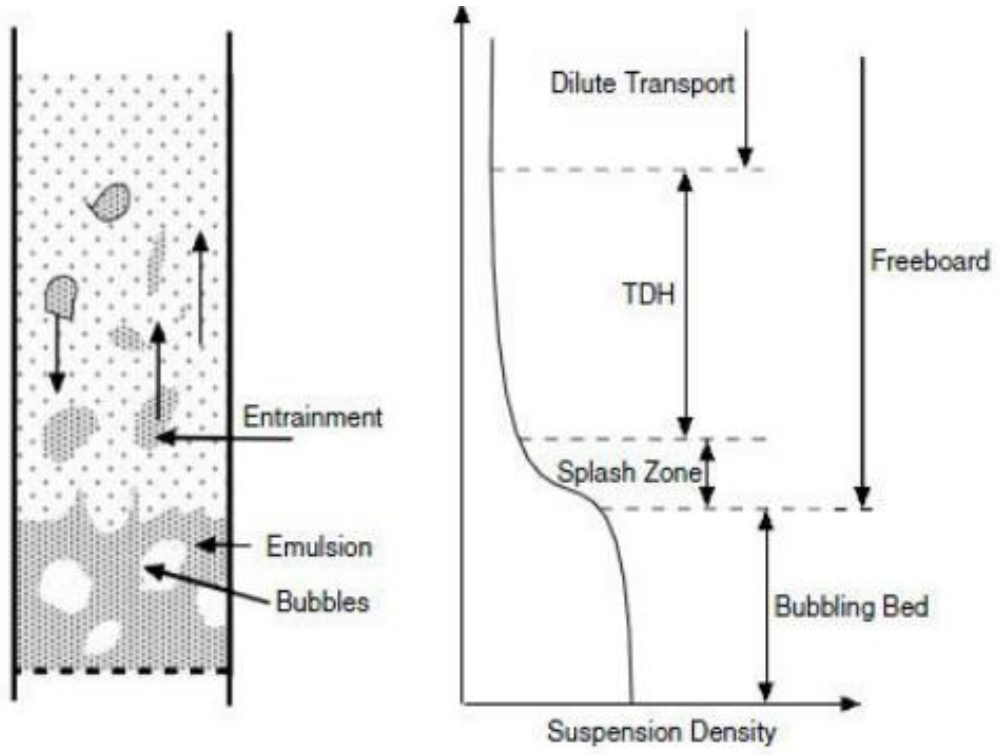


Figure 2.10. Zones in the fluidized bed freeboard (Folayan et al., 2015).

The height from the bed surface to the top of the disengagement zone is called the transport disengagement height (TDH) – it is shown in Figure 2.10. The concentration of the particles and the entrainment flux are constant above the TDH. Entrainment can be measured by means of a value called the elutriation constant (k_i). Kuni and Levenspiel (1991) describe the method of determining the elutriation constants by doing batch experiments. The flux of the particles out of the bed may be described by equation (2.40) (Kunii and Levenspiel, 1991):

- Assumption: the flux rate of a particular size of solid i is proportional to its weight x_i in the bed, all other factors being constant.

$$-\frac{1}{A}\frac{dW_i}{dt} = k_i{}^* x_i = k_i{}^* \left(\frac{W_i}{W}\right) \qquad (2.40)$$

If the total mass of the sample does not change by more than 20% during the experiment, the integration of equation (2.40) results in equation (2.41).

$$\frac{W_i}{W_{io}} = \exp\left(\frac{k_i^* A_t}{W}\right) \quad (2.41)$$

W_{io} Initial weight of mass fraction i

W_i Final weight of mass fraction i

W Total weight of sample before fluidization

A Area of reactor, m^2

t Time, s

k_i^* Elutriation constant, $kg/m^2.s$

The elutriation constant can only be calculated using equation (2.41) if the particle size distribution of the initial bed and after some time is known (Moodley, 2011).

2.6. SUMMARY OF LITERATURE

REEs are commonly extracted from their mineral concentrates using hydrometallurgy-based decomposition processes such as alkaline or acid-baking. These processes are known to be highly efficient for the extraction of REEs as they are associated with high recoveries of these metals. Although this is the case, the processes tend to co-extract major gangue constituents such as Fe, Mn, Al, and Th and are therefore rendered to be unselective. Co-extraction of gangue metals requires multiple purification stages to produce a more sellable product stream. These purification stages tend to make the process flowsheet complicated, tedious, and very expensive (Amer et al., 2013; Bisaka et al., 2016).

High temperature processes such as carbochlorination, soda roasting and smelting, have been investigated for the pre-treatment of mineral concentrates and/or REE-bearing ores prior to leaching stages. These processes were found to be successful in producing a product stream that is amenable leaching but were also found to be unselective because they were associated with co-extraction of major gangue constituents. These processes have not been applied on an industrial scale due to the unattractive process economics associated with energy and reagent consumption, erosion of the fluxes and large slag volumes.

High temperature acid roasting has been investigated for the extraction of REEs from low grade ore concentrates. This process allows for the selective conversion and extraction of REEs into

water-soluble sulfates while keeping the gangue metals as oxide compounds. These insoluble metal oxides are separated from the REE sulfates during the leaching stage therefore simplifying the process flowsheet. However, the use of H_2SO_4 at high temperatures presents some technical challenges associated with the decomposition and volatilisation of H_2SO_4. Higher bake temperatures increase the overall acid requirement due to an increased rate of acid loss to the gas phase. The main process disadvantage is the additional roasting stage which is included in the flowsheet (Borra et al., 2015). Gas-based sulfation roasting is proposed in this study as an alternative technique for the selective extraction of REEs from various South African resources. The process reduces the amount of reagent consumed during the study while producing equivalent results as the acid-based process. Gas-based sulfation roasting also known as sulfation roasting or sulfatizing roasting has been investigated for the extraction of base metals from sulfidic ores. Literature on the application of the gas-based sulfation roasting process for REE extraction from various resources was not obtained during this study.

3. METHODOLOGY

3.1. INTRODUCTION

This chapter discusses the materials, equipment and procedures utilised in this study. The analytical methods used during the study are also summarized in this section. The experimental test work consisted of three stages i.e. preliminary sulfation roasting studies, fluidization parameter determination as well as fluidized sulfation roasting studies.

3.2. MATERIALS

Preliminary sulfation roasting experiments were performed on synthetic CeO_2 and a mixture of synthetic $Ce_2(SO4)_3$ and $Fe_2(SO_4)_3$ was used to conduct stability tests at specific temperatures. All the synthetic materials were obtained from Merck.

Fluidized sulfation roasting studies were conducted on two industrial materials: a Zandkopsdrift (ZKD) ore sample and a PyEarth ™ slag sample. These materials were supplied by Mintek as part of an ongoing REEs project. Elemental analysis of these head samples was determined through Inductively Coupled Plasma – Optical Emission Spectroscopy techniques. The chemical composition of the industrial materials is given in Table 3.1 and 3.2.

The ZKD ore contains considerable amounts of REEs, with the LREEs namely Ce, La, Nd, Pr, being more prevalent than the other REE groups. The ore also contained significant amounts of Fe, which constitutes as the major gangue element in the material. The PyEarth ™ slag which is produced from the PyEarth ™ smelting process of REE-bearing carbonatite deposits, such as the ZKD ore deposit, contains REEs in higher concentrations than the ore. The slag also contains lower amounts of Fe and higher concentrations of Al, Ca, Mg, Mn, Si and Ti than the ZKD ore.

Table 3.1. Bulk chemical composition of the Zandkopsdrift head sample.

Element	**Al**	**Ca**	**Fe**	**Mg**	**Mn**	**Si**	**Ti**	**V**
% mass	2,65	1,19	35,30	0,36	6,33	2,69	1,57	0,06
Element	**Zn**	**Ce**	**La**	**Nd**	**Pr**	**Y**	**Gd**	**Dy**
% mass	0,20	0,96	0,62	0,33	0,10	0,06	0,04	0,02
Element	**Er**	**Eu**	Sm	Yb	Ho	**Tb**	**Tm**	**Lu**
% mass	0,01	0,01	0,05	0,01	<0,01	<0,01	<0,01	<0,01

Table 3.2. Bulk chemical composition of the PyEarth ™ slag head sample.

Element	**Al**	**Ca**	**Fe**	**Mg**	**Mn**	**Si**	**Ti**	**V**
% mass	11,50	4,18	14,20	1,89	8,12	7,09	6,41	0,05
Element	**Ce**	**La**	**Nd**	**Pr**	**Y**	**Dy**	**Er**	**Eu**
% mass	3,20	2,09	1,10	0,33	0,22	0,06	0,03	0,04
Element	**Gd**	**Ho**	**Lu**	**Sm**	**Tb**	**Tm**	**Yb**	
% mass	0,14	0,01	<0,00	0,15	0,02	<0,00	0,02	

The bulk density of the materials summarized in Table 3.3, showed that the ZKD ore is lighter than the PyEarth ™slag. These physical properties suggest that the materials are likely to behave differently during fluidization and therefore, fluidization properties for each head sample would have to be determined.

Table 3.3. Bulk density calculated for the feed materials.

Material	**Bulk Density (kg/m^3)**
Zandkopsdrift ore	1480
PyEarth ™ slag	1730

3.3. EXPERIMENTAL PLAN

The aim of the experimental work was to determine the technical feasibility of the sulfation roasting and leaching process for the extraction of REEs from various South African resources. The following set of tasks were formulated to achieve the aim of the study:

- Determination of the thermal conditions suitable for the sulfation roasting of LREEs, through calculation of predominant phase diagrams using FactSage 7.2 © software.
- Investigation of the suitable operational conditions of the sulfation roasting process by conducting preliminary tests on synthetic REO compounds.
- Calculation of the fluidization parameters to predict the behaviour of the different head samples during the fluidized sulfation roasting tests.
- Investigation on the effect of operational parameters; temperature, reaction time and stoichiometric ratio of SO_2 to O_2, on the conversion efficiency of LREEs in the ZKD ore and the PyEarth ™ slag using fluidized sulfation roasting experiments.
- Investigation of the sulfation efficiency through mineralogical analysis of the head and roast bed samples.

The experimental plan and its relation to the objectives listed in the introduction are described in Figure 3.1.

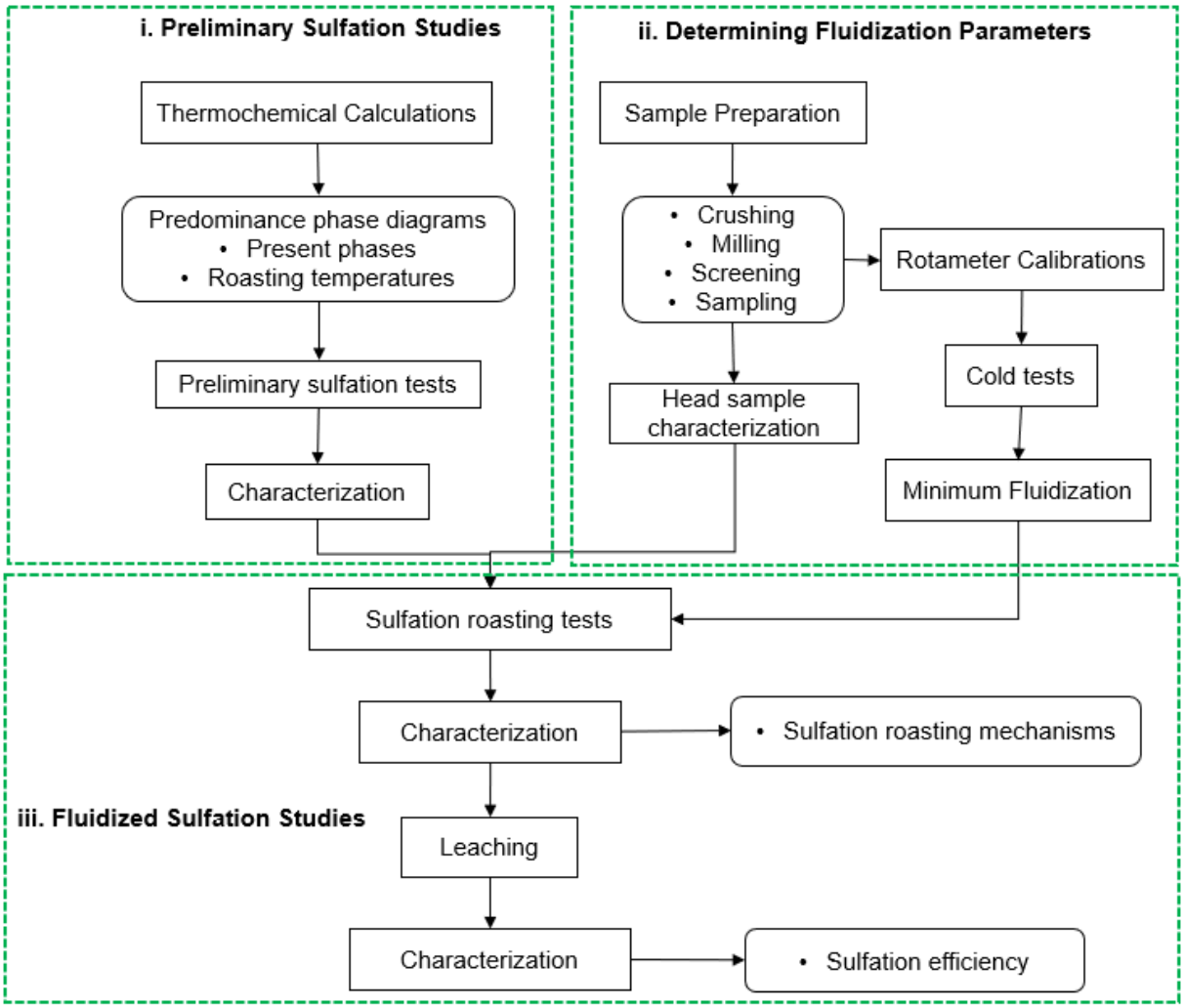


Figure 3.1. Experimental Plan.

3.4. PRELIMINARY SULFATION ROASTING

3.4.1. Thermochemical Calculations

Temperature and gas composition are the main parameters which affect the selectivity aspect of the sulfation roasting process; and therefore need to be controlled within a narrow range to avoid decomposition of formed sulfates and/ or the formation of gangue metal sulfates. The relationship between roasting temperature and the gas composition for metal-gas systems can be described through predominance phase diagrams. Predominance phase diagrams of the metals of interest are important in deducing the probable conditions which needed to be verified by empirical lab-scale tests.

3.4.1.1. Experimental Procedure

FactSage 7.2 © was used to conduct the thermochemical calculations in the study. The PREDOM module was used to calculate and plot isothermal 1- and 2-metal predominance phase diagrams. The first step in the calculations was to specify the metallic and non-metallic elements in the system. The second step was to determine parameters such as pressure constants, axes, labels, and display instructions. A summary of the inputs is presented in Table 3.1. The module also required the specification of species (gas, liquids, and solids) for the predicted final products. The Predom module window used for these calculations is described in Figure 3.2. The use of temperatures between 600°C and 800°C in the study was guided by the need for highly sulfated REEs under the conditions where the base metals or gangue mineral sulfates are unstable, to avoid paired leaching of REE sulfates with gangue metal sulfates.

Table 3.4. PREDOM module inputs for the calculation of predominance phase diagrams.

Parameter/variable	Specification
Metallic elements	Ce, La, Nd, Pr, Fe and Mn
Non-metallic elements	S and O
Pressure	1 atmosphere (atm)
Temperature (°c)	600, 630, 700, 750, 800
Y-axis (log10(y)) (atm)	Min = - 20, Max = 20
X-axis (log10(x)) (atm)	Min = - 20, Max = 20

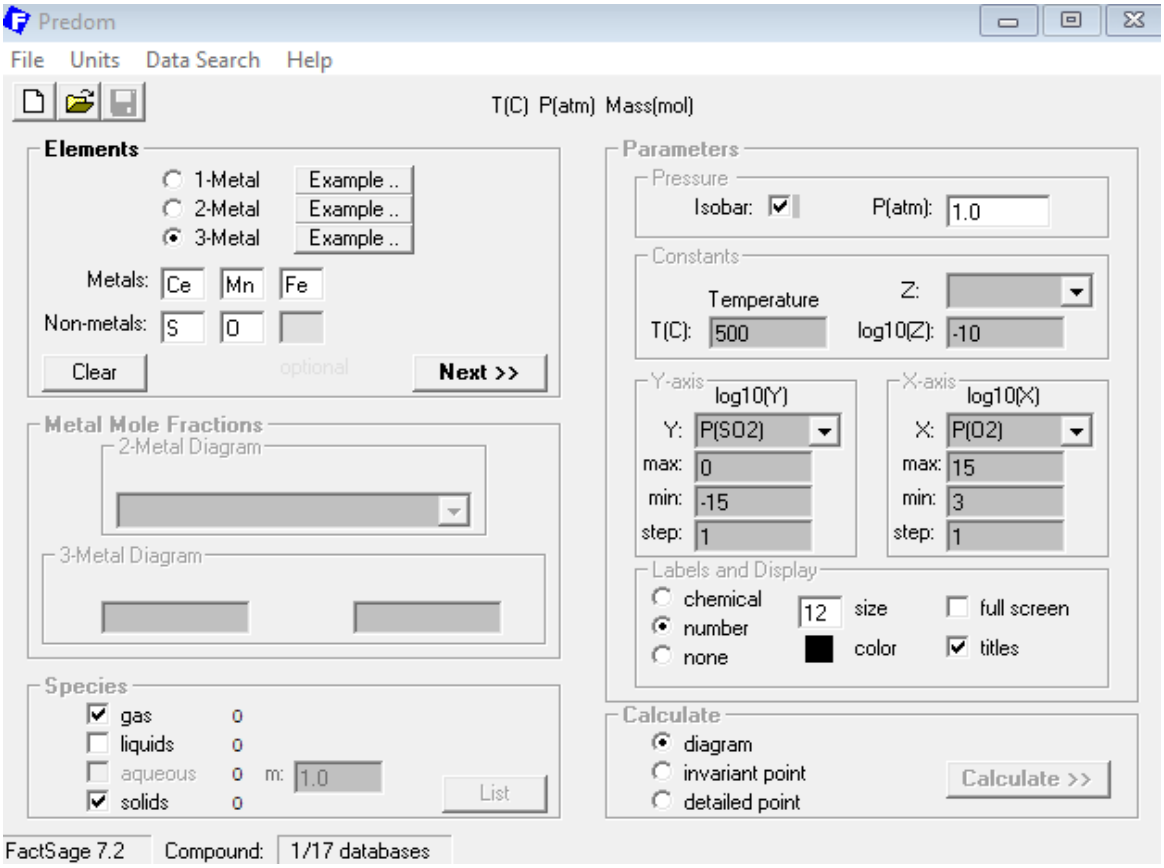


Figure 3.2. PREDOM Module window on FactSage 7.2 ©.

3.4.2. Preliminary Sulfation Roasting

Preliminary sulfation roasting tests were conducted on synthetic metal oxides to investigate the suitable thermal and operational conditions of the sulfation roasting process obtained from the FactSage thermochemical calculations for the extraction of LREEs. The preliminary study consisted of a series of sulfation roasting and leaching test work.

3.4.2.1. Experimental Apparatus

A schematic representation of the horizontal tube furnace used in the preliminary studies is shown in Figure 3.3. The reactor is made up of a 30 mm diameter quartz tube, which was heated to a set temperature in a resistance-type furnace. A K-type thermocouple was placed next to the sample boat inside the furnace to monitor the sample temperature throughout the experiment. The furnace controller was connected to the sample thermocouple for automatic regulation of the furnace resistance to control the temperature (Sithole et al., 2017).

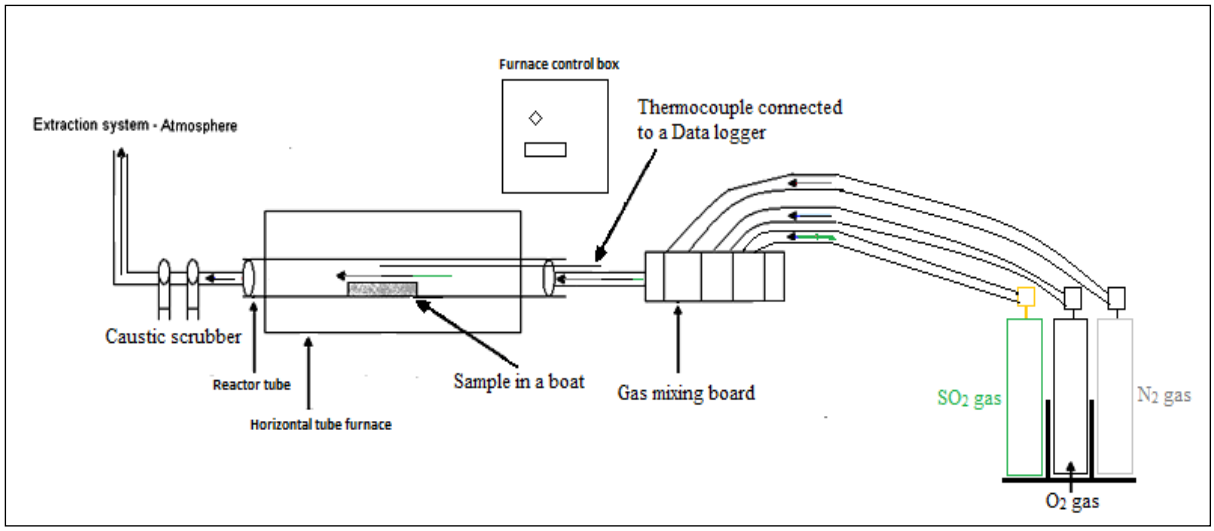


Figure 3.3. Schematic representation of the sulfation roasting experimental setup (Sithole et al., 2017).

3.4.2.2. Experimental Procedure

3.4.2.2.1. Sulfation Roasting and Stability Tests

Discrete masses of 10 g synthetic CeO_2 samples were weighed into respective sample boats and placed at the centre of the 30 mm quartz reactor in the horizontal tube furnace. SO_2, O_2 and N_2 gases were mixed and controlled using a gas mixing board that was connected to the furnace inlet. The total flow of gases was 300 standard cubic centimetres per minute (SCCM) or 5.46×10^{-6} m^3/s. The outlet of the reactor was connected to a double caustic scrubber (made up of 10% NaOH) to ensure that the surplus toxic SO_2 gas was not emitted directly to the atmosphere but reacted to form Na_2SO_4 in the solution. A summary of the test matrix is given in Table 3.5. The main parameters were roasting time, varied between 24 and 48 hours, and temperature, which was varied between 630°C and 800°C in a reaction gas composition of 16% O_2, 32% SO_2 (or 1:2 ratio of O_2 to SO_2) and 52% N_2.

Stability sulfation roasting test was conducted using a 10 g mixed synthetic cerium (III) sulfate ($Ce_2(SO4)_3$) and iron sulfate ($Fe_2(SO_4)_3$) sample, 50:50 mass ratio. The test was conducted at 750°C for 24 hours using the same setup and procedure described for the sulfation roasting tests.

Table 3.5. Summary of the preliminary sulfation roasting tests.

Test	Test material	Reaction time (hours)	Roasting temperature (°C)
Sulfation roasting of CeO_2			
1	CeO_2	24	630
2	CeO_2	48	630
3	CeO_2	24	700
4	CeO_2	48	700
5	CeO_2	24	750
6	CeO_2	48	750
7	CeO_2	24	800
8	CeO_2	48	800
Sulfate stability test- Sulfation roasting of $Ce_2(SO4)_3$- $Fe_2(SO_4)_3$			
9	$Ce_2(SO4)_3$-$Fe_2(SO_4)_3$ (1:1 mass ratio)	24	750

3.4.2.2.2. Mass Change Evaluations

Mass change calculations were conducted on the roast products to determine the occurrence or lack thereof of sulfation of the synthetic cerium oxide. The mass change evaluations were determined using the mass of the feed and product samples according to equation 3.1.

$$\%\text{Mass Change} = \frac{(\text{Mass}_{\text{product}} - \text{Mass}_{\text{Feed}})}{\text{Mass}_{\text{Feed}}} \times 100 \quad (3.1)$$

3.4.2.2.3. Leaching

The leaching experiments were conducted on the roast products generated from Test 1 to Test 8 to study the effect of roasting time and temperature on the leaching efficiency of Ce, La, Nd and Fe. The methodology used to leach the various samples was the same.

The test work involved leaching 5 g of sulfated material in 80 mL deionised water. The pH of the system was adjusted to 3.5–4 by adding 98% sulfuric acid to the water. The sulfated solid samples were transferred into 250 mL glass reactors. The leaching solution was transferred into a glass reactor that was fixed to an overhead stirrer. A hotplate was used to maintain the reactor contents at the required temperature. The pulp density of the slurry used in the tests was 10%. The tests were conducted at a temperature of 80°C for 4 hours, with hot water additions every 30 minutes to account for evaporation. At the end of each test the slurries were filtered using a

vacuum filtration unit. The residue was dried at 50°C for 8 hours in an oven. The mass of the residue and the volume of the filtrate were recorded. The filtrate was subjected to chemical analysis and the residue was analysed using X-ray diffraction.

3.5. FLUIDIZED SULFATION ROASTING STUDIES

3.5.1. Sample Preparation

Sample preparation was conducted for the feed materials, i.e. ZKD ore and PyEarth slag, utilised in the fluidized sulfation roasting tests. The aim of the sample preparation was to produce representative samples that were in the size range that would be suitable for fluidization

3.5.1.1. Experimental Procedure

The head samples were subjected to crushing using a jaw crusher to reduce the particle size from 60-80 mm to approximately 1 mm. The crushed samples were sampled using a riffle splitter to divide the material into representative samples. The riffle splitter was chosen as it produces the lowest variance between the samples (Khan, 1968). The split samples were sized using a vibrating sieve shaker equipped with sieves with aperture sizes of 600, 425, 300, 212, 150 and 125 µm. The aperture size range was determined by the size of particles which would be suitable and amenable for fluidization. The particle size range was also classified using the Geldart classification chart. The coarse samples (+600 µm) were milled using the Sieb Technik Mill and were re-sized. Samples were weighed into 50 g sub-samples for the roasting step. Other sub-samples were subjected to chemical analysis using inductively coupled plasma optical emission spectroscopy as well as mineralogical analysis using X-Ray diffraction (XRD) and scanning electron microscopy coupled with energy dispersive spectroscopy (SEM-EDS). The equipment utilised is described in **Appendix A**.

3.5.2. HEAD SAMPLE CHARACTERIZATION

Characterization studies were conducted on both the Zandkopsdrift ore and the PyEarth ™ slag which served as head samples for the fluidized bed sulfation roasting studies. The characterization of the materials included SEM-EDS analysis for the identification and characterization of mineral and material phases as well as surface features. XRD analysis was

utilised for identification of the crystalline phases while ICP-OES was used for quantification and identification of the chemical elements present in the materials.

3.5.2.1. SEM-EDS Analysis

SEM-EDS analysis was conducted on sub-samples obtained from the milled ZKD ore and PyEarth ™slag materials. Polished sections, coated with carbon, were prepared for analysis by scanning electron microscopy (SEM). A Zeiss EVO Scanning Electron Microscope equipped with a Bruker Energy Dispersive Spectrometer was used to determine the mode of occurrence of the phases in the samples. Annotated back-scattered electron (BSE) images were acquired to show phases of interest, and the semi quantitative elemental composition of annotated phases were determined.

3.5.2.2. XRD Analysis

XRD was used to determine the bulk mineralogical composition and crystalline phases of the ZKD ore and the PyEarth ™ slag. The bulk mineralogical composition of each sample was determined using the Bruker X-Ray Diffraction. The XRD characterization was carried out using nickel-filtered Cu K_α radiation with a scanning speed of 2 seconds/step within a step size of 0.02° over 2 h. This was carried out on a Siemens D500 diffractometer equipped with an atomic emission technique. The XRD patterns were detected within the range of $2\theta = 4 - 80°$.

3.5.2.3. ICP-OES Analysis

ICP-OES analysis was conducted on the feed materials to identify and quantify the chemical elements present in materials. ICP-OES is the more preferred method as it can detect elements even at trace-levels. The method was used to determine the elemental composition (REEs, base metals, phosphorus, and radioactive elements such as uranium or thorium) of the materials.

3.5.3. ROTAMETER CALIBRATIONS

Gas flowrate plays a significant role in the fluidized sulfation roasting tests as it affects the fluidization mechanisms and the residence time of the sulfation process. The sulfation roasting process is conducted using a system of gases in calculated stoichiometric amounts. The gas composition in the system is controlled by using rotameters. Rotameters consist of plastic, metal, or glass tube with a float. The gas control on the rotameter is achieved as the gas enters

the reaction system by passing upwards through the rotameter, therefore allowing control and adjustment of the gas flow. The rotameters used in the study required calibration for the gases used in the fluidized bed sulfation roasting process prior to conducting the sulfation roasting tests.

3.5.3.1. Experimental Apparatus

The rotameters that were calibrated are shown in Figure 3.4. The measurement principle for the rotameters is in Appendix B. These rotameters are ABB Fischer and Porter Glass Tube VA Meters consisting of a ¼'' NPTF connection size with a scale length of 125 mm. Rotameter calibrations were conducted using a soap bubble meter setup shown in Figure 3.5. The soap bubble setup consists of a glass cylinder, with volume measurements, that is connected to a soap reservoir through an inlet pipe (where the soap solution is introduced). A stopwatch was also utilised in the calibration studies.

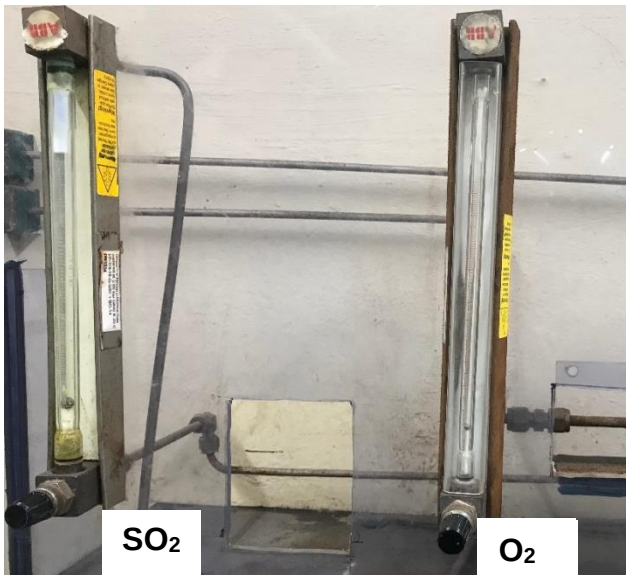


Figure 3.4. Picture of the ¼'' NPTF rotameters used for the sulfation roasting experiments.

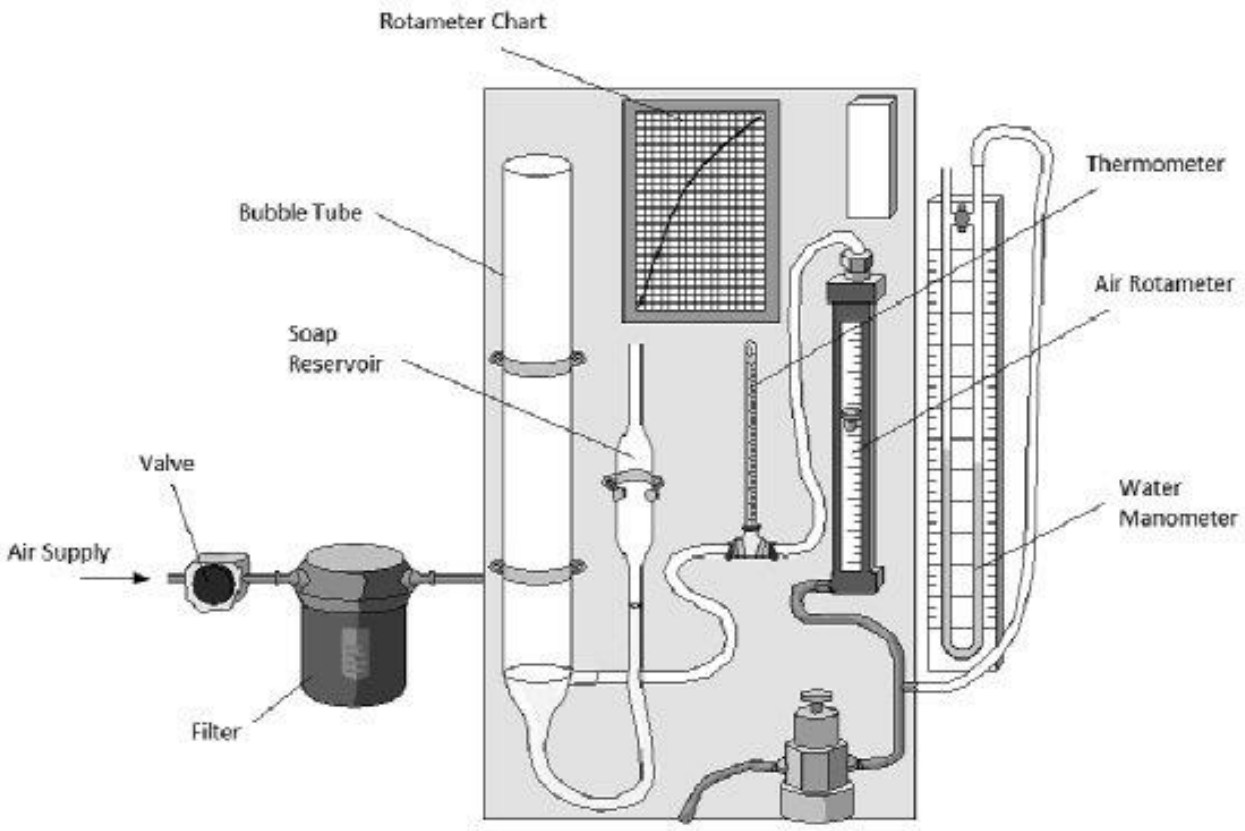


Figure 3.5. Schematic of the soap bubble meter setup.

3.5.3.2. Experimental Procedure

The soap water reservoir was used to produce bubbles. The bubbles produced were allowed to travel up the cylinder with volume measurements. The bubble speed was dependent on the rotameter setting, higher rotameter settings resulted in higher bubble speed and vice versa. The soap bubble meter setup was used to measure the gas volumetric flowrate by measuring the time that the bubble takes to travel from a starting point (A) to a final point (B) as a function of volume of the column. The gas pressure of the gas cylinder was kept at 200 kilopascals (kpa) for all three gases. The volume that the bubble travels was kept at 100 cm^3 for the rotameter setting from 0-8, and 300 cm^3 for rotameter setting 10-20. The calibrations were conducted for O_2 and N_2 rotameters.

Calibration readings were conducted a minimum of 3 times at every rotameter setting to obtain the average volume change (ΔV) and the average time (Δt) in seconds. The volumetric flowrate (Q) was calculated using the formula described in equation (3.1). The calibration calculations

were conducted to produce calibration curves which allow for the conversion between the rotameter setting and the actual gas flow rate and vice versa.

$$Q = \frac{\Delta(V_B - V_A)}{\Delta t} \quad (3.1)$$

A, B = reference marks on the tubes.

V_A = volume at point A (cm^3)

V_B = volume at point B (cm^3)

Δt = bubble travel time from point A to point B (seconds)

SO_2 calibrations using the soap bubble method were unsuccessful as the SO_2 gas was reacting with the soap. The soap was sodium hydroxide (NaOH) based, thus it produced sodium sulfite and water, according to the reaction described by equation (3.2).

$$SO_2 + 2NaOH \rightarrow Na_2SO_3 + H_2O \quad (3.2)$$

The calibration curve for the SO_2 gas was calculated using the calibration curve of chlorine gas as the same rotameter was used during the tests. The conversion was conducted using the specific gravities (SG) of the two gases (SO_2 and Cl_2). At every selected point on the Cl_2 calibration curve the volumetric flowrate for the Cl_2 was multiplied by the factor obtained from dividing the SG of SO_2 gas and the SG of Cl_2 (described by equation 3.3 and 3.4) to obtain the new points for the SO_2 calibration curve.

$$\frac{SG_{SO_2}}{SG_{Cl_2}} = \frac{Q_{SO_2}}{Q_{Cl_2}} \quad (3.3)$$

$$\therefore Q_{SO_2} = \frac{SG_{SO_2}}{SG_{Cl_2}} \times Q_{Cl_2} \quad (3.4)$$

Rotameter conversion curves produced from the rotameter calibration tests are shown in Figure 3.6 and 3.7. These curves are useful in determining the gas flowrate utilised when using rotameters to control the gas.

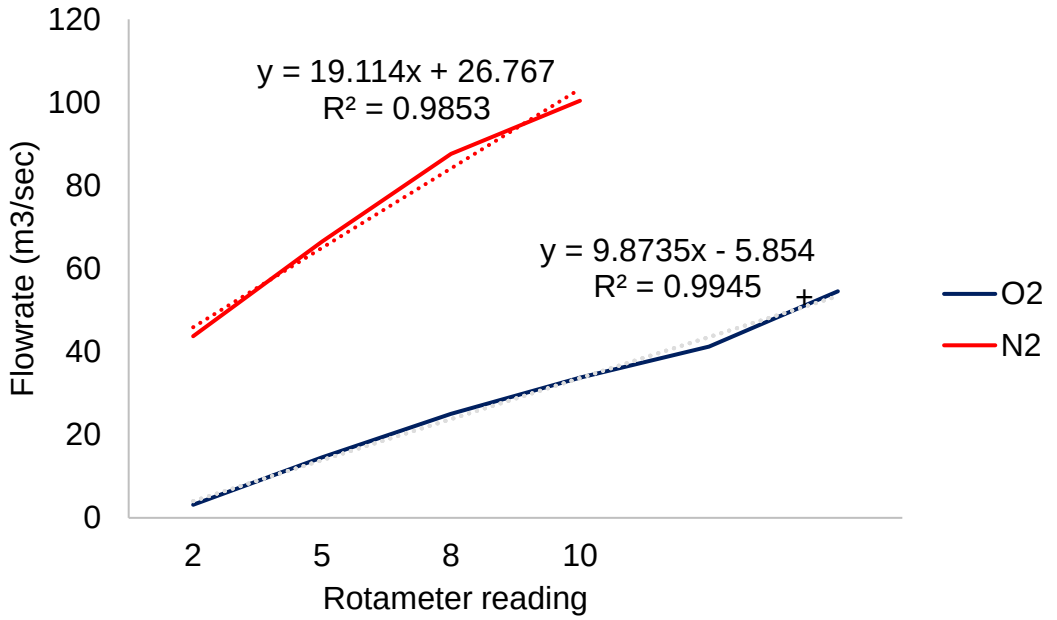


Figure 3.6. Calibration curve for oxygen and nitrogen gas rotameters.

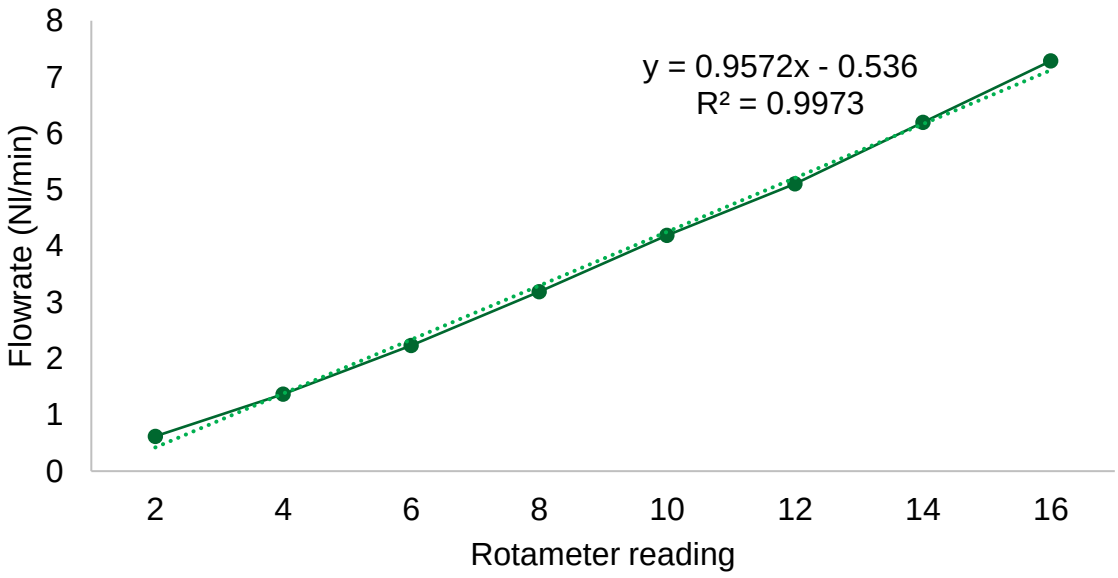


Figure 3.7. Calibration curve for the sulfur dioxide rotameter.

3.5.4. FLUIDIZATION STUDIES

Fluidization studies (cold tests and elutriation tests) were conducted on the head samples, i.e. ZKD ore and PyEarth ™ slag because these materials have different bulk densities. Particles become fluidized when the gas velocity is high enough that the drag force on the particles equals the weight of the particles. This point is commonly referred to as the minimum

fluidization velocity (U_{mf}). The minimum velocity can be determined through theoretical calculations or through a series of cold tests. Cold fluidization tests are also conducted on the different materials to determine the elutriation rate constants.

Elutriation is the process by which fine particles are carried out of the fluidized bed by the upward fluid flow as the fluid passes through the bed. The elutriation rates affect the particle residence time which in turn affects the efficiency of the process. This, therefore, makes it important to compare blow over behaviours of the different feed materials prior to the sulfation roasting tests. The carryover is measured using elutriation constants (k_i^*) that are determined during batch fluidization experiments. The elutriation constant can be calculated using equation 3.5 if the particle size distribution of the initial and final bed is known.

$$\frac{W_i}{W_{io}} = \exp\left(-\frac{k_i^* A t}{W}\right) \quad (3.5)$$

W_{io} = Initial weight of mass fraction i
W_i = Final weight of mass fraction i
W = Total weight of sample before fluidization
A = Area of reactor (m^2)
t = Time (s)
K_i^* = Elutriation constant (kg/m^2. s)

3.5.4.1. Experimental Apparatus

Fluidization tests were conducted using a vertical quartz tube reactor (i.e. 895 mm height and 36 mm diameter), shown in Figure 3.8. The reactor consists of a silica-based porous distributor plate that divides the quartz reactor into two zones, a lower region where the gases enter and an upper region where the gases escape. The reactor was connected to a collection flask. N_2 gas was used as the fluidizing agent in the cold tests and its flowrate was controlled by rotameters.

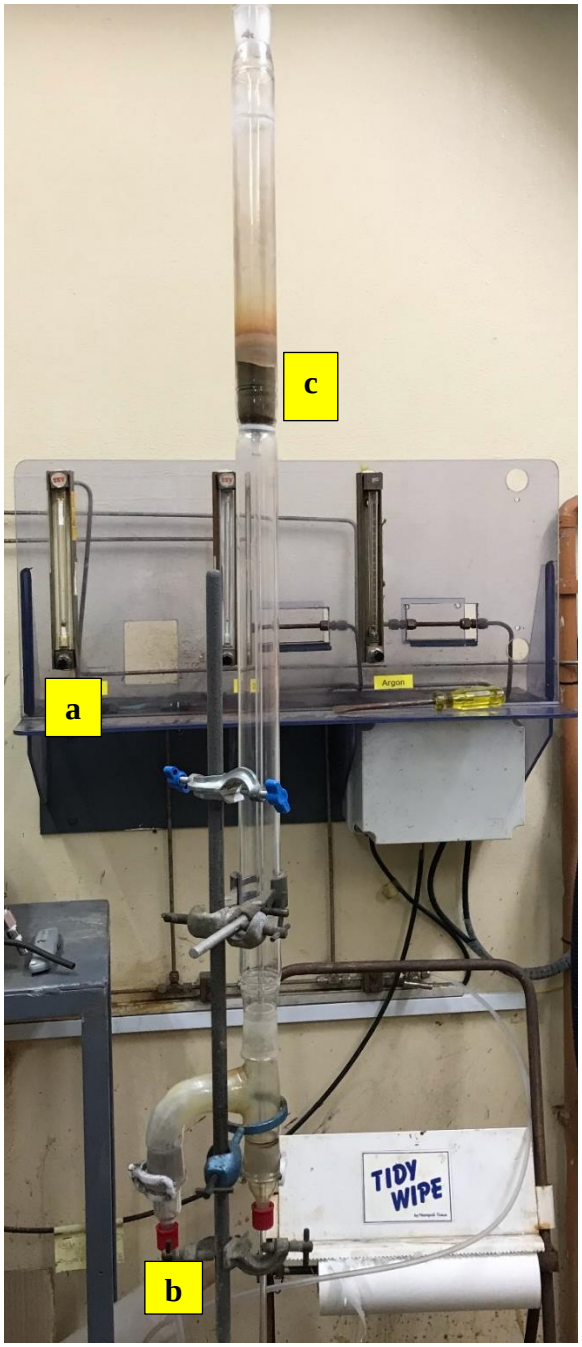


Figure 3.8. Visual representation of the cold test setup consisting of (a) rotameters for control of gas flow, (b) gas inlet and (c) the material lying on the porous bed.

3.5.4.2. Experimental Procedure

3.5.4.2.1. Cold N_2 Tests

A mass of 50 g of the sample was placed onto the distributor plate of the quartz reactor. The reactor was connected to the collecting flask. N_2 gas was introduced into the reactor at different rotameter settings until the material was observed to be fluidized. The volumetric flowrate at

the inception of fluidization was recorded and the minimum velocity was calculated using equation (3.6).

$$Q = \text{cross sectional area} \times \text{velocity}$$

$$Q = (\pi \times r^2) \times U_{mf}$$

$$\therefore U_{mf} = \frac{Q}{(\pi \times r^2)} \quad (3.6)$$

3.5.4.2.2. Elutriation Studies

Elutriation studies were conducted using 50 g samples that were poured onto the distributor plate in the reactor. The collection system was connected to the reactor prior to switching on the gas. The material was fluidized for 1 h using N_2 and the volume flowrates were obtained from the cold tests. After the time had elapsed, the remaining bed sample and elutriated fines were collected, weighed, and screened. Screen sizes 600, 425, 300, 212, 150 and 106 µm were used for the determination of the particle size distribution.

3.5.5. SULFATION ROASTING STUDIES

Fluidized sulfation roasting and leaching tests were conducted on two industrial REE-bearing materials (ZKD ore and PyEarth ™ slag) to investigate the applicability of the sulfation roasting process on real REE resources.

3.5.5.1. Fluidization Sulfation Roasting Studies

3.5.5.1.1. Experimental Apparatus

The fluidized bed reactor setup located at Mintek was used for the sulfation roasting experiments. The reactor setup consisted of a quartz tube reactor, furnace, K-type thermocouple, crossover L-tube, a condenser, blow-over collector flask, off gas duct that is connected to the scrubber system illustrated in Figure 3.9. For the sulfation roasting experiments, the quartz reactor (895 mm height and 36 mm diameter) was placed vertically in an electrically heated furnace shown in Figure 3.10. The sample in the reactor was heated using the heating elements in the furnace. The heating of the furnace and the heating rate was setup using a controller. The reactor contains a porous silica distributor plate which serves the

function of supporting the charge and allowing even distribution for the sulfation roasting gases and fluidization of the sample bed. The gas flow (i.e. SO_2, O_2 and N_2) was controlled by rotameters and the minimum fluidization velocity was kept at 9.9 cm/s and 23.9 cm/s for the ZKD ore and the PyEarth ™ slag, respectively. The flowrates of SO_2, O_2 and N_2 were maintained at the flowrates summarized in Table 3.6. The total gas pressure inside the fluid bed reactor was approximately 200 kPa and the partial pressure of SO_2 gas in the fluid bed reactor was kept constant at approximately 64 kPa.

Table 3.6. Summary of rotameter gas settings for sulfation roasting experiments.

Gas flowrate (l/min)		**SO_2**	**O_2**	**N_2**
ZKD Ore	**O_2 Rich**	1.9	1.0	3.2
	O_2 depleted	1.9	-	4.1
PyEarth ™ Slag	**O_2 Rich**	4.7	2.3	7.6
	O_2 depleted	4.7	-	9.9

The temperature of the sample bed was controlled by a K-type thermocouple, connected to a data logger that was protruding through the sample bed. The L-tube was used to allow for flow of the product gases from the quartz reactor through to the condenser and into the round bottomed flask where the solids and condensed gases settled out. The gases were passed into the scrubber setup through an extraction system connected to the condenser and round flask by a scrubber system, setup shown in Appendix C.

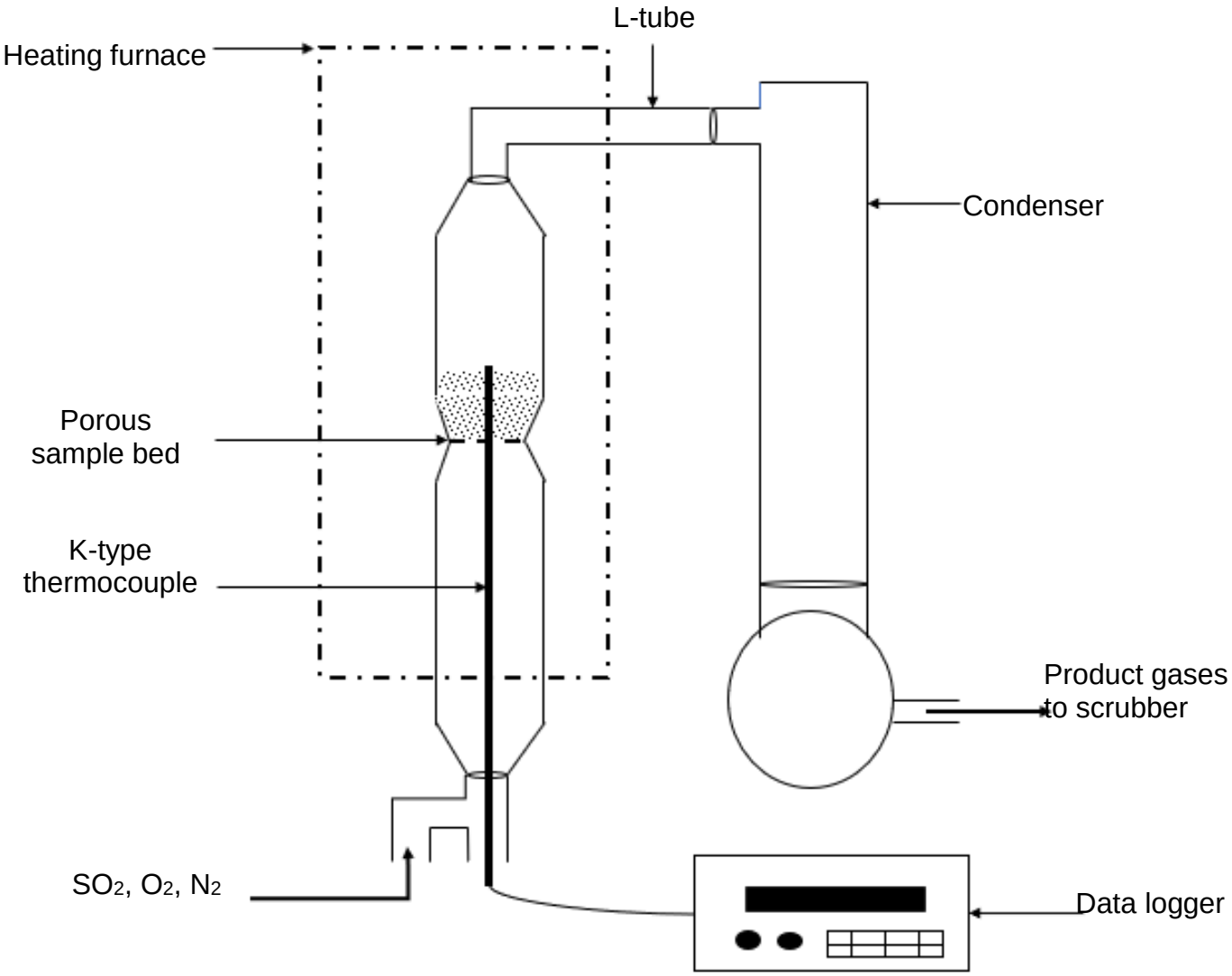


Figure 3.9. Schematic of sulfation roasting experimental setup.



Figure 3.10. A picture of the sulfation roasting experiments furnace and reactor setup.

3.5.5.1.2. Experimental Procedure

Head samples (-600 + 125 µm) were split into 50 g sub-samples for the sulfation roasting experiments. The particle size was chosen to avoid blow over during fluidization. The 50 g sample was loaded into the reactor and onto the distributor plate. The loaded reactor was placed vertically in the furnace and the L-tube, condenser, round bottom flask and the extraction system were connected. N_2 gas was used to fluidize the sample during the heat up period. A heating rate of 10°C/min was utilised to reach the desired operation temperature in the furnace. Once the furnace and the sample bed had reached the desired operation temperature, the N_2 air flow was reduced to the calculated ratio and SO_2 (32%) was introduced into the system. O_2, when required, was introduced into the system after introducing SO_2 to avoid temperature spikes in the reactor. The introduction of SO_2 and/or O_2 marked the start of the experiment. The sulfation roasting tests and conditions are summarized in Table 3.7.

Once the test duration was reached, the SO_2 and O_2 flow were switched off and the sample was cooled down in a N_2 atmosphere. The remaining bed sample was removed once the furnace and reactor reached room temperature. These samples were weighed and subjected to chemical

analysis by ICP-OES. Mineralogical studies were conducted on the roast bed samples to identify the main phases present, i.e. the main REE-bearing phases and the major gangue metal phases after sulfation roasting. X-ray diffraction was utilised to determine the bulk modal mineralogy in the roasted samples, while the Scanning Electron Microscope was used to determine the mode of occurrences of the REE and Fe-bearing minerals in both the roasted ZKD ore and PyEarth ™ slag bed samples.

Table 3.7. Sulfation roasting experiment test plan.

Test No.	Material	Gas Composition	Reaction time (hours)	Temperature (°C)
1	ZKD Ore	32% SO_2 + 68% N_2	1	600
2				700
3				800
4		32% SO_2 + 16% O_2 + 52% N_2		600
5				700
6				800
7		32% SO_2 + 68% N_2	4	600
8				700
9				800
10		32% SO_2 + 16% O_2 + 52% N_2		600
11				700
12				800
13		32% SO_2 + 68% N_2	8	600
14				700
15				800
16		32% SO_2 + 16% O_2 + 52% N_2		600
17				700
18				800
19	PyEarth ™ Slag	32% SO_2 + 68% N_2	1	700
20			4	
21			8	
22		32% SO_2 + 16% O_2 + 52% N_2	1	
23			4	
24			8	

3.5.5.2. Leaching

3.5.5.2.1. Experimental Apparatus

Leaching experiments were conducted using 250 mL Erlenmeyer flasks which were placed into a shaking water bath with holders, Figure 3.11. The shaking bath had temperature and agitation speed controls. The pH was measured using a benchtop pH meter. A Buchner funnel filtration setup was used to filter the slurry, and an oven was used to dry the residues

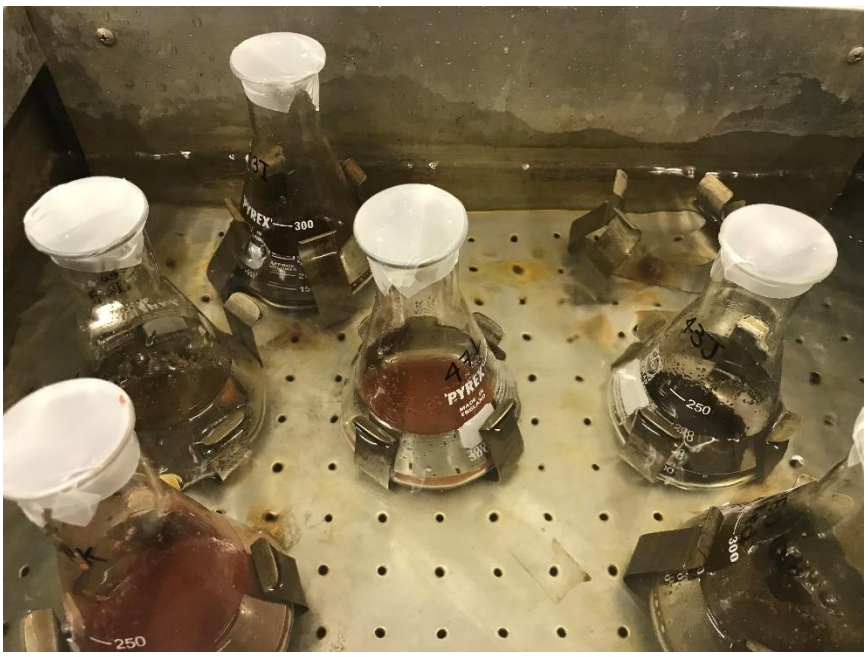


Figure 3.11. A picture of the shaking bath and Erlenmeyer flasks containing the leach slurries.

3.5.5.2.2. Experimental Procedure

Leaching experiments were conducted on the roasted ZKD ore and PyEarth ™ slag samples to study the effect of the sulfation roasting time, temperature, and gas composition on the leaching efficiency of the targeted LREEs (Ce, La, Nd and Pr) and on the Fe. The test work involved leaching 8 g of sulfated ZKD ore material in 40 mL deionized water and 3 g of sulfated PyEarth ™ slag samples in 15 mL of deionized water. The pH of the system was adjusted to a range of 3–4 using 1M sulfuric acid solution at the beginning of the experiments. The roasted sample and deionized water were transferred into 250 mL glass Erlenmeyer flasks and covered using parafilm to reduce the effect of evaporation. The flasks were placed in a shaking water bath that was equipped with temperature and agitation controls. The tests were conducted at 25°C for 24 hours as guided by literature (Borra et al., 2015). A solid: liquid ratio of 1:5 was maintained throughout the study. The agitation of the shaking bath was kept at 140 rpm during

the study. At the end of the test, the pH of the slurries was measured and recorded. The slurries were filtered in a vacuum filtration unit. Syringe filters were also utilised for further filtration as the material contained fines after leaching. The residue was dried at 50°C for 8 hours in an oven. The mass of the residue and the volume of the filtrate were recorded, and the residue was subjected to chemical analysis. The test plan for the leaching conditions is summarized in Table 3.8.

- The safety, health and environmental procedures followed in the study are attached in Appendix D.

Table 3.8. Summary of the ZKD ore leaching studies.

Test No.	Gas Composition	Material	Reaction Time (hours)
1	32% SO_2 + 68% N_2	ZKD Ore	Time = 24 hours Temperature =25°C Solid: Liquid Ratio = 1:5 Agitation Speed= 140 rpm
2			
3			
4	32% SO_2 + 16% O_2 + 52% N_2		
5			
6			
7	32% SO_2 + 68% N_2		
8			
9			
10	32% SO_2 + 16% O_2 + 52% N_2		
11			
12			
13	32% SO_2 + 68% N_2		
14			
15			
16	32% SO_2 + 16% O_2 + 52% N_2		
17			
18			
19	32% SO_2 + 68% N_2	PyEarth ™ Slag	
20			
21			
22	32% SO_2 + 16% O_2 + 52% N_2		
23			
24			

4. PRELIMINARY SULFATION ROASTING RESULTS

4.1. INTRODUCTION

A series of preliminary tests were conducted to investigate the suitable thermal and operational conditions of the sulfation roasting process for the extraction of LREEs. The investigation consisted of thermochemical calculations, stationary bed sulfation roasting tests, stability, and leaching tests. Stationary sulfation roasting tests were conducted to determine suitable conditions for fluidized sulfation roasting. Parameters investigated in the study included the sulfation temperature and residence time.

4.2. THERMOCHEMICAL CALCULATIONS

Thermochemical calculations were conducted for temperatures between 600°C and 800°C for the LREEs (cerium, lanthanum, praseodymium, and neodymium) and Fe in a sulfur dioxide (SO_2) – oxygen (O_2) gas system. The LREEs are the target metals, while Fe is the major gangue metal in the ZKD ore feed material. Predominance phase diagrams were produced for 1- and 2-metal systems to determine the stable phases present during sulfation roasting as a guide to determine the suitable roasting conditions.

4.2.1. One Metal – SO_2 – O_2 Calculations

Figure 4.1 shows the predominance phase diagrams for the Ce-S-O_2 system calculated at 630°C, 700°C, 750°C and 800°C. The axes on the diagram are the logarithms of the partial pressures of SO_2 and O_2 in the gas phase. The predominance phase diagram is divided into areas or domains of stability of the various solid compounds of the metal, S and O. The conditions for coexistence of two and three solid phases are indicated by the lines and triple points on the diagram (Pelton, 2014). LREEs are chemically similar and are expected to result in similar trends with respect to the predominance phase diagrams. Therefore, discussion of these diagrams was predominantly based on the Ce-S-O_2 system.

The diagram showed that Ce can exist as a stable sulfate phase, $Ce_2(SO_4)_3$, at all the sulfation temperatures. This indicates that sulfation of Ce is possible at these isothermal temperatures. Figure 4.1 also shows that the stable Ce sulfate phase occurs over a wide range of SO_2 - O_2 partial pressures for all the isothermal calculations. The diagrams also show that CeO_2 is stable

over a wide range of SO_2 - O_2 partial pressures for all calculated temperatures. An increase in temperature results in a shift in the stable $Ce_2(SO_4)_3$ phase, to higher O_2 partial pressures, as new Ce sulfide phases are introduced.

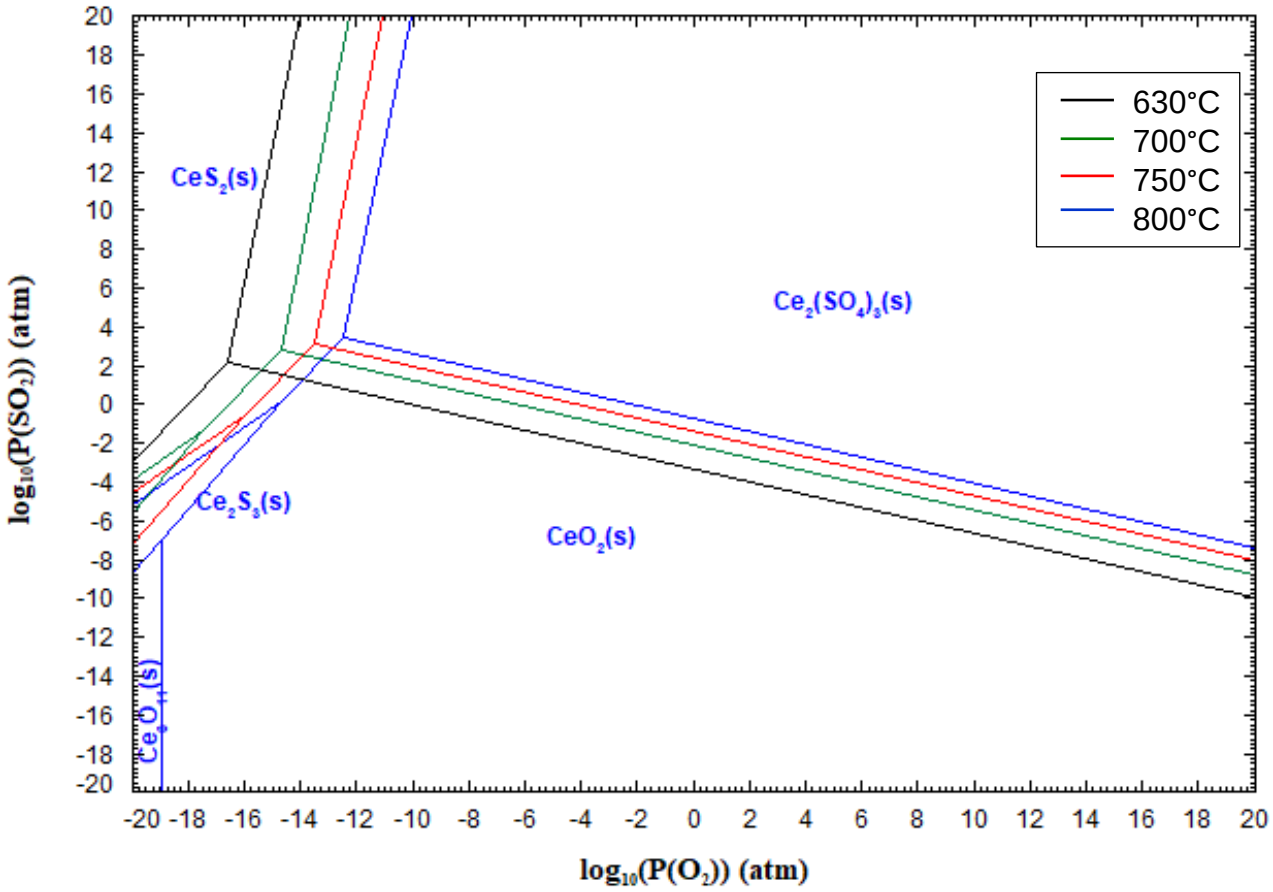


Figure 4.1. Predominance diagram for Ce–O–S system at temperatures between 630°C and 800°C.

A similar trend was observed for La and Nd, Appendix E. However thermochemical calculations for praseodymium (Pr), shown in Figure 4.2, resulted in a different trend. According to this diagram, Pr does not exist as a stable sulfate at all the roasting temperatures, instead it was calculated to exist as oxide and sulfide compounds. This predicted behaviour contradicts what has been observed in literature with Pr being part of the REEs that form sulfates at temperatures between 200°C and 900°C (Teixeira et al., 2019). Further investigations into the FactSage © software database showed that the software does not contain thermochemical data for Pr-sulfates in solid phases. The software can conduct calculations for Pr-sulfates in aqueous systems as it contains thermochemical data for these compounds in these phases. This highlights some of the limitations of the PREDOM mode on FactSage ©.

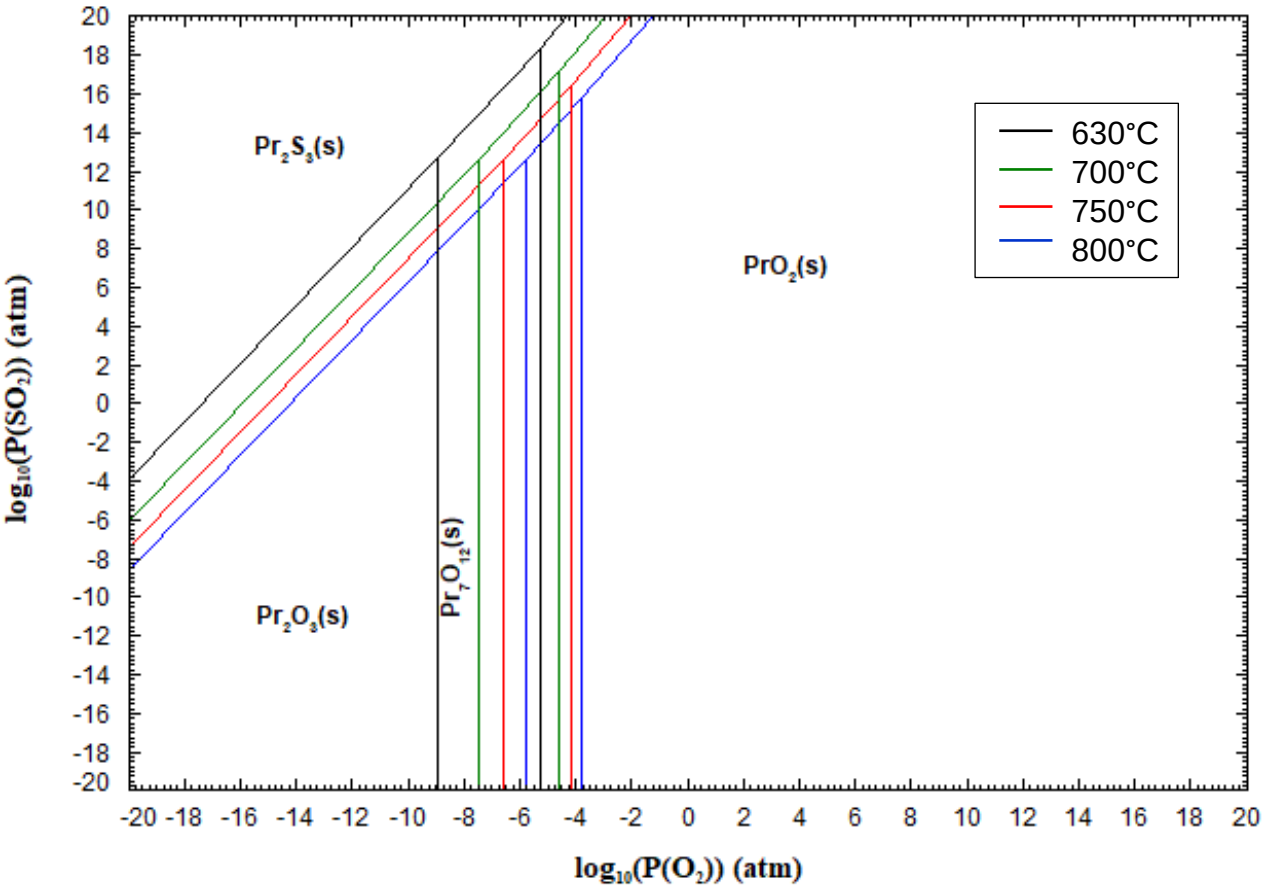


Figure 4.2. Predominance diagram for Pr–O–S system at temperatures between 630°C and 800°C.

4.2.2. Two Metal-SO_2 – O_2 Calculations

The sulfation roasting process is attractive as it allows for selective conversion of targeted metals through the manipulation of operational parameters such as temperature and gas composition. The roasting temperature can be used for selectivity by choosing a temperature where targeted metal sulfates are stable while those of the major gangue constituents decompose into their respective metal oxides. The selection of the temperature is based on thermodynamic data and calculations of diagrams such as the predominance phase diagrams. 2–metal–SO_2–O_2 predominance phase diagrams have been utilised to predict whether selectivity is achievable, and at which conditions this selectivity can be attained.

Predominance phase diagrams were calculated for Ce–Fe–SO_2–O_2 systems at temperatures between 600°C and 800°C and the results are described in Figure 4.3 to 4.5. These diagrams were calculated to predict the suitable roasting temperatures where cerium exists as a metal sulfate, while maintaining iron in its oxide form. This information was important for sulfation of REE-bearing materials that have significant amounts of Fe, such as the Zandkopsdrift ore

from South Africa Figure 4.3 to 4.5 show that both Ce and Fe can exist as stable metal sulfates, metal sulfides and/ or metal oxides and that there is only a narrow region that exists where where Ce exists as a sulfate while maintaining Fe in its oxide or sulfide phases. According to the predominance phase diagrams selective roasting of REEs in a material containing high Fe concentrations would only be possible at high SO_2 partial pressures, where Ce is in the form of $Ce_2(SO_4)_3$ and Fe is in the form of FeS_2.

These thermochemical calculations highlighted some of the limitations associated with using predominance phase diagrams to select suitable roasting conditions for selectivity. The diagrams only describe phases that exist under equilibrium conditions and do not consider the kinetics of these phases. Therefore, a particular phase that is described in the phase diagram may have slow rates of reactions and may not be formed under specific conditions investigated. The diagrams are also calculated outside of external factors such as reaction time, phase composition of the feed and the heating rates during the process. Therefore, the indication of when the phases form or decompose requires additional knowledge from thermodynamic data and diagrams such as thermal stability and Gibbs free energy diagrams.

The PREDOM mode can only calculate a maximum of 3-metal systems even though many materials might contain multiple metals that might interact or take part in reactions during the roasting process. The other significant limitation is that the Predom module accesses compound databases and not solution databases. This is a significant limitation considering that REEs are defined as “elements with similar chemical properties” there is a possibility of the formation of solution sulfate phases.

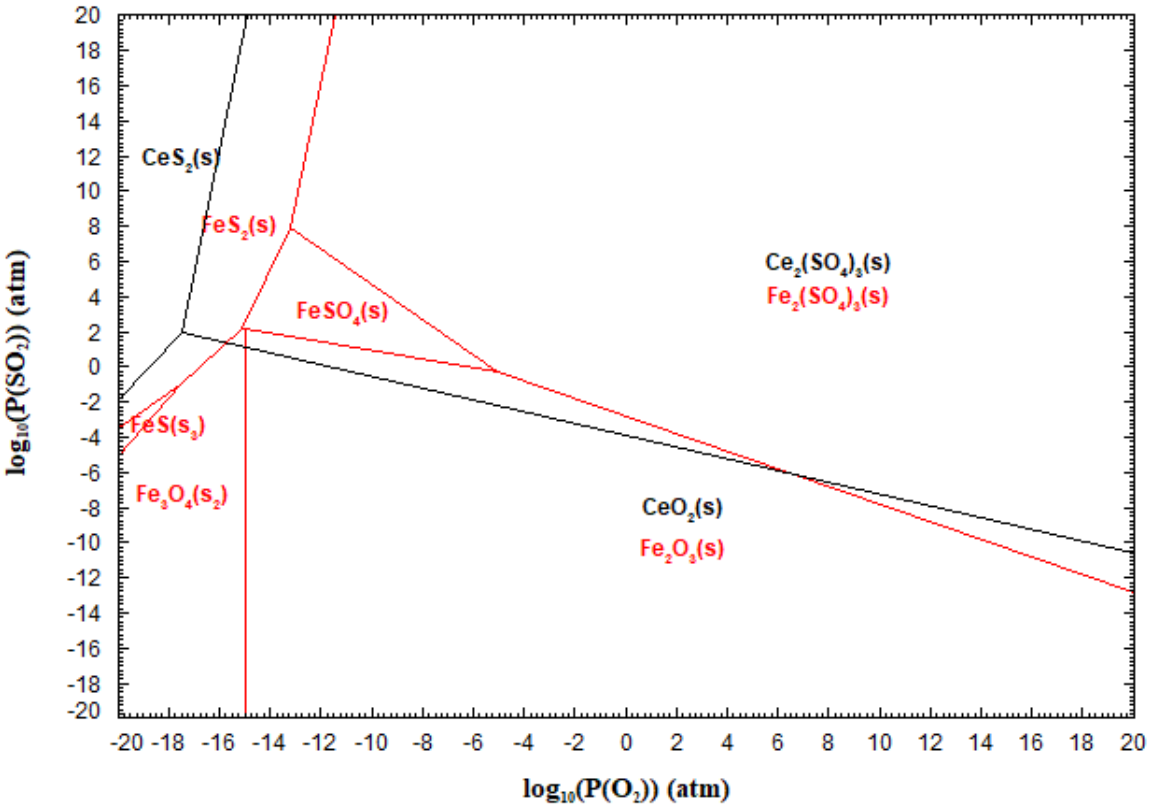


Figure 4.3. Predominance diagram for Ce-Fe–O–S system at 600°C.

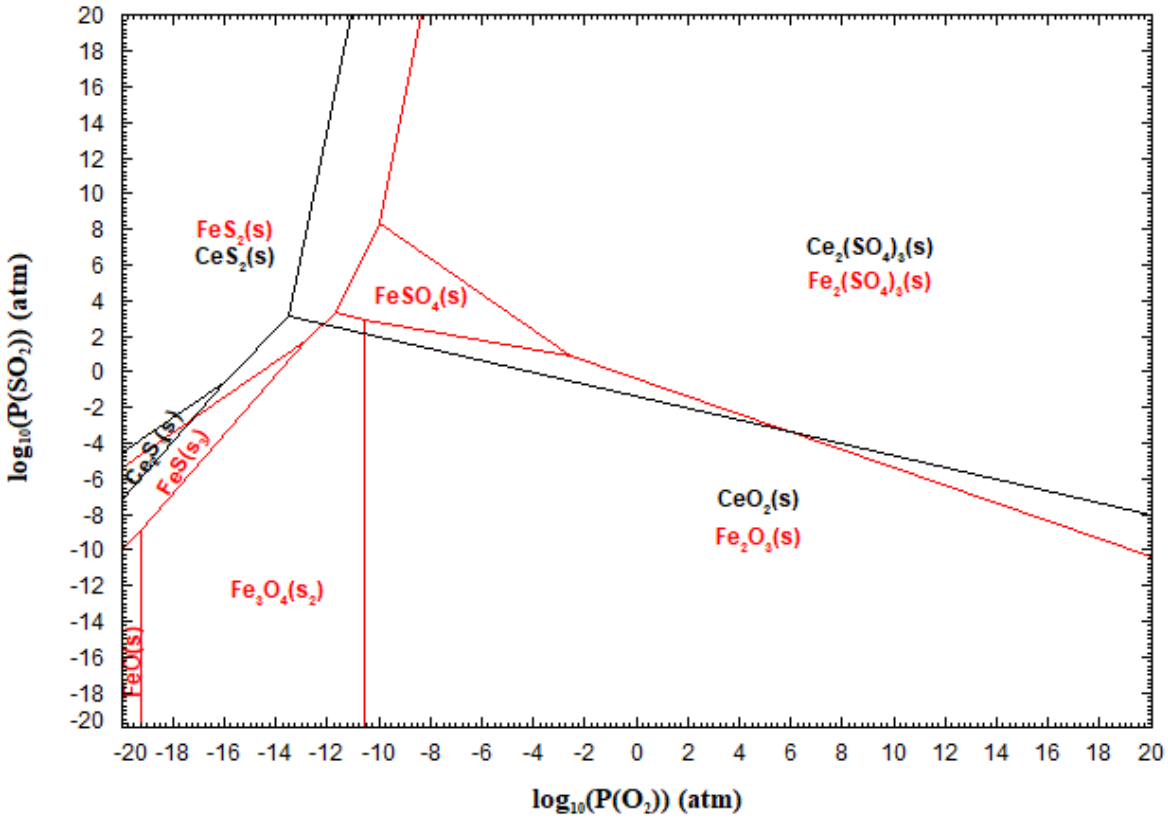


Figure 4.4. Predominance diagram for Ce-Fe–O–S system at 750°C.

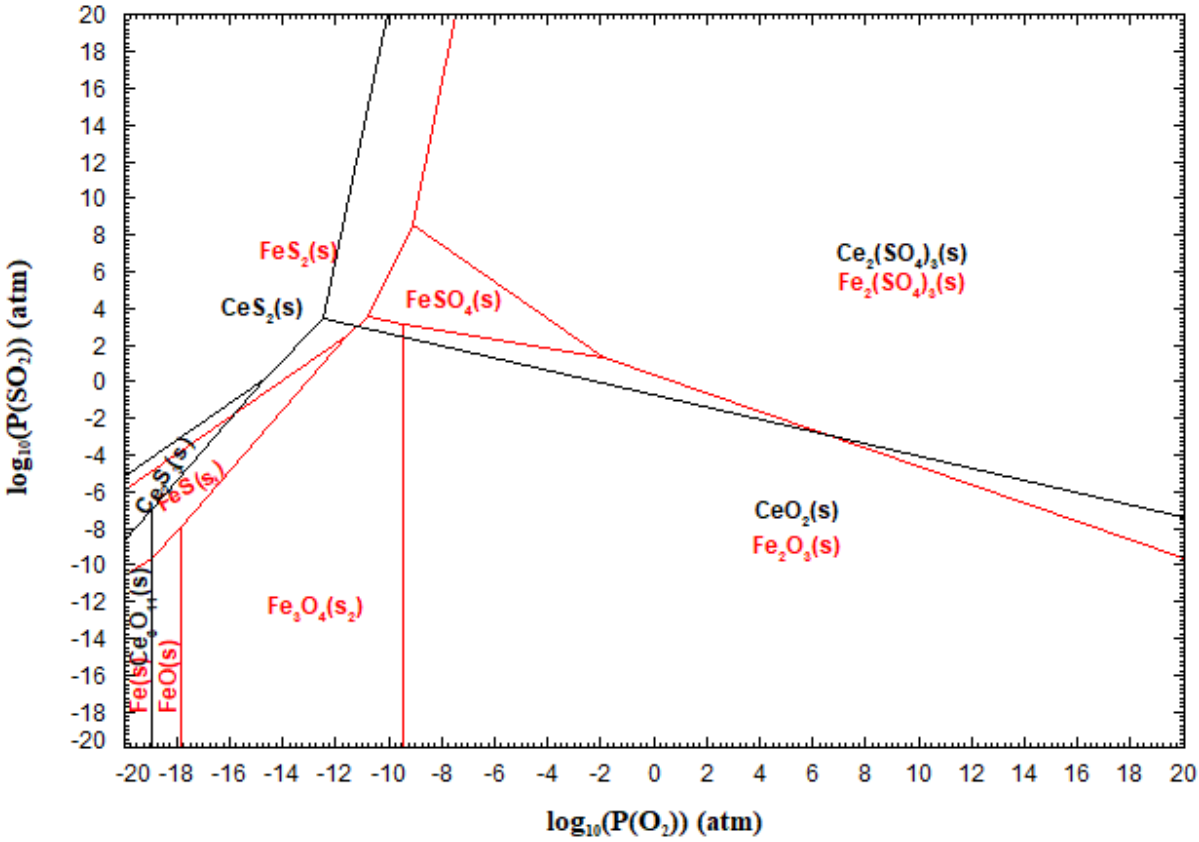


Figure 4.5. Predominance diagram for Ce-Fe–O–S system at 800°C.

4.3. MASS CHANGE EVALUATION

Mass change calculations were conducted on the roast products to determine the occurrence or lack thereof of sulfation of the synthetic cerium oxide. A positive mass change indicates the sulfation of oxides, whereas a negative mass change is an indication of the decomposition of sulfate and/ or oxide phases. The mass changes as a result of the sulfation roasting of the synthetic CeO_2 are presented in **Error! Reference source not found.**.

The net mass change for the sulfation of synthetic CeO_2, Test 1 to 8, was found to be consistently positive suggesting that sulfation of the cerium oxide occurred under these roasting conditions. The net mass changes were found to be lower at lower roasting temperatures and shorter roasting times. The highest net mass change was obtained at 750°C, for both 24 hour and 48 hour periods therefore suggesting that this is the best temperature for sulfation of CeO_2. However, to investigate the selectivity of the roasting process, stability tests including major gangue metal sulfates needed to be evaluated at this temperature, discussed in section 4.4.

The results obtained for temperatures between 630°C and 750°C deviated from observations reported in literature by Tagawa. (1984) and Gmelin. (1978) who indicated that cerium sulfates start decomposing at temperatures of 666°C and 700°C. A decrease in mass change was observed at roasting temperatures of 800°C for both roasting times. A similar trend in results was reported by Poston et al. (2003), where the prevalent phase present after roasting cerium (III) sulfate and cerium (IV) sulfate at 800°C was CeO_2, therefore indicating decomposition of cerium sulfates at this temperature.

The mass change results also showed that the sulfation of CeO_2 is dependent on both roasting temperature and time. The effect of time on the mass change deviated from common roasting trends, where prolonged roasting times are known to destabilize the metal sulfates therefore resulting in lower mass changes. This was only true for tests conducted at 800°C, where the mass change observed was lower for tests conducted for 48 hours. At the other roasting temperatures, the mass changes reported for tests conducted for 48 hours were higher than the ones obtained for tests conducted for 24 hours. This therefore indicated that roasting duration had a bigger impact on metal sulfate stability as compared to the roasting temperature.

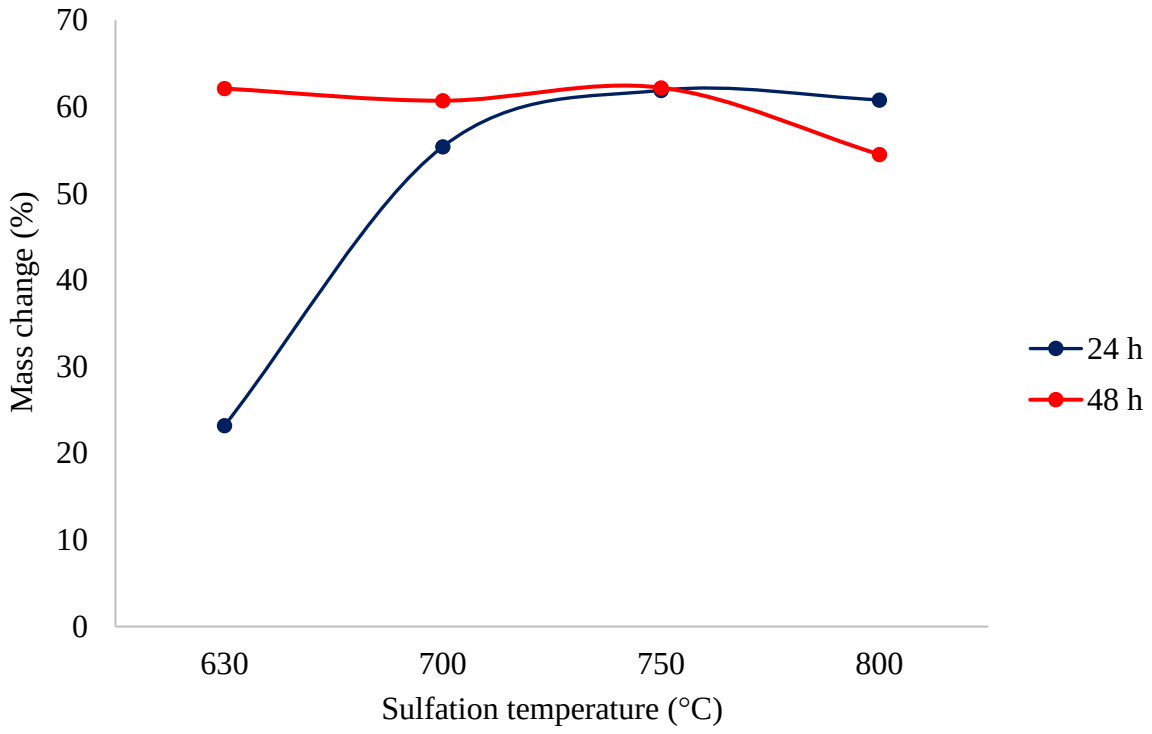


Figure 4.6. Graphical representation of mass changes for the sulfation of synthetic CeO_2 at different sulfation temperatures.

4.4. MINERALOGICAL CHARACTERIZATION

XRD characterization of the roast products was conducted to determine the products formed during the sulfation roasting process. A summary of the phase chemical compositions of the sulfated synthetic CeO_2, is presented in Table 4.1. The phases are listed in order of decreasing abundance, i.e., the most abundant is recorded first. The characterization results showed the formation of cerium oxy-sulfate ($CeOSO_4$) and not a complete sulfate as predicted by FactSage. The formation of the oxy-sulfate phase was attributed to the prolonged roasting durations utilised in the study which are known to result in metal sulfate instabilities, resulting in decomposition of sulfate phases to form oxy-sulfates and/or oxides. The cerium oxy-sulfate phase was the prevalent phase at all the sulfation conditions investigated. $CeOSO_4$ was the only phase present for roasting tests conducted at 700°C for both 24 and 48 hours. The CeO_2 phase was also detected in tests conducted at 630°C, 750°C and 800°C for both roasting durations. The presence of $CeOSO_4$ and CeO_2 phases are an indication of the decomposition of cerium (IV) sulfate, $Ce(SO_4)_2$, which occurs at approximately 600°C (Poston et al., 2003). The phases detected at 700°C, 750°C and 800°C are contrary to what is reported by Poston et al. (2003), who indicated that only CeO_2 exists at these temperatures as presented in Table 4.2. These observations were strongly attributed to the prolonged roasting times utilised in the study.

Table 4.1. Summary of the phase chemical compositions of the sulfated CeO_2.

Temperature (°C)	REE products after 24 hours (order of decreasing abundance)	REE products after 48 hours (order of decreasing abundance)
630	$CeOSO_4$, CeO_2	$CeOSO_4$, CeO_2
700	$CeOSO_4$	$CeOSO_4$
750	$CeOSO_4$, CeO_2	$CeOSO_4$, CeO_2
800	$CeOSO_4$, CeO_2	$CeOSO_4$, CeO_2

According to the mineralogical analysis, the best suitable roasting temperature for sulfation of CeO_2 is 700°C because the CeO_2 phase was not detected. This contradicts what was observed from the mass change calculations, where the highest mass changes were obtained at a roasting temperature of 750°C for both roasting times. The difference between the mass changes obtained at 700°C and those obtained at 750°C were minute therefore indicating that optimal sulfation roasting for LREEs can be achieved at temperatures between 700°C and 800°C.

Table 4.2. X-Ray Diffraction results of various cerium sulfate materials at different temperatures (extracted from Poston et al., 2003).

Compound Temperature (°C)	Cerium (III) sulfate	Cerium (IV) sulfate
600	$Ce_2(SO_4)_3 > Ce_2O_3 > Ce_6O_{11} > Ce_2O_2S_2$	$CeOSO_4$
650	$CeOSO_4$, $Ce_2(SO_4)_3$, CeO_2	$CeOSO_4$
700	$Ce_2(SO_4)_3$, CeO_2, > $Ce_2(SO_4)_3$	CeO_2
750	$CeOSO_4$, CeO_2	CeO_2
800	CeO_2	CeO_2

4.5. METAL SULFATE STABILITY TESTS

Stability sulfation roasting tests were conducted using hydrated $Ce_2(SO4)_3$ and $Fe_2(SO_4)_3$ at 750°C for 24 hours. These tests were conducted to investigate the stability of the formed sulfates at 750°C, where the highest mass change was observed during the sulfation of synthetic CeO_2. Stability tests were also conducted to investigate the behaviour of the formed metal sulfates under sulfation conditions. These tests were important as they were used to predict whether selectivity using the sulfation roasting process was possible. South African resources such as the ZKD ore are known to be associated with high Fe amounts and therefore the behaviour of Fe sulfates is required. The selectivity would be indicated by the presence of predominantly Ce-sulfates, while the Fe is present as an oxide or sulfide compound.

The mass change results for the stability tests are summarized in Table 4.3. The test resulted in a negative net mass change. This was due to the dehydration of Ce- and Fe- hydrated sulfates as well as the decomposition of $Fe_2(SO_4)_3$ to Fe oxide and $Ce_2(SO4)_3$ to oxysulfates and/or oxides. This behaviour was expected because the roasting temperature utilised in the test was higher than the decomposition temperature of both Fe and Ce sulfates as indicated in Table 4.4.

These results were further verified through XRD characterization of the roast products to determine the phases present. XRD analysis showed that the roast product contained $CeOSO_4$, Fe_2O_3, and $Fe_2(SO_4)_3$ in order of decreasing abundance. The presence of $CeOSO_4$ and Fe_2O_3 phases in the roast products indicate that the metal sulfates that are formed during the sulfation roasting study are not stable under these roasting conditions. The prolonged roasting times also play a role in the destabilization of the metal sulfates and therefore shorter roasting periods were investigated in the fluidized roasting studies. The stability results also indicate that selective sulfation can be achieved during roasting as the Fe exists predominantly as Fe_2O_3, while Ce exists as an oxysulfate with no detection of Ce oxides. These results further indicate

the limitation of the thermochemical calculations as the predominance phase diagrams only indicated that Fe and Ce can exist as sulfates, oxides or sulfides at these temperatures.

Table 4.3. Summary of the mass changes for the stability tests and the sulfation of the REE-bearing ore.

Material	Operational temperature (°C)	Roasting time (hours)	Mass change (%)
$Ce_2(SO4)_3$- $Fe_2(SO_4)_3$	750	24	-29.0

Table 4.4. Stability of metal sulfates of interest

Compound	Onset of thermal decomposition (°C)	Heating rate (°C/min)	Source
Iron (III) sulfate	545	5	Tagawa, 1984
Cerium (III) sulfate	666 700	5 -	Tagawa, 1984 Gmelin, 1978
Neodymium (III) sulfate	800	1.5	Gmelin, 1978
Lanthanum (III) sulfate	840	2.5	Gmelin, 1978

4.6. LEACHING OF ROAST PRODUCTS

Leaching tests were conducted on the roast products obtained from stationary sulfation studies of synthetic CeO_2 to quantify the sulfation efficiency of Ce as a function of roasting temperature and time.

Results obtained to investigate the effect of sulfation roasting temperature and time on the extraction of Ce are presented in Figure 4.7. Higher Ce extractions were obtained for sulfation roasting tests conducted for 24 hours than those at 48 hours at temperatures below 800°C. This therefore indicates that the sulfation of CeO_2 is dependent on both the roasting temperature and time. The results also showed that prolonged roasting times have a negative effect on the stability of the formed metal sulfates. The highest Ce extraction for the 24 and 48h hour experiments were 89% and 79%, respectively observed at 700°C. This correlates with the mineralogical analysis results where complete sulfation of CeO_2 to $CeOSO_4$ was observed at 700°C for both roasting times. This suggests that optimal sulfation of LREEs can be attained at this temperature. An increase in temperature to 750°C is associated with a decrease in Ce extraction for experiments conducted at both roasting durations. This is expected according the thermal stability diagrams and the decomposition temperatures obtained from literature, which

indicate that Ce sulfates start decomposing at temperatures between of 666°C and 700°C as reported by Tagawa. (1984) and Gmelin. (1978) respectively.

The lowest Ce extractions for sulfation tests conducted for 24 hours was observed at 800°C, while those for tests conducted for 48 hours were observed at 750°C. The increase in Ce extraction at 800°C for the 48 hour tests could have occurred as a result of the leaching conditions utilised in the study. The low Ce extractions observed at 630°C, 750°C and 800°C can be strongly associated with the phases present at these temperatures. The XRD results showed that both $CeOSO_4$ and CeO_2 were detected at these temperatures. The leaching was conducted in an acidic environment at pH levels between 3 and 4, which from the Pourbaix diagrams and from literature are suitable conditions for the leaching of LREEs including CeO_2 (Borra et al., 2015). Janos et al. (2015) reported a similar trend in a study conducted on the recovery of CeO_2 from spent glass-polishing slurry. The study reported that the solubility of CeO_2 in acid solutions was significantly reduced by processing at temperatures between 600°C and 1000°C. These temperatures are very similar to the ones utilised in the sulfation roasting of CeO_2 and therefore could have an impact on the solubility of this phase after roasting. Leaching of such materials should be conducted using concentrated acid solutions and/or high leaching temperatures.

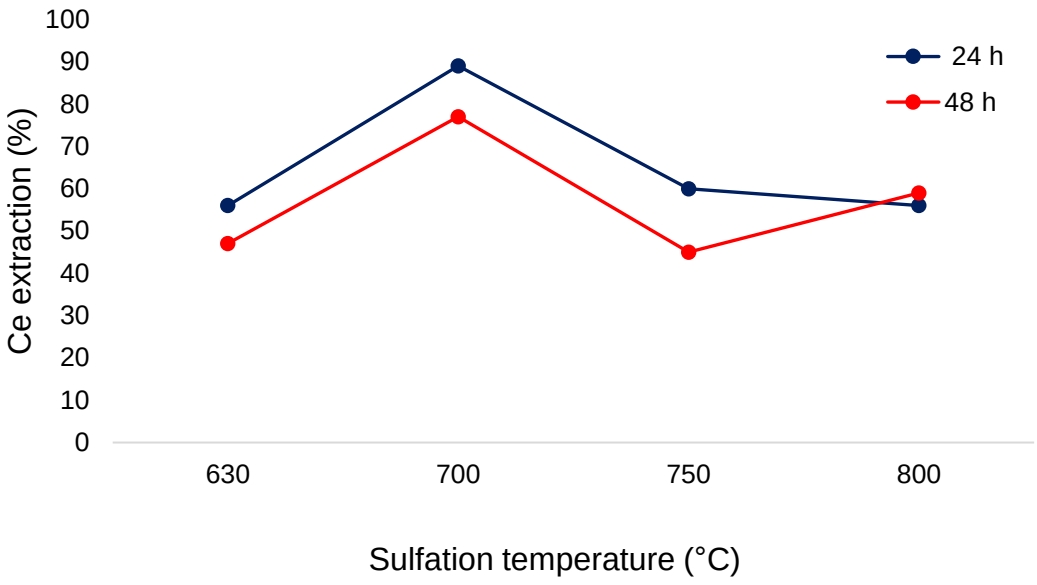


Figure 4.7. Graphical representation of the effect of sulfation temperature and time on Ce leaching efficiency.

4.7. SUMMARY

A preliminary study consisting of thermochemical calculations, sulfation roasting and leaching tests was conducted to investigate the suitable thermal and operational conditions of the sulfation roasting process for the extraction of LREEs. Thermochemical calculations to produce predominance phase diagrams for the LREEs and Fe were conducted to predict the stable phases at the proposed roasting temperatures. The diagrams showed that all the LREEs except Pr can exist as metal sulfates at these temperatures. The diagrams further showed that Fe, the major gangue constituent in the ZKD ore, also can form sulfates at these temperatures. Calculation of these diagrams highlighted some of the limitations associated with using predominance phase diagrams to select suitable roasting conditions for selectivity. The diagrams only describe phases that exist under equilibrium conditions and do not consider the kinetics of these phases. Sulfation roasting of synthetic CeO_2 was conducted at temperatures between 630°C and 800°C as well as roasting periods of 24 and 48 hours to investigate the applicability of the conditions obtained from the predominance phase diagrams. CeO_2 was successfully sulfated to $CeOSO_4$, an oxy-sulfate at temperatures between 630°C and 800°C as well roasting periods of 24 and 48 hours. The presence of $CeOSO_4$ indicated the decomposition of $Ce(SO_4)_2$, as well as the negative effect of prolonged roasting times on the stability of metal sulfates. The highest Ce extractions were obtained at 700°C for both roasting durations, therefore indicating that this temperature is the most suitable for cerium sulfation. Metal sulfate stability tests using hydrated $Ce_2(SO4)_3$ and $Fe_2(SO_4)_3$ were conducted at 750°C for 24 hours. The presence of hematite and $CeOSO_4$ after the test indicated that the metal sulfates are not stable under these roasting conditions. The results also showed that selective sulfation of Ce can be attained using the sulfation roasting process. Results obtained from the stability tests further indicated the limitations associated with using the diagrams to predict suitable roasting conditions and that other thermodynamic information such as the Gibbs free energy diagrams and thermal stability diagrams is required to decide on roasting conditions. The presence of $CeOSO_4$ throughout the preliminary tests indicated that shorter roasting times should be investigated in the fluidized roasting tests and that the effect of the roasting temperatures utilised should be investigated on REE-bearing resources.

5. FLUIDIZED SULFATION ROASTING STUDIES

5.1. INTRODUCTION

Fluidized sulfation roasting studies were conducted on REE-bearing materials, Zandkopsdrift ore and PyEarth ™ slag, to investigate the applicability of the roasting process on real REE-bearing resources from South Africa. The effect of sulfation temperature, residence time and gas composition on the sulfation roasting was investigated in the study. The selectivity of the sulfation roasting-leaching process was investigated throughout the study.

5.2. MINERALOGICAL CHARACTERIZATION – FEED MATERIALS

Mineralogical characterization of the feed samples was conducted to identify the main phases present, i.e. the main REE-bearing phases and the major gangue metal phases. Special focus was on the occurrence and distribution of the REEs between mineral phases. The phases identified in the head samples and their formulae by XRD are summarized in Table 5.1 and 5.2. The REEs in the ZKD ore were predominantly contained in monazite and florencite phosphate phases. Fe was mainly contained in the goethite, hematite, and biotite phases. These Fe phases were the predominant phases in the ore therefore, making the ZKD ore a Fe-rich REE-bearing ore. Characterization of Fe-rich carbonatite deposits from Southern Africa conducted by Bisaka et al. (2016) also showed that the REEs were predominantly contained in monazite minerals. The REEs in the PyEarth ™ slag were predominantly contained in the perovskite phase. The perovskite phase was as a result of the high amounts of lime (CaO) utilised as fluxing agent in the smelting process. Development of this phase was predicted through the addition of CaO to slags low in FeO which leads to the precipitation of $CaTiO_3$ (a perovskite type structure) (Bisaka et al., 2017). The decomposition of the perovskite phase is important during the sulfation roasting process because this phase has been reported by Bisaka et al. (2018) to be difficult to leach even in concentrated solutions.

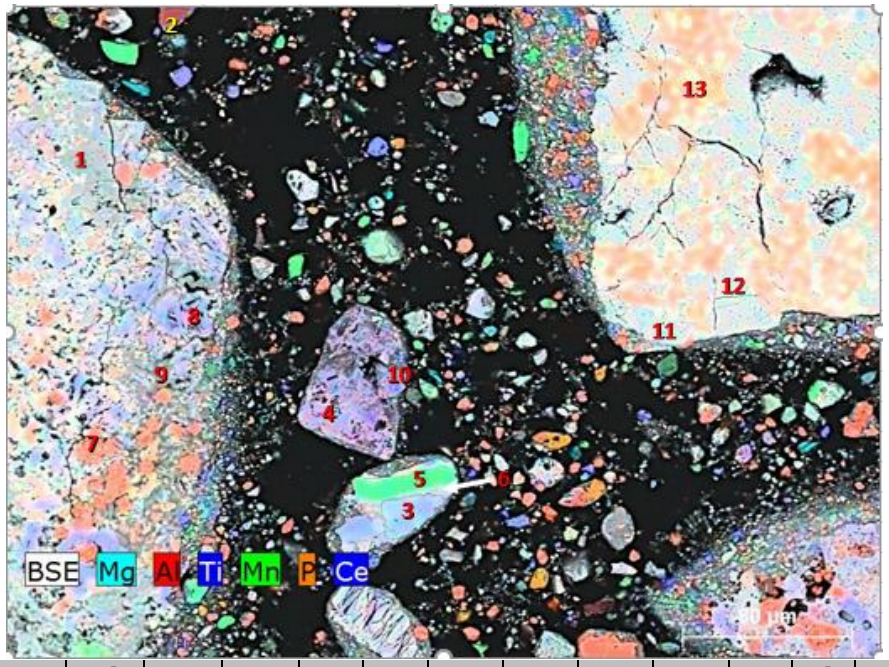
Table 5.1. Phases identified in the ZKD ore head sample and their formulae.

Compound Name	Formula	ZKD ore
Goethite	$FeO(OH)$	*xxx*
Florencite	$(La,Ce)Al_3(PO_4)_2(OH)_6$	*xx*
Monazite	$(Ce,La,Nd,Th)(PO_4,SiO_4)$	*xx*
Hematite	Fe_2O_3	*xx*
Biotite	$K(Mg,Fe)_3(Al , Fe)\ Si_3O_{10}(OH,F)_2$	*xx*
Rutile	TiO_2	*x*
x < 5 mass %; xx 5-20 mass %; xxx 20-50 mass %; xxxx >50 mass %		

Table 5.2. Phases identified in the PyEarth ™ slag sample and their formulae.

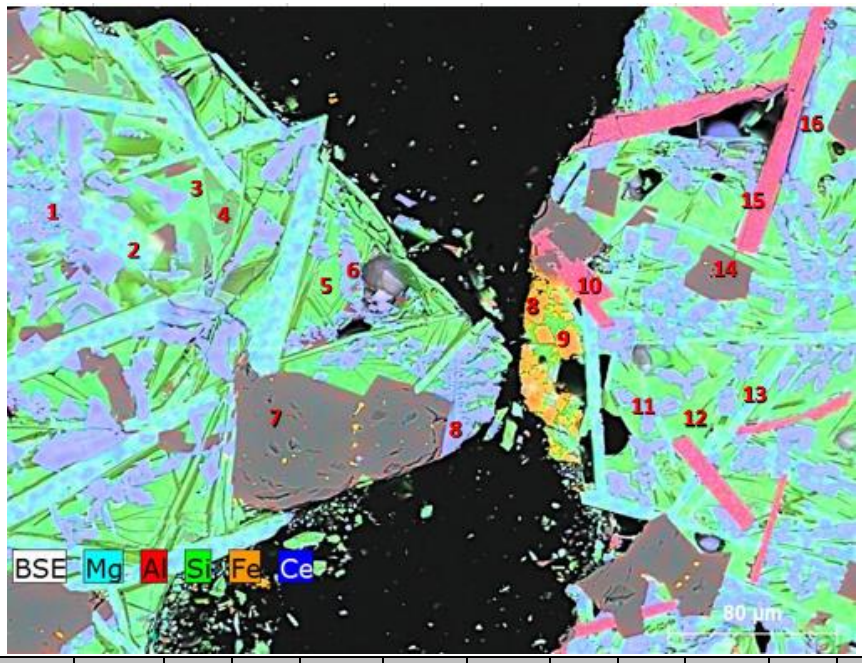
Compound Name	Formula	PyEarth ™
Perovskite	$(Ce, La, Nd, Pr)_{0.5}\ (Ca_{0.75}\ Sr_{0.25})\ (TiO_3)$	*xxx*
Spinel	$(Mg,Mn,Al)_3O_4$	*xxx*
Rankinite	$Ca_3Si_2O_7$	*xx*
Hexacelsian	$BaAl_2Si_2O_8$	*xx*
Fayalite	$(Fe,Mn\ )_2SiO_4$	*xx*
x < 5 mass %; xx 5-20 mass %; xxx 20-50 mass %; xxxx >50 mass %		

SEM-EDS analysis of the ZKD ore and the PyEarth ™ slag feed materials is presented in Figure 5.1 and 5.2. The EDS analysis further shows that the REEs occur in the florencite and monazite phases of the ZKD ore while those of the PyEarth ™ slag were contained in the perovskite phase. The REE-bearing phases of the ore were found to exist as fine grains disseminated in the hematite/ goethite matrix. This type of material precludes liberation. Iron, which is a major gangue constituent of the ZKD ore was not detected by EDS in the PyEarth slag. Manganese was detected in significant amounts in the favalite and spinel phases, while aluminium was detected mostly in the spinel phase and calcium in the perovskite phase of the slag. The REE-bearing phases in the slag were found to occur as dendrites and subhedral phases in the slag that were evenly scattered throughout the sample.



Spectrum	O	Na	Mg	Al	Si	P	S	K	Ca	Ti	Mn	Fe	Sr	Nb	Ba	La	Ce	Phase
1-4	25,4	0,7	0,4	1,5	2,3	0,7	0,3				1,5	67,4						Goethite
5, 6	21,0			0,7	0,1	0,2		0,7			62,6				14,7			Biotite
7	31,6			10,1		6,9	0,3		1,1		1,0	34,8	3,5			5,3	5,3	Florencite
8	22,9		1,1	1,3		3,5	0,5		0,6	2,0	1,7	19,4	2,1				44,9	Florencite
6-11	25,4			1,4	2,4	0,8				0,6	1,9	67,5						Biotite
12	26,0		0,0	0,3	0,8	5,2	0,2		0,9			52,5				3,9	10,2	Monazite
13	24,1			0,2	1,0	1,3					0,5	72,8						Hematite

Figure 5.1. Backscattered electron images and EDS analyses for the ZKD ore head+ sample.



Spectrum	O	Mg	Al	Si	S	K	Ca	Ti	Mn	Sr	Zr	Ba	La	Ce	Nd	Phase
1	29,1		1,4				10,5	27,2		2,1			8,9	16,0	4,8	Perovskite
2	33,9		14,2	14,3		0,3	1,5		1,4			34,5				Hexacelsian
3	36,0	1,0	5,2	13,7	1,2	0,1	7,1	2,7	22,7		1,9		3,2	5,3		Spinel
4	38,2	2,5	12,6	7,9			10,2	10,5	18,0							Spinel
5	38,8	0,8	8,8	14,7	0,8		8,3	3,7	18,8		1,4			3,9		Favalite
6	29,5	0,2	1,6		0,0		11,0	27,0	1,9	1,8	0,2		8,0	14,2	4,6	Perovskite
7, 8, 9	41,2	8,8	33,8					1,8	14,5							Spinel
10, 11	41,8	2,0	38,3				1,8	5,2	3,0	1,8				6,1		Spinel
12	39,2	1,0	10,6	13,8	0,9		7,1	3,8	18,8		1,7			2,5		Favalite
13	33,1		14,1	13,8		0,3	0,7					38,0				Hexacelsian
14	41,0	8,1	33,4					2,3	15,2							Spinel
15	41,4	1,7	35,9				1,8	7,7	4,0	1,8				5,7		Spinel
16	34,1		14,9	14,4		0,3	0,6					35,6				Hexacelsian

Figure 5.2. Backscattered electron images and EDS analyses for the PyEarth ™ slag sample.

5.3. FLUIDIZATION PARAMETERS

5.3.1. Particle Size and the Geldart Classification

Particle size and bulk density of the feed materials influence the success of the fluidization process. These physical properties are used in the calculation of fluidization parameters such as the minimum fluidization velocity and elutriation constants. A particle size range of -600 + 125 µm for both materials was maintained throughout the study. The particle size distribution curves of the feed samples determined through sieve analysis are described in Figure 5.3. The

d_{50} of the materials was calculated by interpolation is summarized in Table 5.3. From the size distribution curves the ZKD ore material was found to be finer and lighter than the PyEarth ™ slag and therefore fluidization parameters were calculated for each material.

The behaviour of the particles used in the fluidization process was predicted using the Geldart classification. The Geldart system classifies powders into 4 groups, i.e. Geldart group A, B, C and D, according to their fluidization properties at ambient conditions as summarized in Table 5.4. The size fractions of the feed materials were plotted onto the Geldart group classification chart described in Figure 5.4. The results from the Geldart chart showed that approximately 80% of the ZKD ore particles fell into group B and 20% fell in Group A (finer particles), while 90% of the particles in the PyEarth ™ slag were Group B particles and 10% were Group A particles. Classification of these two materials showed that fluidization was relatively easy as they contain particles that exhibit a combination of aeratable and bubble forming characteristics on the onset of fluidization.

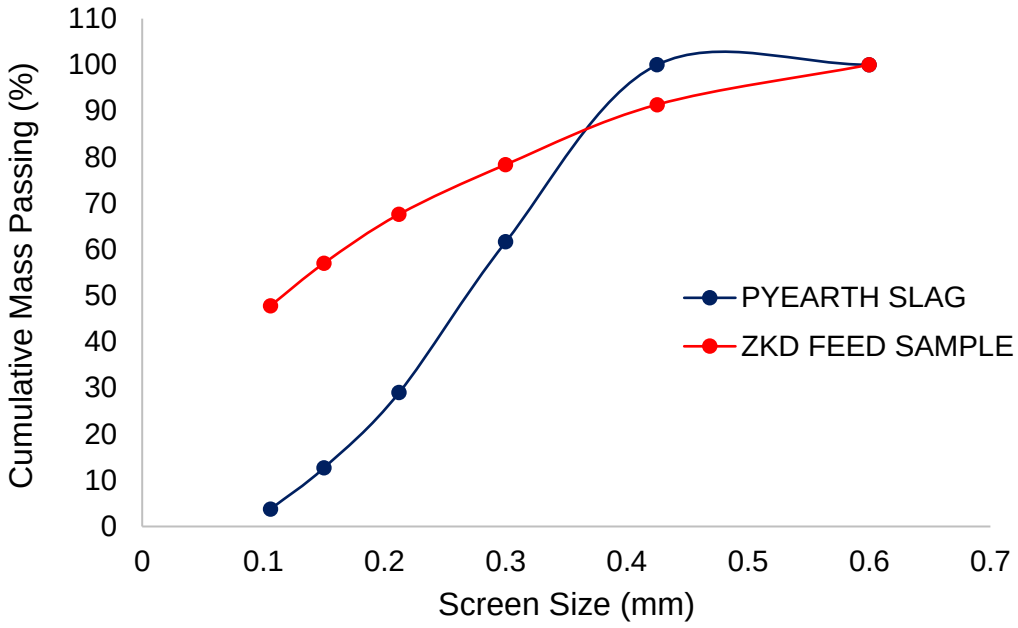


Figure 5.3. Cumulative frequency distributions of the PyEarth ™ slag and ZKD ore feed materials prior to roasting.

Table 5.3. Feed material d50.

Feed Material	D_{50} (µm)
ZKD ore	72.24
PyEarth ™ slag	290

Table 5.4. Summary of the Gerldart Classification.

Geldart Group A	Particles are aeratable, i.e. have a small mean particle size and/or low particle density and fluidize well (smooth fluidization).
Geldart Group B	Particles exhibit sand-like behaviour (bubbles form at onset of fluidization.
Geldart Group C	Particles are cohesive and experience significant channelling during fluidization.
Geldart Group D	Particles are spoutable (bubbles formed are enormous therefore, the bed tends to exhibit sluggish behaviour.

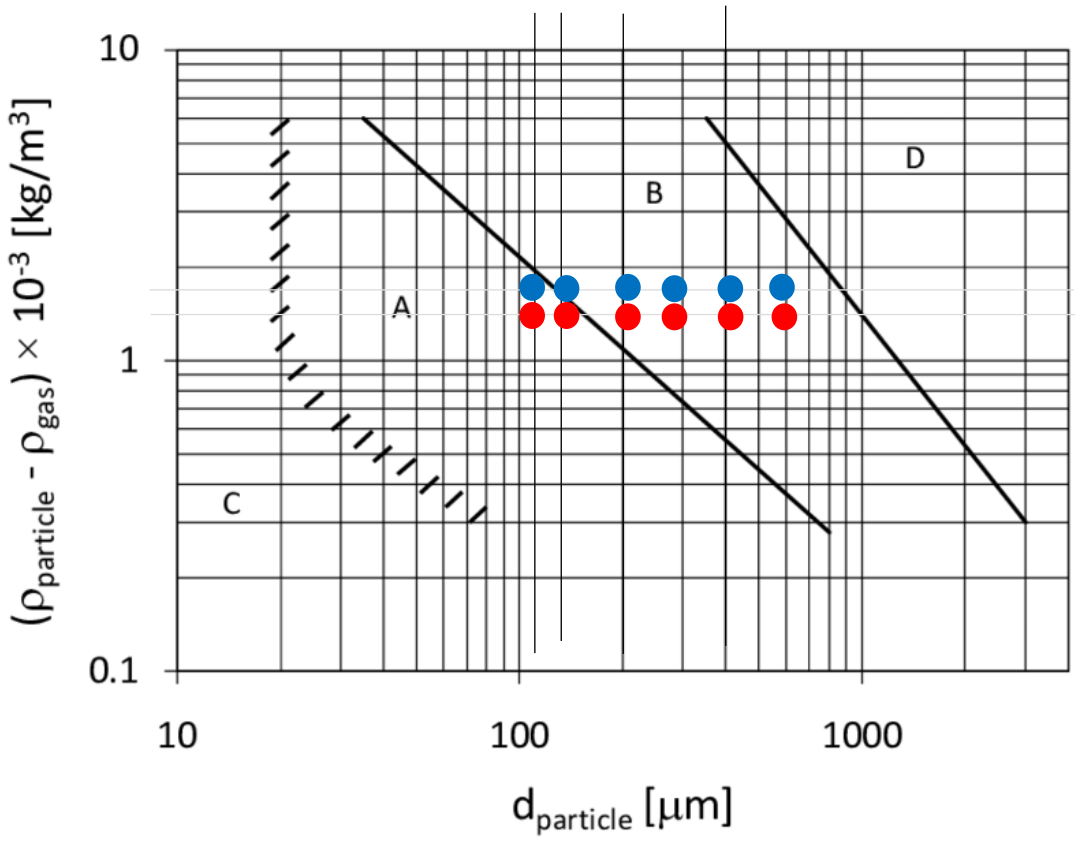


Figure 5.4. Geldart Classification- ZKD Ore (Red) and PyEarth slag (Blue).

5.3.2. Minimum Fluidization Velocity

The velocity that marks the onset of fluidization is known as the minimum fluidization velocity or the velocity at inception fluidization. The minimum fluidization velocity was determined manually through a series of cold tests using nitrogen gas as the fluid medium. The volumetric flowrate of the gas at inception of fluidization was used to calculate the minimum fluidization velocity according to equation 6.1

$$\therefore U_{mf} = \frac{Q}{(\pi \times r^2)} \quad (6.1)$$

The minimum fluidization calculation results for the two head samples are presented in Table 5.5. The minimum fluidization velocity for the PyEarth ™ slag was calculated to be higher than that of the ZKD ore. This was expected as the PyEarth ™ slag consisted of a larger average particle size and was heavier than the ZKD ore. The calculation of other fluidization parameters, i.e. terminal velocity, and elutriation rate constants, is summarized in Appendix E.

Table 5.5. Minimum fluidization velocity.

Material	Volumetric flowrate at inception of fluidization (cm^3/s)	Cross-sectional area (cm^2)	Minimum fluidization velocity (cm/s)	Minimum fluidization velocity (m/s)
ZKD Ore	101.17	10.18	9.94	0.10
PyEarth ™ Slag	243.13		23.88	0.24

5.4. FLUIDIZED SULFATION ROASTING RESULTS

5.4.1. Mineralogical Characterization of Roast Samples

Mineralogical analysis was conducted to investigate the occurrences and distribution of the REE and iron-bearing phases in the roasted samples as an indication of the sulfation roasting efficiency.

5.4.1.1. Zandkopsdrift Ore

The relative abundances for the ZKD ore sulfated at 600, 700, and 800°C, for varying roasting times (1, 4, and 8 hours) in a O_2-rich and/or O_2-depleted atmosphere, and their formulae are summarized in Table 5.7 to 5.9. Hematite was the most prominent phase in most of the roasted

samples as it was detected to make up 20-50% of the material. Trace amounts of monazite, the main REE-bearing phase in the ZKD ore, were detected in the samples processed at 600°C and 700°C, while no florencite was detected in all the samples. The presence of monazite at roasting temperatures between 600°C and 700°C has been reported by Yuan et al. (2017) who observed that the monazite decomposition was between 600°C and 650°C during a kinetic study on the roasting decomposition of REEs by CaO and coal. This was further confirmed by the lack of konazite in the samples roasted at 800°C. The reduced amounts of monazite and the lack of detection of the florencite phases indicated the decomposition of the phosphate phases during the sulfation roasting process. The presence of Fe oxide and alloy phases as predominant phases in the roasted materials indicated that Fe was not sulfated during the roasting process and that selectivity was achieved. This further proved the results obtained from the preliminary roasting study which indicated that any formed Fe sulfates would have decomposed at roasting temperatures above 545°C.

Titanium minerals, rutile, anatase, pseudobrookite, perovskite, and ulvospinel, were also detected in the samples. These phases were found to occur in minor quantities (5-20%) in the samples roasted in an O_2-rich environment. The presence of these phases in the investigated samples indicated that their formation is dependent on the concentration of O_2 in the system. Apatite was also detected as a minor constituent (5-20%) in the roasted samples.

Table 5.6. Bulk mineralogical composition of the ZKD ore roasted at 600°C.

Phase	**Formula**	**No O_2**	**O_2 enriched**
Spinel, Mn	$Mg_{0.899}Mn_{0.351}Al_{1.75}O_4$	*xxx*	*xxx*
Hexacelsian	$BaAl_2Si_2O_8$	*xx*	*xxx*
Manganese Strontium Cerium Oxide	$(Sr_{0.75}Ce_{0.25})MnO_3$	*xx*	*xxx*
Monazite (Ce)	$(Ce,La,Th)PO_4$	*x*	
Hematite	Fe_2O_3	*xxxx*	*xxxx*
Iron Manganese	$(Fe_{0.8}Mn_{0.2})$	*x*	*x*
Pyrrhotite	Fe_9S_{10}	*xx*	*x*
Manganese Aluminium Oxide	$Mn2AlO_4$	*xxx*	*x*
Anatase	TiO_2		*x*
x < 5 mass %; xx 5-20 mass %; xxx 20-50 mass %; xxxx >50 mass %			

Table 5.7. Bulk mineralogical composition of the ZKD ore roasted at 700°C.

Compound Name	Formula	No O_2	O_2 enriched
Spinel	$MgAl_2O_4$	*xx*	*x*
Rutile	TiO_2	*xx*	*xx*
Muscovite	$KAl_2(AlSi_3O_{10})(F,OH)_2$	*xx*	*x*
Monazite (Ce)	$(Ce,La,Th)PO_4$	*x*	
Hematite	Fe_2O_3	*xxxx*	*xxx*
Hausmannite	$Mn^{3+}{}_3O_4$	*xx*	
Goethite	$Fe^{3+}O(OH)$	*xx*	
Apatite	$Ca_{10}(PO_4)_6(OH)_2$	*xx*	*xx*
Ramsdellite	MnO_2		*xx*
Cristobalite	SiO_2		*x*
Anatase	TiO_2		*x*
x < 5 mass %; xx 5-20 mass %; xxx 20-50 mass %; xxxx >50 mass %			

Table 5.8. Bulk mineralogical composition of the ZKD ore roasted at 800°C.

Phase	Formula	No O_2	O_2 enriched
Spinel, Mn	$Mg_{0.899}Mn_{0.351}Al_{1.75}O_4$	*xxx*	*xxx*
Hexacelsian	$BaAl_2Si_2O_8$	*xxx*	*xxx*
Monazite (Ce)	$(Ce,La,Th)PO_4$	*x*	
Hematite	Fe_2O_3	*xxx*	*xxx*
Iron Manganese	$(Fe_{0.8}Mn_{0.2})$	*x*	*x*
Pyrrhotite	Fe_9S_{10}	*x*	*x*
Manganese Aluminium Oxide	$Mn2AlO_4$	*xx*	*x*
Anatase	TiO_2		*x*
x < 5 mass %; xx 5-20 mass %; xxx 20-50 mass %; xxxx >50 mass %			

SEM-EDS was used to determine the mode of occurrences of the REE and Fe-bearing minerals in the roasted ZKD ore samples. The results obtained from the sulfation roasting tests conducted at 700°C were used to discuss this section and are summarized in Figure 5.5. The primary phases detected in the SEM included iron oxides, hematite, and iron oxyhydroxides, goethite, manganese oxides, typically occurring as Mn oxyhydroxides, and titanium minerals, rutile, anatase and ilmenite. REEs were detected to occur in the form of monazite, in some cases showing chemical weathering or alterations (Figure 5.5B). The monazite in these samples had a very unusual composition, as sulphur (S) and calcium (Ca) were consistently detected in the compositions. S and Ca have been described in monazite by Chen et al. (2017) for carbonatite REE deposits. In some samples the REE mineralisation was found to occur as finely intergrown grains within the iron oxides (hematite) and iron-manganese oxyhydroxides phases

(Figure 5.5A, E, and F). The monazite detected in these samples was fine-grained <30µm commonly locked in hematite precluding liberation.

In rare cases, the REE-bearing phase was found to occur as coatings on the hematite or goethite phases (Figure 5.5C). Gangue minerals detected include apatite, biotite, zircon, barite, quartz, orthoclase and spinel. The iron oxide grains vary in size, with most of the grains being >300µm. Goethite displayed colloform texture while hematite occurred as a clean, smooth surface often with some cracks. Iron bearing minerals and oxyhydroxides were the most predominant phases in the samples which confirms the XRD analysis results. The REE-bearing phases in the roasted samples were predominantly exposed on the surface of the particles. These phases occurred as coatings of major gangue phases. The roasted samples contained a fair amount of cracks and were of a porous nature, indicating that the REE-bearing phases were significantly exposed for adequate leaching and therefore did not require size reduction prior to leaching.

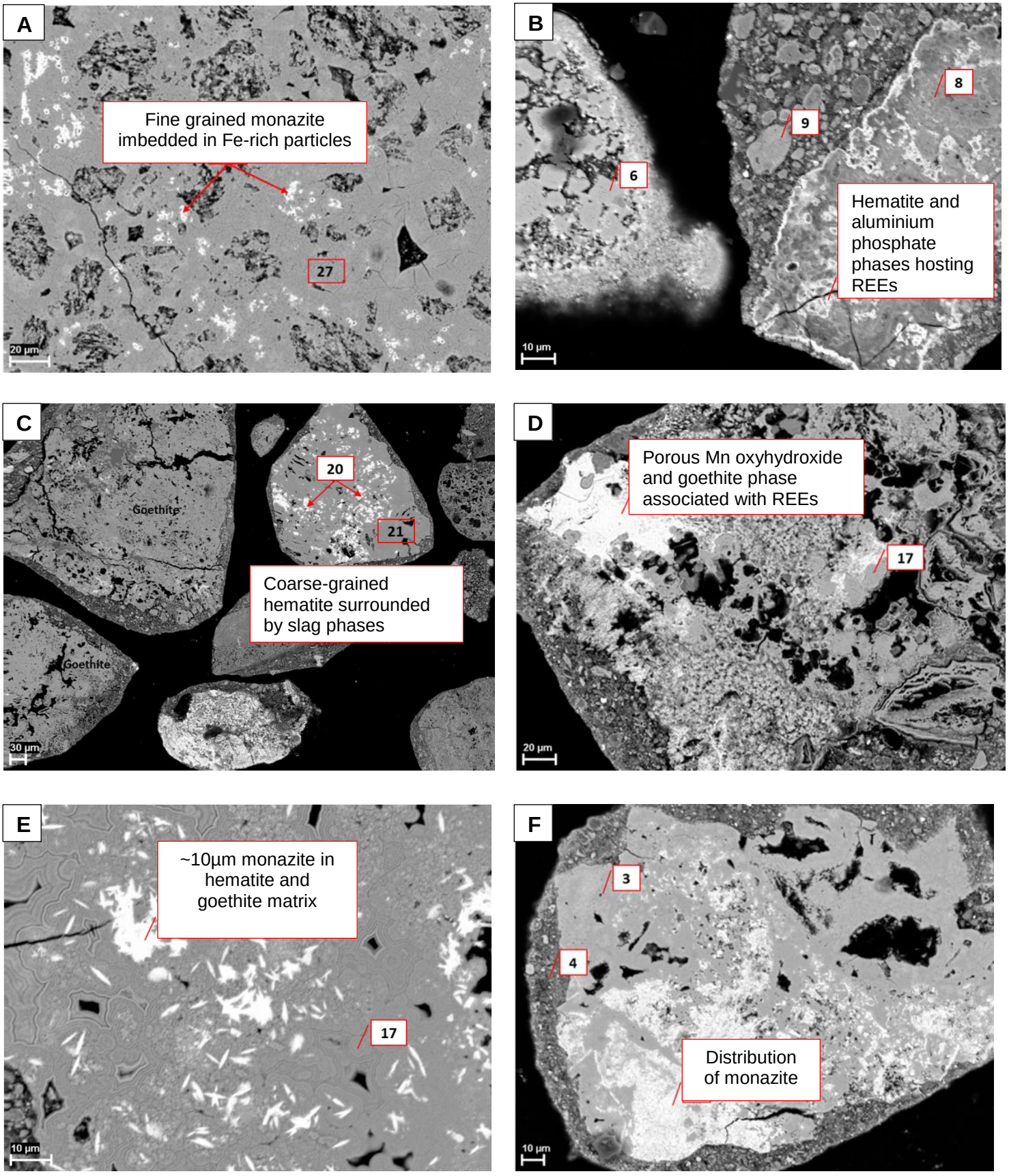


Figure 5.5. SEM-EDS results showing the mode of occurrence of the REE-bearing phases in the roasted ZKD ore samples. Diagram A-F represent group samples obtained at 700°C.

5.4.1.2. PyEarth ™ Slag

The phases identified in the PyEarth ™ slag samples sulfated at 700°C, at varying roasting times (1, 4, and 8 hours) in a O_2-rich and O_2-depleted atmosphere, and their formulae by XRD are summarized in Table 5.11. The roasted slag samples presented similar characteristics for the different tests conducted. Prior to roasting the REEs were contained predominantly in the perovskite phase which was detected to make up 20-50% of the slag. The sulfated slag samples contained significantly reduced amounts of the perovskite phase, 5-20%. Sulfation roasting of the slag resulted in the formation of an amorphous phase which constituted over 50% of the material. Fe which was contained in the fayalite prior to roasting was detected in the magnetite and the grossular phase.

Table 5.9. Phases identified in the PyEarth ™ slag sample after sulfation roasting and their formulae.

Compound Name	**Formula**	**Relative Abundance**
Perovskite	$(Ce, La, Nd, Pr)_{0.5}$ $(Ca_{0.75}$ $Sr_{0.25})$ (TiO_3)	*xx*
Grossular	$Al_{1.89}Ca_{2.869}$ $Fe_{0.241}$ O_{12} Si_3	*x*
Gypsum	H_4CaO_6S	*x*
Zeolite	$Al_2Ba_{0.995}O_8Si_2Yb_{0.005}$	*xx*
Spinel	$Al_{1.844}Fe_{0.142}Mg_{1.012}O_4$	*xx*
Magnetite	Fe_3O_4	*x*
Amorphous		*xxxx*
xxxx 50-100 mass % xxx 20-50 mass %; xx 5-20 mass %; x < 5 mass %		

SEM-EDS was used to determine the mode of occurrences of the REE and Fe-bearing minerals in the roasted PyEarth ™ slag samples. The SEM-EDS results obtained from the roasted PyEarth ™ slag samples are summarized in Figure 5.6 and 5.7. The characterization showed that the slag samples were dominated by Fe and Fe-alloys with variable Mn and P contents. Other phases detected in the slags were aluminium silicate (celsian) and spinel. The REEs were found to be concentrated in perovskite (Ti-Ca oxide) and amorphous structures containing; manganese barium aluminium silicate (Mn-Ba-Al silicate), barium-manganese-aluminium-calcium silicate (Mn-Ba-Ca-Al silicate), barium aluminium silicates (Ba-Al silicate) and calcium silicates (Ca silicates). Perovskite was found to occur as dendrites and subhedral phases in the slag as shown in Figure 5.6A point 9 and Figure 5.6C1 point 8, respectively. The Mn-Ba-Ca-Al silicate phase containing the REEs occurred as a background in the phases

largely hosting the spinel, Figure 5.6A point 10, and as dendritic crystals, Figure 5.6B1 point 10. These Ba-Al silicate structures occurred as fine-grained (<30µm) white particles in the slag, Figure 5.6B1 point 9. Calcium silicates hosting REE's occurred as fine-grained particles contained in Fe oxide phases Figure 5.6C2. Figure 5.7E showed occurrences of REE silicates, point 16, and a rare occurrence of a NbTi alloy, point 15, intergrown in the FeMn alloy, point 17. The occurrences of the REE's in these phases was generally fine-grained (<30µm) precluding liberation.

The slag samples displayed some porosity either in the matrix or around the rims. Figure 5.6B2 and C3 showed that the particles contained a porous rim between the Fe oxide and silicates. The rims in Figure 5.6C3 were more concentrically formed than those in Figure 5.6B2. The spinel phases, Figure 5.7D1, point 20, showed zoning, still forming with some graphitic silicate texture, point 19, within the crystals.

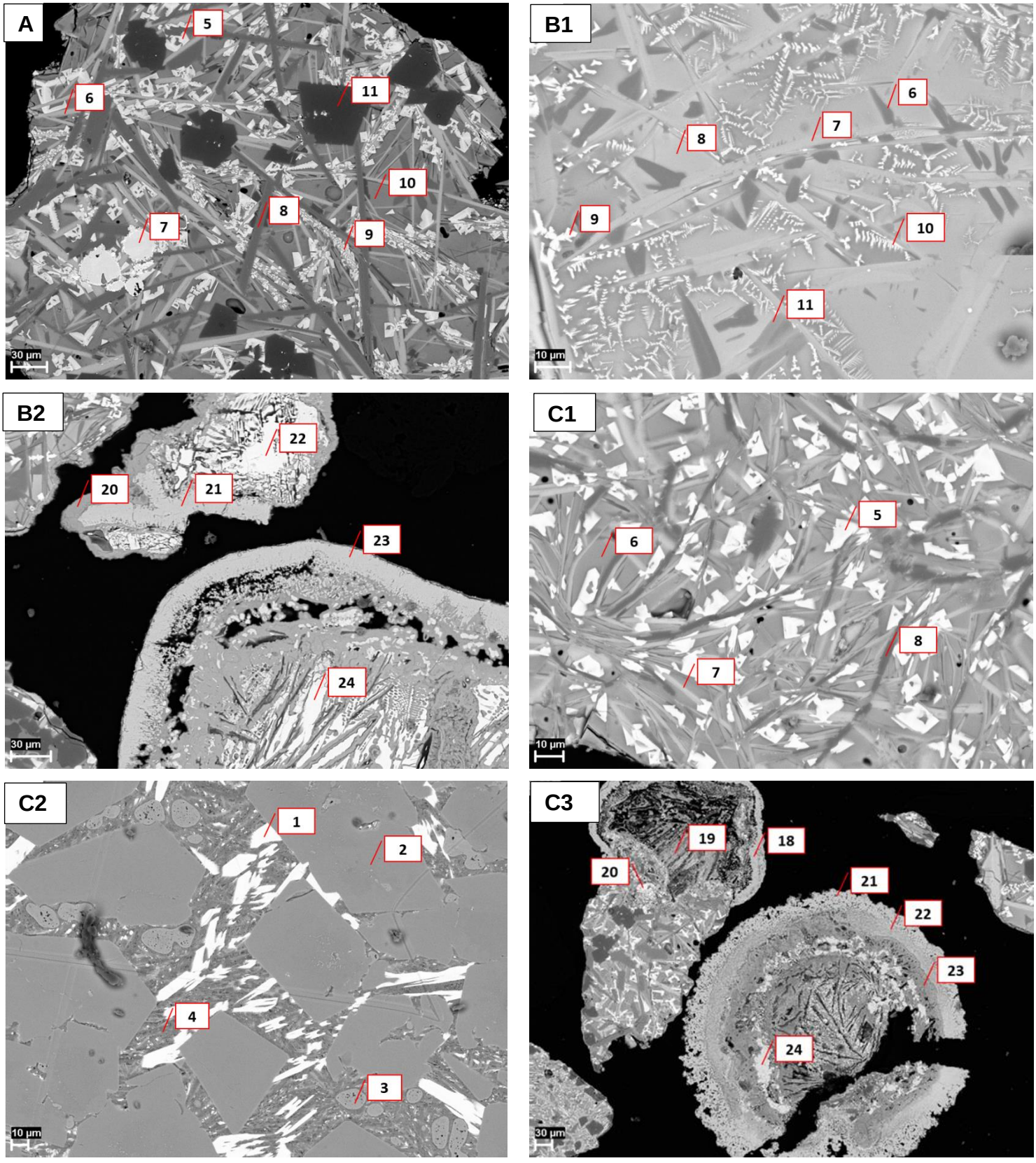


Figure 5.6. SEM-EDS results showing the mode of occurrence of the REE-bearing phases in the roasted PyEarth ™slag samples. Diagram A-C represent group samples roasted at 700° C in an O_2-depleted atmosphere for 1, 4, and 8 hours, respectively.

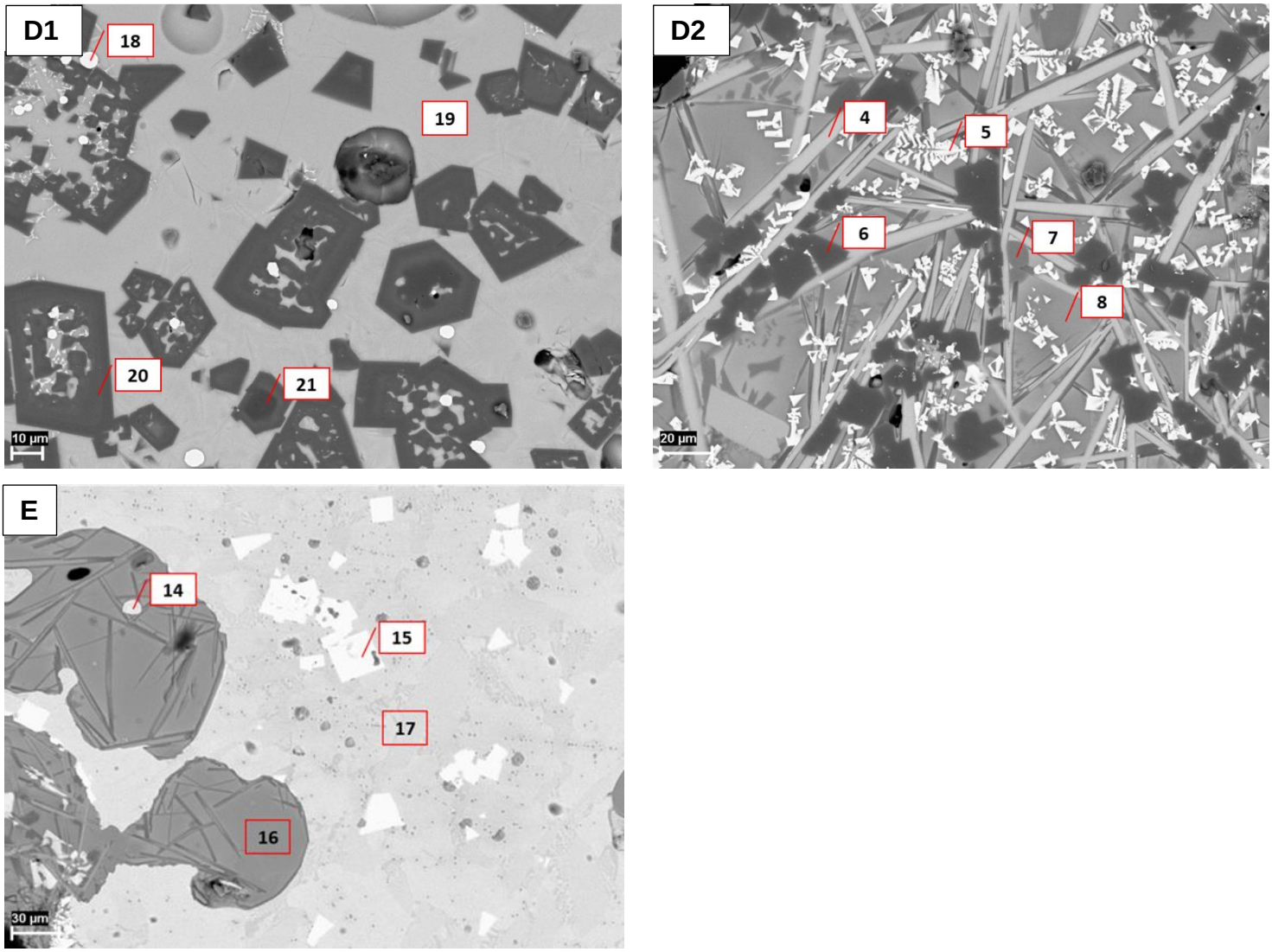


Figure 5.7. SEM-EDS results showing the mode of occurrence of the REE-bearing phases in the roasted PyEarth ™slag samples. Diagram D-E represent group samples roasted at 700° C in an O_2-enriched atmosphere.

5.4.2. ZKD Ore Sulfation

The sulfated materials were subjected to water dissolution under a controlled pH in the range between 3 and 4, and ambient temperature. The metal extraction was calculated for each sample. The metal extraction, defined as the ratio between the amount of remaining metal in the residue after water leaching and the initial amount contained in the roasted samples, was calculated using equation (5.1). The metal extraction was used to quantify the sulfation efficiency of the roasting process.

$$\text{Metal Extraction (\%)} = \frac{\text{Mass Of Metal In Residue}}{\text{Mass Of Metal In Feed}} \times 100 \qquad (5.1)$$

5.4.2.1. The Effect of Roasting Temperature on Leaching

The effect of roasting temperature on the dissolution behaviour of the LREEs and Fe was investigated by conducting sulfation roasting experiments on a ZKD ore at a constant roasting time of 4 hours, and gas composition consisting of 32% SO_2, 16% O_2, and 52% N_2, while varying the roasting temperatures between 600°C, 700°C and 800°C. The roasted samples were leached in deionized water at 25°C for 24 hours.

Figure 5.8 shows the effect of roasting temperature on the extraction of the LREEs and Fe. Maximum REE extraction was observed at 700°C, which varied from 37% to 24% for La and Nd, while a decrease in REE extraction was observed at a roasting temperature of 800°C. These results were expected as an increase in roasting temperature is known to increase the decomposition kinetics of metal sulfates (Borra et al., 2015). It was further observed that La had the highest extractions at all the roasting temperatures, while the lowest extractions were associated with Nd. This trend was expected from thermodynamic data and literature where La has been reported to produce the most stable sulftates amongst the LREEs and Nd produced the least stable sulfates (Teixeira et al., 2018). This trend is also associated with the decomposition temperatures of these metal sulfates, where La sulfates only start decomposing at temperatures of 1100°C, while the other LREE sulfates decompose at lower temperatures (Teixeira et al., 2018). These results indicate that selectivity amongst the LREEs can be attained using the sulfation roasting process. The presence of Pr in the solution further validates the limitations associated with the predominance phase diagrams which predicted Pr to only exist as stable oxides when sulfated at 600°C, 700°C and 800°C.

The selective roasting of LREEs was a crucial step in this study and was measured by the metal extractions of the LREEs in comparison with that of major gangue constituents, i.e. Fe. Fe constitutes approximately 35% of the ZKD ore and therefore selectivity against Fe was one of the significant goals of this study. The leaching results showed that Fe was the lowest extracted metal at all the roasting temperatures. The lowest Fe extraction of ~2% was obtained at 700°C. Borra et al. (2015) observed a similar trend where lower Fe extractions were obtained for roasting tests conducted at 700°C as compared to those obtained at 650°C. The low Fe extractions are also closely related to the phase composition of the roasted ZKD ore samples where Fe was predominantly detected as hematite, Fe_2O_3. This mineral phase is insoluble in water at the pH range utilised in the study as shown in the Pourbaix diagram in Figure 5.9. These results showed that 700°C was the suitable roasting temperature where selective

extraction could be attained, i.e. the highest LREE extractions and the lowest Fe extractions were recorded at this temperature.

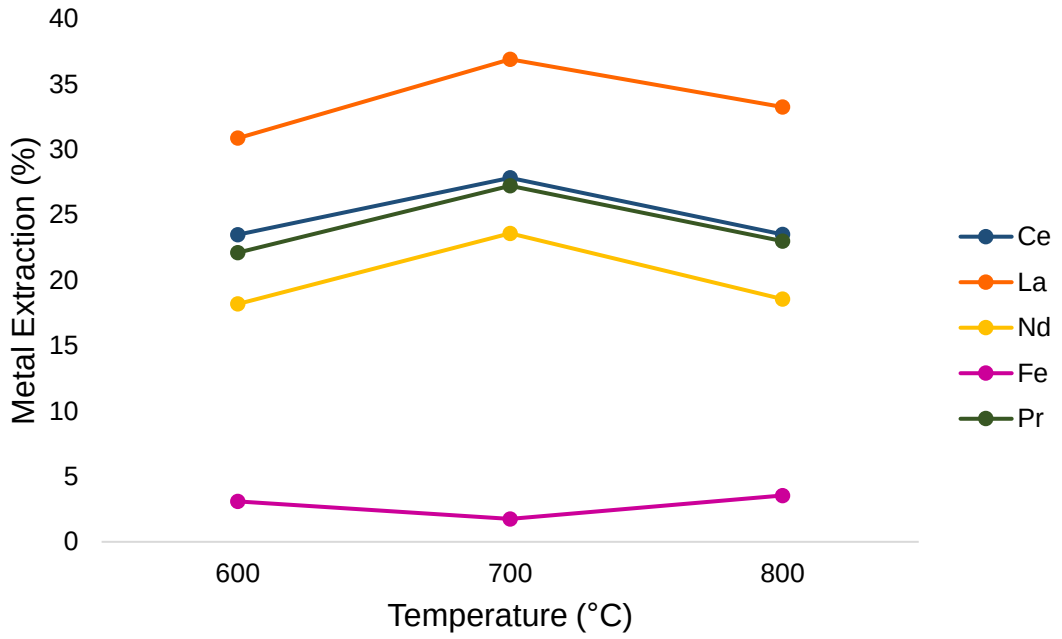


Figure 5.8. The effect of sulfation temperature on the LREE and Fe extraction efficiencies from the roasted ZKD ore.

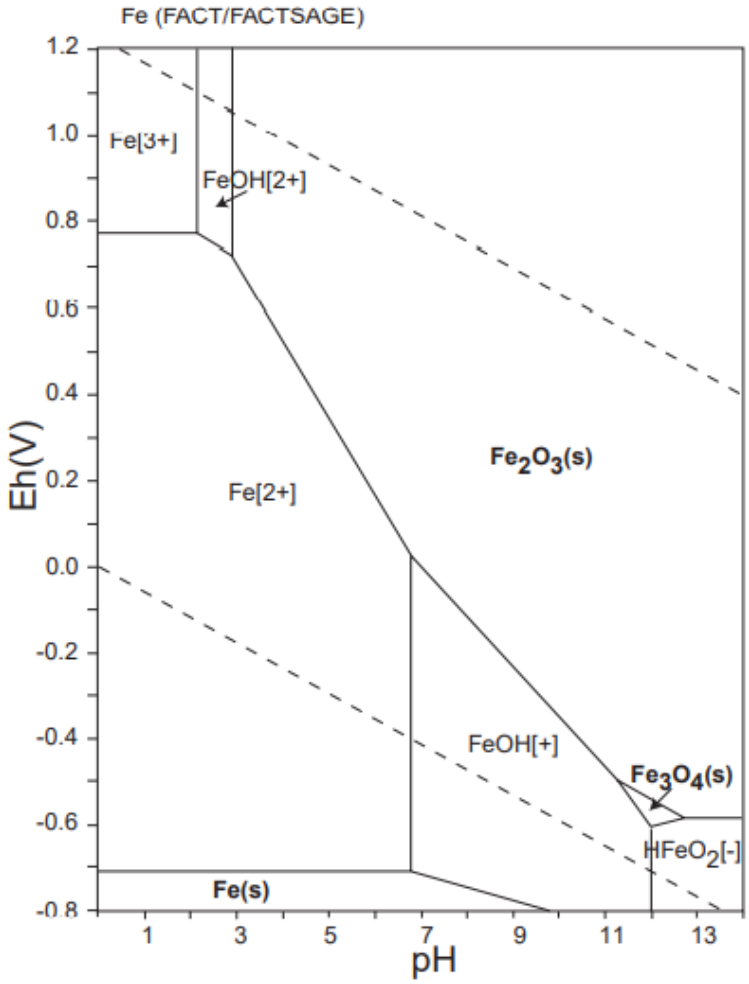


Figure 5.9. Eh-pH diagram of the system Fe-O-H (1). Fe = 10^{-10}, 298.15K, 10^5 Pa (Takeno, 2005).

5.4.2.2. The Effect of Roasting Time

The effect of roasting time on the sulfation and dissolution of LREEs and Fe was investigated by conducting sulfation roasting experiments at a constant roasting temperature of 600°C**,** 700°C and 800°C, and constant gas composition (32% SO_2, 16% O_2, and 52% N_2), while varying the time between 1-, 4-, and 8- hours. The samples were leached at a constant temperature of 25°C for 24 hours in a pH range of 3-4. Figure 5.10 to 5.12 show the effect of roasting time on the leaching of the LREEs and Fe at 600°C**,** 700°C and 800°C, respectively. The LREE extractions were observed to increase with increasing roasting time at all the temperatures. Even though this is the case, the highest extractions, 88% La, 87% Pr, 86% Nd and 61% Ce, were observed for samples roasted for 8 hours at 700°C. These results do not follow the trends reported in literature where the LREE extraction decreases with increasing time due to the decomposition of metal sulfates into oxysulfates and oxides which are insoluble

in water (Borra et al., 2015). This is mainly attributed to the phase composition of the roasted samples, which contained Fe predominantly in the hematite phase and not as Fe sulfates. Borra et al. (2015) reported that the presence of Fe sulfates in the roast product is associated with hydrolysis of the REEs due to the high pH associated with the decomposition of Fe sulfates. This was avoided in the study by maintaining the pH of the slurry between 3 and 4. The directly proportional relationship between the LREE extractions with the increase in roasting time at all the studies undertaken may also be associated with the rate of formation of the LREE sulfates. The low extractions observed at the shorter roasting times could be indicative of the instability of the formed metal sulfates or the slow rate of formation of the metal sulfates. This can be further investigated through kinetic studies of the process.

The effect of roasting time seemed to have a more pronounced effect on the results obtained for Fe. The Fe extractions were observed to be the lowest at all the roasting temperatures and times. Although this is the case, Fe extraction was observed to decrease with increasing time at 600°C, constant at 700°C and increase with increasing time at 800°C. The more usual trend from literature is similar to the one observed at 600°C, where Fe extraction decreases with increasing roasting time. The suitable roasting time is determined by considering the REE and Fe dissolution. From these results the suitable conditions for the selective extraction of the LREEs was observed to be at a roasting time of 8 hours and a temperature of 700°C. This does not follow the reported trend where an increase in roasting temperature results in shortened roasting durations because the metal sulfates decompose faster (Borra et al., 2015). This trend can be further investigated through kinetic and optimization studies.

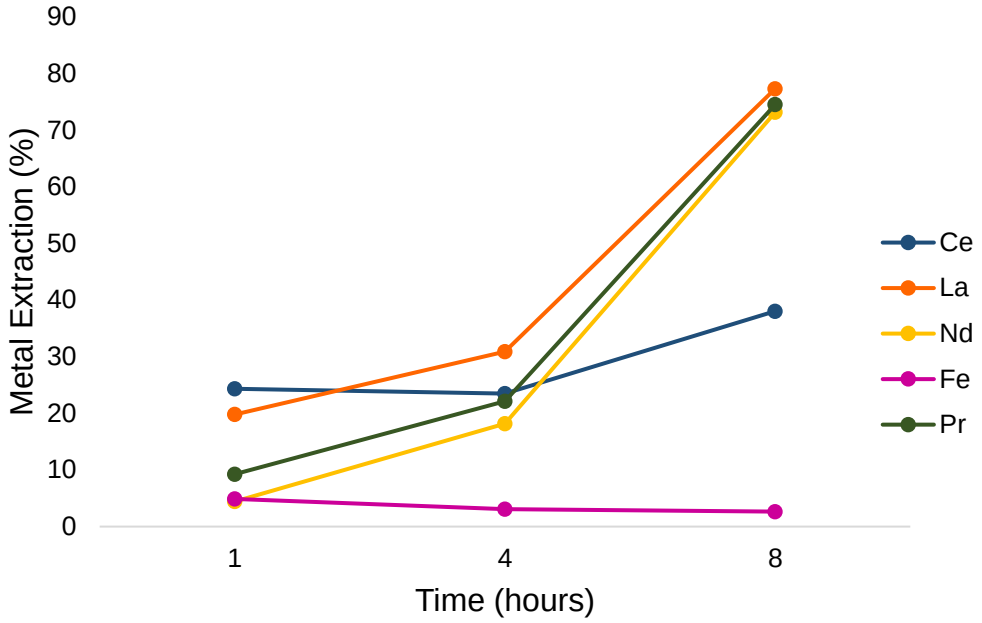


Figure 5.10. The effect of roasting time on the LREE and Fe extraction efficiency of the ZKD ore (600°C).

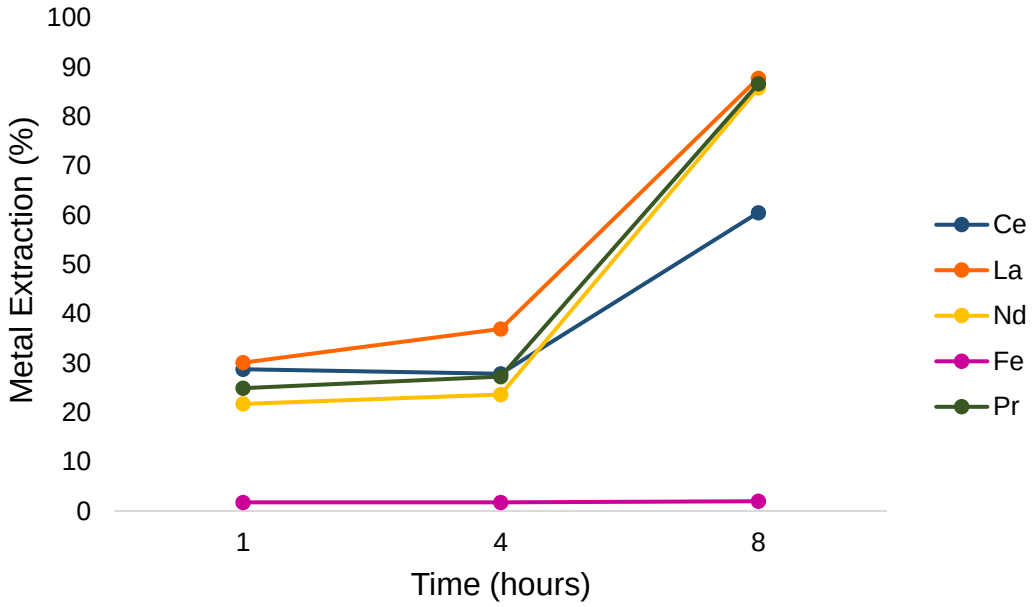


Figure 5.11. The effect of roasting time on the LREE and Fe extraction efficiency of the ZKD ore (700°C).

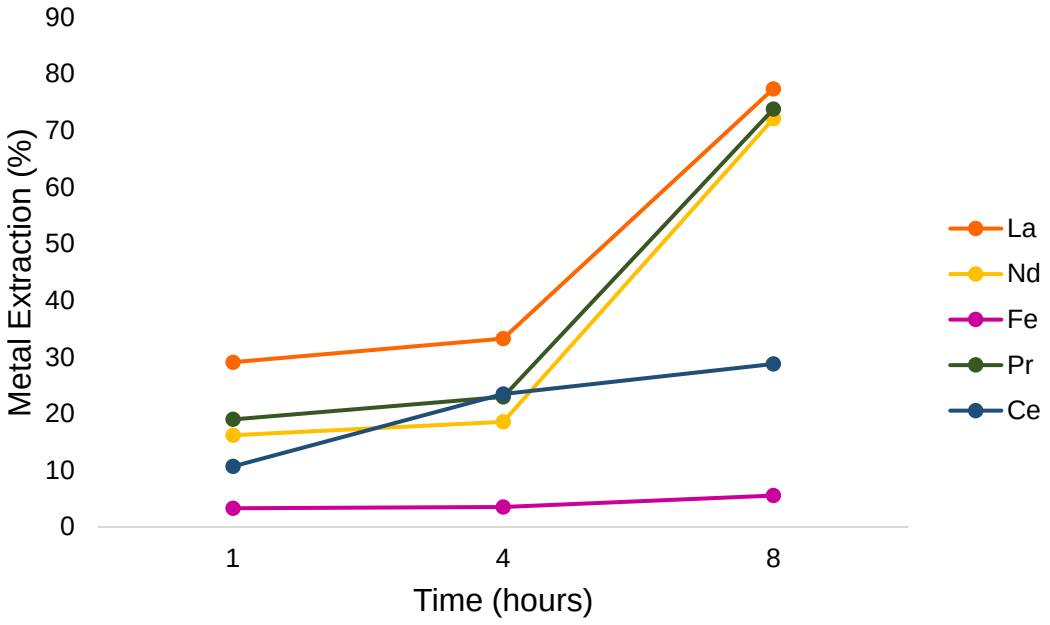


Figure 5.12. The effect of roasting time on the LREE and Fe extraction efficiency of the ZKD ore (800°C).

5.4.2.3. The Effect of Gas Composition

The effect of the gas composition during the sulfation roasting process was investigated in the study because from literature it was reported that Fe oxides sulfate only in the presence of both SO_2 and O_2 or when using SO_3 as a reductant (Bainbridge, 1973). With Fe, being contained in significant amounts in the ZKD ore, it was important to observe the sulfation behaviour of Fe in the presence and absence of oxygen. It was also important to investigate the effect of LREE sulfation in a gas atmosphere that is not oxygen enriched. Sulfation roasting studies were conducted at a constant roasting temperature of 700°C. The gas composition was varied between an O_2-rich (32% SO_2, 16% O_2, and 52% N_2) atmosphere and a O_2-depleted (32% SO_2 and 68% N_2) atmosphere.

Figure 5.13 and 5.14 describe the results obtained in an O_2-enriched and O_2-depleted atmosphere at 700°C. From the results, higher LREE extractions were observed for samples that were roasted in a O_2-enriched atmosphere as compared to those in the in a O_2-depleted atmosphere. The removal of O_2 from the system was shown to have a negative effect on the LREE sulfation. This result can be due to the slowing down of reaction kinetics for the formation of sulfur trioxide (SO_3) according to equation (5.2), which in turn affects the formation of LREE sulfates.

$$SO_2 + {}^1/_2\, O_2 \rightarrow SO_3 \qquad (5.2)$$

Fe extractions were reported to be higher in the O_2-depleted atmosphere as compared to the results obtained in the O_2-rich atmosphere. The extractions in the O_2-rich atmosphere are constant with increasing reaction time, with the lowest being ~1.8% at 1 hour and the highest being ~2% after 8 hours. Fe extractions in the O_2-depleted atmosphere were observed to increase with increasing time. These results contradict the thermodynamic claims by Bainbridge, 1973, stating that Fe sulfation only occurs in the presence of SO_2 and O_2 in the system. The results indicate that the removal of O_2 from the roasting atmosphere has minimal effect on inhibiting the formation of Fe sulfates because O_2 can still be introduced into the system through the decomposition of metal phases. From these results the suitable conditions for the selective extraction of the LREEs was observed to be at a roasting time of 8 hours and a temperature of 700°C using a gas system that contains oxygen.

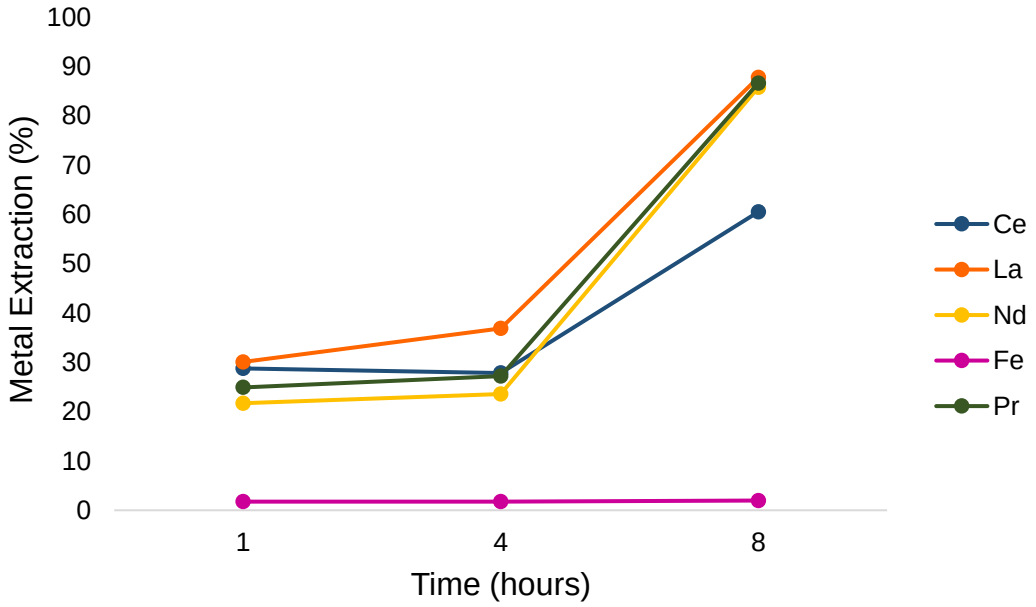


Figure 5.13. Metal extraction as a function of roasting time for sulfation roasting of the ZKD ore in an O_2-rich atmosphere at 700°C.

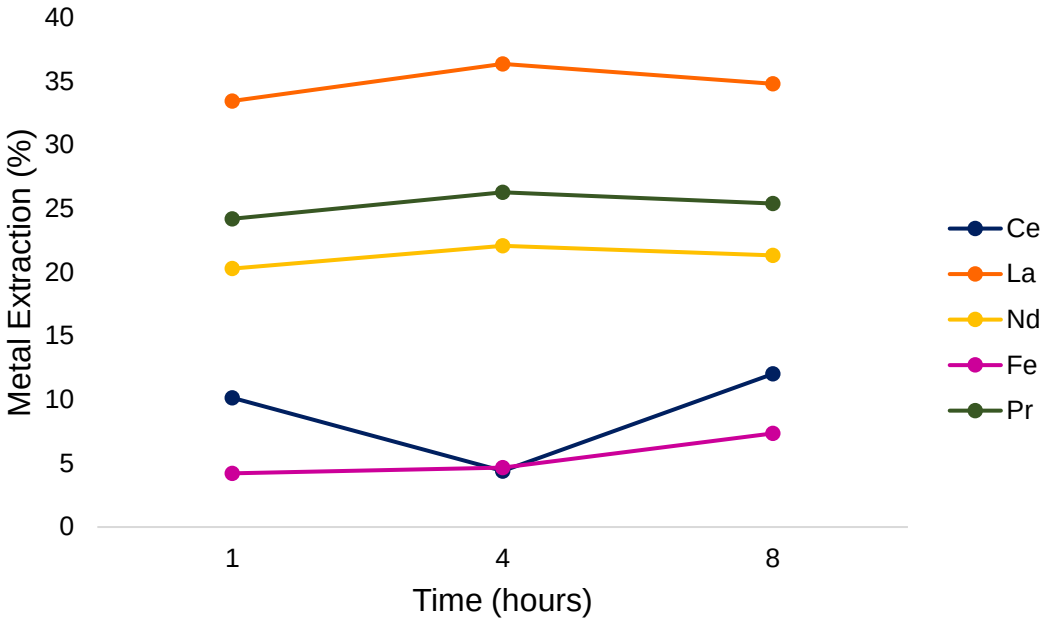


Figure 5.14. Metal extraction as a function of roasting time for sulfation roasting of the ZKD ore in an O_2-depleted atmosphere at 700°C.

5.4.3. PyEarth ™ Slag Sulfation

The PyEarth ™ slag was roasted at selected conditions to investigate the applicability of the conditions obtained from the ZKD ore. The material was roasted at 700°C and the effect of roasting time and gas composition was investigated.

5.4.3.1. The Effect of Roasting Time and Gas Composition on Leaching

The effect of roasting time on the sulfation and dissolution of LREEs and Fe was investigated by conducting sulfation roasting experiments at a constant roasting temperature of 700°C, and constant gas composition (32% SO_2, 16% O_2, and 52% N_2), while varying the time between 1-, 4-, and 8- hours. Figure 5.15 describes the effect of roasting time on LREE and Fe extraction. The LREE extractions were observed to increase with increasing roasting time, where the highest extractions were observed after 8 hours. A similar behaviour was observed during the roasting of the ZKD ore indicating that the sulfation of LREEs is dependent on time. The LREE extraction in the PyEarth™ slag was significantly lower compared to those obtained in the ZKD ore under the same conditions. These results are attributed mainly to the complex phase composition of the slag. The REEs were predominantly contained in the perovskite phase which was shown by mineralogical analysis to be partially decomposed after roasting at 700°C.

This decomposition of the perovskite phase was also accompanied by the formation of alloy and amorphous phases which were not adequately sulfated during the roasting process. The perovskite phase is also known to be difficult to decompose even under extreme conditions. The low extractions also indicate that the reaction kinetics for the formation of LREE sulfates are quite slow in the PyEarth ™ slag as compared to the ZKD ore.

Fe extractions were observed to decrease with increasing time, with the highest extraction of 69% obtained at 1 hour and the lowest of 40% obtained after 8 hours. This behaviour follows observations from literature where roasting time has a negative effect on the metal extractions due to the instability of the metal sulfates (Borra et al., 2015). Fe extractions were observed to be higher than the LREE extractions at all the roasting times. This is mainly due to the phase composition of the slag, where Fe was contained in a mixture of alloys, spinel, grossular and magnetite phases which might be easier to leach. These results showed that selective extraction of the LREEs, while keeping Fe extractions low was unsuccessful. These results, increase in REE extraction versus a decrease in Fe extraction as a function of time, also show that there is a room for improvement in leaching kinetics through the investigation of longer roasting times.

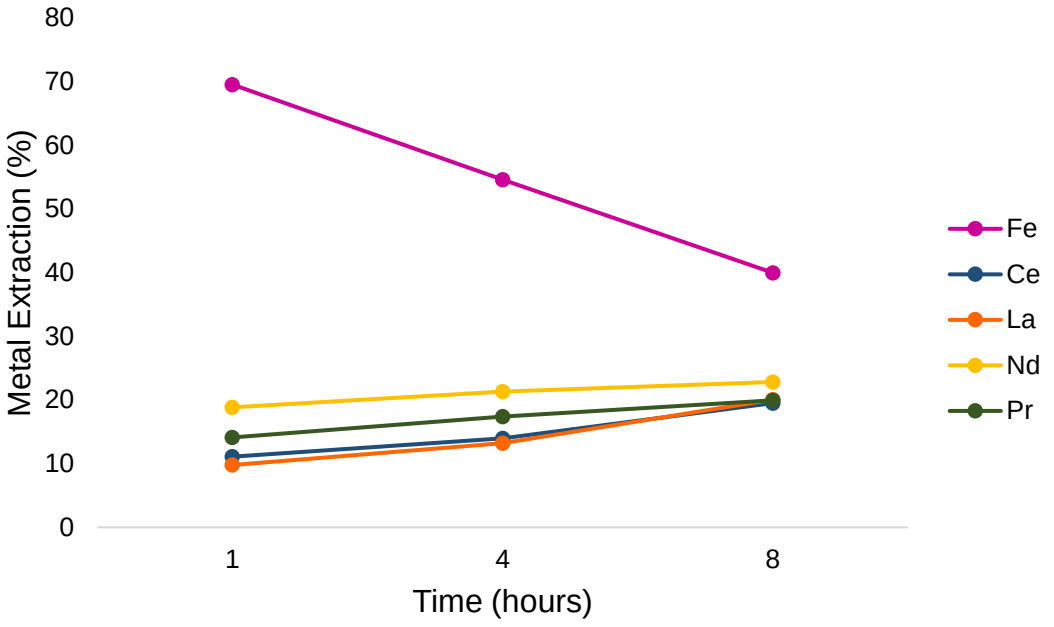


Figure 5.15. Metal extraction as a function of roasting time for sulfation roasting of the PyEarth ™ in an O_2-enriched atmosphere at 700°C.

Figure 5.16 describes the results obtained in an O_2-depleted atmosphere at 700°C. LREE extraction in the O_2-enriched atmosphere was observed to increase with increasing roasting time. An irregular trend was observed in the O_2-depleted atmosphere, where the lowest

extractions were obtained at 4 hours. This observation indicated that both the decomposition of the perovskite phase and the formation of sulfates is dependent on the presence of oxygen in the system. The results further indicated that the gas atmosphere plays a significant role in the sulfation of LREEs and that the removal of O_2 gas has a negative effect on the sulfation of these metals in the PyEarth ™ slag.

The results in both roasting conditions showed that Fe was the highest extracted metal in the solution. For tests conducted in a O_2-enriched environment, Fe extractions were observed to decrease with increasing time, while in the O_2-depleted environment the highest Fe extraction was obtained after 4 hours. The results obtained in the tests conducted without O_2 indicate that the removal of oxygen in the system may cause the formed metal sulfates to be unstable with increase in roasting time, this is shown by the irregular trend in the metal extractions. These results showed that the sulfation and leaching process was technically feasible and applicable for the extraction of LREEs from the PyEarth ™ slag. Although this was the case, the high Fe extractions associated with roasting of the slag makes the process economically unattractive because selectivity was not achieved. Further experiments at varied conditions are recommended to determine suitable conditions for the roasting of this material.

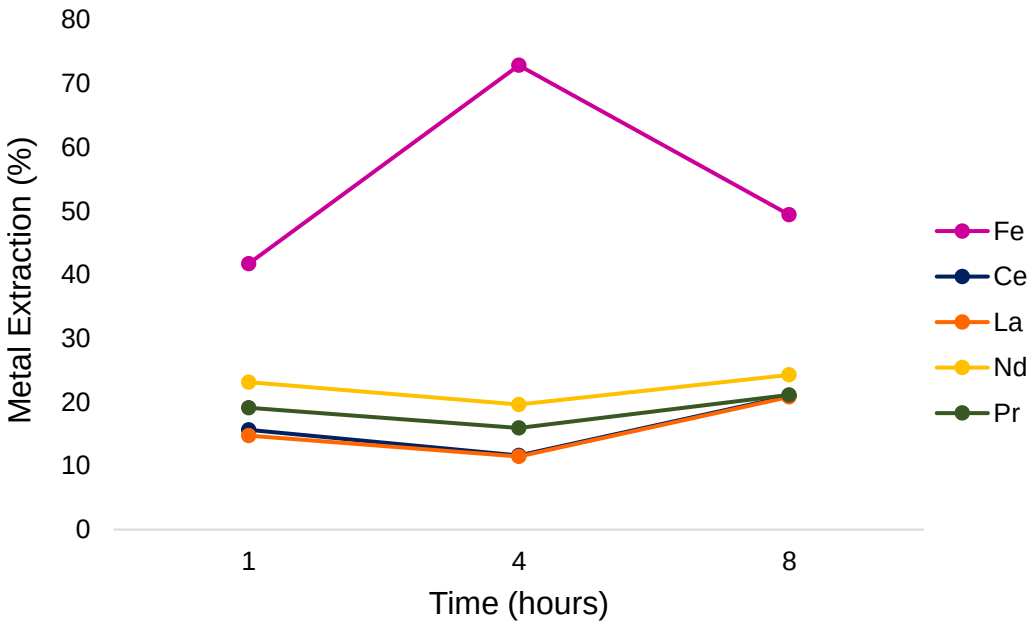


Figure 5.16. Metal extraction as a function of roasting time for sulfation roasting of the PyEarth™ slag in an O_2-depleted atmosphere at 700°C.

5.5. SUMMARY

The applicability of the sulfation roasting and leaching process on REE-bearing industrial materials, ZKD ore and PyEarth ™ slag, was successfully investigated in the study. The results showed that the process was more applicable with the ZKD ore than the PyEarth ™ slag as indicated by the high LREE extractions obtained at the various conditions. Selective extraction was achieved during the roasting of the ZKD ore as shown by the high LREE extractions as compared to Fe extraction. The low Fe extractions obtained with the ZKD ore were attributed to the phase composition of the roasted samples, where Fe predominantly occurred as hematite. The leaching conditions also contributed to the insoluble nature of Fe observed in the study. The sulfation of the ZKD ore was found to be dependent on the roasting temperature, time, and the composition of gas atmosphere. The best results (88% La, 87% Pr, 86% Nd, 61% Ce and 2% Fe) were obtained from tests conducted at 700°C for 8 hours in a O_2-enriched gas atmosphere. Sulfation roasting of the PyEarth™ slag was associated with significantly high Fe extractions, highest of 72%, therefore rendering the process unselective for this material. Although this was the case, process achieved a significant degree of decomposition of the perovskite phase which hosts the REEs. The process also resulted in extraction of the LREEs therefore indicating that sulfation was achieved. The LREE extractions obtained for the PyEarth ™ slag were relatively low compared to those obtained with the ZKD ore under the same conditions. Therefore, it is recommended that various conditions are investigated for the sulfation roasting of the PyEarth ™ slag.

6. CONCLUSIONS

REEs are commonly extracted from mineral concentrates using conventional hydrometallurgical processes such as alkaline and/or acid baking. Although these processes are very efficient in extracting REEs, they tend to co-extract gangue constituents such as Fe, Mn and Th, therefore, rendering them unselective. Co-extraction of gangue metals requires multiple purification stages to produce a more sellable product stream. These purification stages tend to make the process flowsheet complicated, tedious, and very expensive. The sulfation roasting and leaching process was proposed in the study for the selective conversion and extraction of LREEs from REE-bearing resources from South Africa. The aim of the study was to investigate the technical feasibility of the sulfation roasting and leaching process. A preliminary sulfation roasting study was conducted to investigate and determine the suitable operational conditions using synthetic REO compounds. This study consisted of:

- The calculation of predominance phase diagrams for the LREEs and Fe to investigate the stable phases present at temperatures between 600-800°C using FactSage thermochemical software's.
- Sulfation roasting and leaching of synthetic cerium oxide, CeO_2, at temperatures between 630°C-800°C,
- Stability tests conducted using hydrated $Ce_2(SO4)_3$ and $Fe_2(SO_4)_3$

Sulfation roasting of synthetic cerium dioxide, CeO_2, at temperatures between 630°C and 800°C, roasting periods of 24 and 48 hours resulted in the sulfation of CeO_2 to $CeOSO_4$, an oxy-sulfate. The presence of $CeOSO_4$ and CeO_2 phases, obtained at 700°C, 750°C and 800°C from XRD analysis, were reported by Poston et al. (2003) to be an indication of the decomposition of cerium (IV) sulfate, $Ce(SO_4)_2$, which occurs at approximately 600°C. The presence of $CeOSO_4$ and CeO_2 at 700°C, 750°C and 800°C contradicted what Poston et al. (2003) reported that only CeO_2 exists at these temperatures. These results indicated the negative effect of prolonged roasting times on the metal sulfate stability. The highest Ce extractions from the leaching tests were 89% and 79% for the roasting tests at 700°C for 24 and 48 hours, respectively. These results correlated with the mineralogical analysis where complete sulfation of CeO_2 to $CeOSO_4$ was observed at 700°C for both roasting times. This, therefore, indicates that optimal sulfation of LREEs can be attained at this temperature. Metal sulfate stability tests conducted using hydrated $Ce_2(SO4)_3$ and $Fe_2(SO_4)_3$ at 750°C for 24 hours

resulted in the presence of $CeOSO_4$, Fe_2O_3, and $Fe_2(SO_4)_3$, in order of decreasing abundance. The presence of these phases indicated that the metal sulfates are not stable under these roasting conditions. The results also showed that selective sulfation of Ce (and the LREEs) can be attained using the sulfation roasting process.

Fluidized sulfation roasting and leaching studies were conducted on REE-bearing industrial materials, Zandkopsdrift (ZKD) ore and the PyEarth ™ slag, from South Africa to investigate the applicability of the roasting process on real REE-bearing resources. The study consisted of:

- The calculation of the fluidization parameters to predict the behaviour of the different head samples during the fluidized sulfation roasting tests.
- Investigation on the effect of operational parameters; temperature, reaction time and stoichiometric ratio of SO_2 to O_2, on the conversion efficiency of LREEs in the ZKD ore and the PyEarth ™ slag using fluidized sulfation roasting experiments.
- Investigation of the sulfation efficiency through mineralogical analysis of the head and roast bed samples.

The two head materials used in the fluidization roasting study were found to possess different bulk densities and were therefore expected to have different fluidization parameters and behave differently during fluidization. The PyEarth ™ slag was found to be heavier and contained a larger fraction of coarse particles as compared to the ZKD ore. This trend was further observed with the minimum fluidization velocity (U_{mf}) calculations, where the ZKD ore reported a lower U_{mf} (0.10 m/s) as compared to the PyEarth ™, 0.24 m/s. Although the ZKD ore was finer than the PyEarth ™ slag, because of the particle size (- 600 + 106 µm) utilised, both materials contained particles that exhibit a combination of aeratable and bubble forming characteristics on the onset of fluidization.

Mineralogical analysis of the head samples showed that the REEs were predominantly contained in the florencite and monazite phosphate phases in the ZKD ore and in the perovskite phase in the PyEarth™ slag. The roasted samples contained minimal amounts of the monazite phase and no florencite phase was detected. This, therefore, indicates that decomposition of these phases was achieved. The perovskite was detected in reduced amounts in the roasted PyEarth ™ slag. An amorphous phase was detected in prevalent amounts in the roasted slag. Fe, which is the most prevalent gangue constituent in the ZKD ore was contained in goethite, hematite, and biotite phases prior to roasting, and in the hematite phase after roasting. The

hematite phase was found to be the predominant phase in the ZKD ore after roasting, therefore indicating that sulfation of Fe was avoided. The extent of REE sulfation was not detected using the mineralogical analysis because these metals were below the detection limit for the techniques utilised.

The fluidized roasting tests on the two materials confirmed that the sulfation roasting process is applicable on real REE-bearing resources. This was seen through the metal extraction results obtained from the leaching tests. The sulfation roasting of the ZKD was observed to be dependent on the roasting temperature, time and gas composition utilised. The highest LREE extractions (88% La, 87% Pr, 86% Nd, 61% Ce and 2% Fe) were obtained for roasting tests conducted at 700°C for 8 hours in an O_2-enriched gas atmosphere. Fe constituted approximately 35% of the ZKD ore and therefore selectivity against Fe was one of the significant goals of this study. Fe was the lowest extracted metal at all the roasting temperatures, times and gas composition variations. The results obtained for Fe confirmed that the leaching behaviour is significantly influenced by the phase composition of the roasted material, i.e. Fe was predominantly detected as hematite, Fe_2O_3, which is insoluble in water. The low Fe extractions obtained were due to the pH range, 3-4, used in the study which is suitable Fe oxide dissolution. Sulfation roasting of the PyEarth™ slag was associated with significantly high Fe extractions, highest of 72%, as compared to the highest LREE extractions of 24% Nd, 21% Pr, 21% La, and 21% Ce obtained at 700°C for 8 hours in an O_2-enriched gas atmosphere. This leaching behaviour was attributed to the phase composition of the slag and the limited conditions investigated with the PyEarth ™ slag.

7. RECOMMENDATIONS

The study conducted on both synthetic REOs and industrial REE-bearing resources highlighted the limitations associated with using predominance phase diagrams to paint an accurate prediction of the occurrences during roasting of REEs alongside major gangue constituents such as Fe. It is therefore recommended that thermal gravimetric analysis (TGA) coupled with mineralogical analysis are utilised to determine the behaviour of the materials and their thermal stability at different temperatures.

The extent of sulfation and the reaction mechanisms involved in the sulfation roasting of REE-bearing materials were difficult to quantify using the characterization techniques used in the study. It is therefore recommended that more robust techniques such as mineral liberation analysis (MLA) are utilised in future studies to identify phases containing trace elements such as the REEs.

Although the sulfation and leaching study conducted on the REE-bearing materials was sufficient in concluding that gas-based sulfation roasting is technically feasible as an alternative process for the selective conversion and extraction of LREEs, therefore, there exists opportunities to optimise further. Kinetic sulfation roasting studies are therefore, recommended to determine the rate at which metal sulfate phases are formed as well as to determine the suitable and optimal roasting conditions for the sulfation roasting of industrial materials. It is also recommended that more conditions are investigated for the PyEarth ™ slag to make a more accurate conclusion in terms of the applicability of the sulfation roasting for slag feed materials.

REFERENCES

Alcock, C. B. (1976). *Principles of pyrometallurgy*. Academic Press

Amer, T. E., Abdella, W. M., Wahab, G. A., & El-Sheikh, E. M. (2013). A suggested alternative procedure for processing of monazite mineral concentrate. *International Journal of Mineral Processing*, *125*, 106-111.

An, E. P. D., & Reddy, R. G. (2017). Applications of Process Engineering Principles in Materials Processing, Energy and Environmental Technologies.

Aplan, F.F. (1988). The processing of rare earth minerals, rare earths, In: Bautista, R.G., Wong, M.M. (Eds.), *The Minerals, Metals and Materials Society*, Warrendale, PA, 15-34.

Bainbridge, D. W. (1973). Sulfation of a nickeliferous laterite. *Metallurgical Transactions*, *4*(7), 1655-1658.

Balaram, V. (2019). Rare earth elements: A review of applications, occurrence, exploration, analysis, recycling, and environmental impact. *Geoscience Frontiers*, *10*(4), 1285-1303.

Bale, C. W., Bélisle, E., Chartrand, P., Decterov, S. A., Eriksson, G., Gheribi, A., & Petersen, S. (2014). Recent developments in FactSage thermochemical software and databases. In *Celebrating the Megascale* (pp. 141-148). Springer, Cham.

Berry, L., Galvin, J., Agarwal, V., & Safarzadeh, M. S. (2017). Alkali pug bake process for the decomposition of monazite concentrates. *Minerals Engineering*, *109*, 32-41.

Bisaka, K., Thobadi, I., & Pawlik, C. (2016). Extraction of rare-earth elements from iron-rich rare-earth deposits. In *Hydrometallurgy Conference 2016: Sustainable Hydrometallurgical Extraction of Metals, Cape Town, 1–3 August 2016, Southern African Institute of Mining and Metallurgy*.

Bisaka, K., Thobadi, I., Mokoena, S., Pawlik, C., & Erwee, M. (2017). Flowsheet Development for The Extraction of Rare Earths Using Mintek's PyEarth ™ Process. *The Conference of Metallurgists (2017): Hosting World Gold & Nickel Cobalt.* Canadian Institute of Mining, Metallurgy and Petroleum. Proceedings ISBN: 978-1-926872-36-0

Bisaka, K., Thobadi, I., & Mphahlele, Y. (2018). EM45 - PyEarthTM Process: 200 kW *DC furnace demonstration -Manganese reduction option and flowsheet development.* Internal Mintek Report: Unpublished.

Borra, C. R., Pontikes, Y., Binnemans, K., & Van Gerven, T. (2015). Leaching of rare earths from bauxite residue (red mud). *Minerals Engineering*, 76, 20-27

Castor, S. B., & Hedrick, J. B. (2006). Rare earth elements. *Industrial minerals and rocks*, 769-792.

Charalampides, G., Vatalis, K. I., Apostoplos, B., & Ploutarch-Nikolas, B. (2015). Rare earth elements: industrial applications and economic dependency of Europe. *Procedia Economics and Finance*, *24*, 126-135.

Chen, W., Honghui, H., Bai, T., & Jiang, S. (2017). Geochemistry of monazite within carbonatite related REE deposits. *Resources*, *6*(4), 51.

Chhabra, R. P., & Gurappa, B. (Eds.). (2019). *Coulson and Richardson's Chemical Engineering: Volume 2A: Particulate Systems and Particle Technology*. Butterworth-Heinemann.

Cocco, R., Karri, S. R., & Knowlton, T. (2014). Introduction to fluidization. *Chem. Eng. Prog*, *110*(11), 21-29.

Coudurier, L., Hopkins, D. W., & Wilkomirsky, I. (2013). Fundamentals of Metallurgical Processes: *International Series on Materials Science and Technology (Vol. 27*). Elsevier.

De Lima, I. B., & Leal Filho, W. (Eds.). (2015). *Rare earths industry: Technological, economic, and environmental implications*. Elsevier.

Demol, J., Ho, E., Soldenhoff, K., & Senanayake, G. (2019). The sulfuric acid bake and leach route for processing of rare earth ores and concentrates: a review. *Hydrometallurgy*, *188*, 123-139.

Ding, Y., Xue, Q., Wang, G., & Wang, J. (2013). Recovery behavior of rare earth from Bayan Obo complex iron ore. *Metallurgical and Materials Transactions B*, *44*(1), 28-36.

Faris, N., Ram, R., Tardio, J., Bhargava, S., McMaster, S., & Pownceby, M.I. (2017). Application of ferrous pyrometallurgy to the beneficiation of rare earth bearing iron ores – A review. *Minerals Engineering*,110, 20-30.

Folayan, C. O., Pam, G. Y., & Habib, Y. B. (2015) Fluidised Bed Combustion: Towards Alternative Ways of Energy Recovery in Rural Nigeria.

Generalic, Eni. Rare Earth Elements (REE). (2020). *EniG. Periodic Table of the Elements.* https://www.periodni.com/rare_earth_elements.html. (date accessed 22-04-2020).

Gao, P., Han, Y. X., Li, Y. J., & Ma, W. Y. (2010). Fundamental research in comprehensive utilization of Bayan Obo ore by direct reduction. In *Advanced Materials Research* (Vol. 92, pp. 111-116). Trans Tech Publications Ltd.

Gao, P., Han, Y., & Wu, H. (2010). Research on reduction-magnetic separation of Bayan Obo ore. In *XXV International Mineral Processing Congress 2010 Proceedings* (pp. 1541-1547).

Gao, P., Sun, Y., Ren, D., & Han, Y. (2013). Growth of metallic iron particles during coal-based reduction of a rare earths-bearing iron ore. *Mining Metallurgy & Exploration, 30(1)*, 74-78.

Geldart, D. (1973). Types of gas fluidization. *Powder technology*, *7*(5), 285-292.

Gmelin, L. (1978). *Gmelin Handbuch der anorganischen Chemie: Seltenerdelemente. Sc, Y, La-Lu. Die Elemente: Scandium, Yttrium, Lanthan und Lanthanide. Sc, Y, La und Lanthanide: Darstellung, Anreichnung und Abtrennung der Isotope (Eu bis Lu); Nachweis und Bestimmung der Isotope; Chemisches Verhalten des Elemente*. Springer-Verlag.

Goodenough, K. M., Wall, F., & Merriman, D. (2018). The rare earth elements: demand, global resources, and challenges for resourcing future generations. *Natural Resources Research*, *27*(2), 201-216.

GUO, M. (1979). Fluidized roasting of oxidic Chinese iron ores. *Scientia Sinica, 22(11)*, 1265-1291.

Güntner, J., & Hammerschmidt, J. (2012). Sulphating roasting of copper-cobalt concentrates. *Journal of the Southern African Institute of Mining and Metallurgy*, *112*(6), 455-460.

Habashi, F. (2003). Review: textbook of pyrometallurgy. *Russian Journal of Applied Chemistry*, *76*, 337.

Habashi, F. (2013). Extractive metallurgy of rare earths. *Canadian Metallurgical Quarterly, 52(3)*, 224-233.

Habashi, F. (2017). Principles of extractive *metallurgy*. Routledge.

Haque, N., Hughes, A., Lim, S., & Vernon, C. (2014). Rare earth elements: Overview of mining, mineralogy, uses, sustainability, and environmental impact. *Resources, 3(4)*, 614-635.

Haxel, G. (2002). *Rare earth elements: critical resources for high technology* (Vol. 87, No. 2). US Department of the Interior, US Geological Survey.

Hower, J. C., Granite, E. J., Mayfield, D. B., Lewis, A. S., & Finkelman, R. B. (2016). Notes on contributions to the science of rare earth element enrichment in coal and coal combustion byproducts. *Minerals*, *6*(2), 32.

Humphries, M. (2013). Rare earth elements: the global supply chain.

Iwasaki, I., & Prasad, M.S. (1989). Processing techniques for difficult-to-treat ores by combining chemical metallurgy and mineral processing. *Mineral Processing and Extractive Metallurgy Review, 4(3-4)*, 241-276.

Jackson, W., & Christiansen, G. (1993). US Geological Survey Circular 930-N. *International Strategic Minerals Inventory Summary Report–Rare Earth Oxides.*

Janoš, P., Kuráň, P., Ederer, J., Šťastný, M., Vrtoch, L., Pšenička, M., ... & Skoumal, M. (2015). Recovery of cerium dioxide from spent glass-polishing slurry and its utilization as a reactive sorbent for fast degradation of toxic organophosphates. *Advances in Materials Science and Engineering*, *2015*.

Jepson, N. (2012). A 21st century scramble: South Africa, China and the rare earth metals industry.

Jha, M. K., Kumari, A., Panda, R., Kumar, J. R., Yoo, K., & Lee, J. Y. (2016). Review on hydrometallurgical recovery of rare earth metals. *Hydrometallurgy*, 165, 2-26.

Jordens, A., Cheng, Y. P., & Waters, K. E. (2013). A review of the beneficiation of rare earth element bearing minerals. *Minerals Engineering*, *41*, 97-114.

KATO, K., KANBARA, S., TAJIMA, T., SHIBASAKI, H., OZAWO, K., & TAKARADA, T. (1987). Effect of particle size on elutriation rate constant for a fluidized bed. *Journal of chemical engineering of Japan, 20(5),* 498-504.

Kellogg, H., & Basu, S. K. (1960). Thermodynamic properties of the system lead-sulfuroxygen to 1100 K. *Trans Metall Soc AIME*, 218, 70-81.

Khan, A. (1968). MSc thesis. *Bradford University.*

Kim, E., & Osseo-Asare, K. (2012). Aqueous stability of thorium and rare earth metals in monazite hydrometallurgy: Eh–pH diagrams for the systems Th–, Ce–, La–, Nd–(PO4)–(SO4)–H2O at 25 C. *Hydrometallurgy*, 113, 67-78.

King, H. M. (2013). REE–rare earth elements and their uses. *Geoscience News and Information*.

Koltun, P., & Tharumarajah, A. (2014). Life cycle impact of rare earth elements. *ISRn Metallurgy*, *2014*.

Komatina, M., & GUDENAU, H. W. (2018). The sticking problem during direct reduction of fine iron ore in the fluidized bed. *Metallurgical and Materials Engineering*.

Krishnamurthy, N., & Gupta, C. K. (2015). *Extractive metallurgy of rare earths*. CRC press.

Kunii, D., & Levenspiel, O. (2013). *Fluidization engineering*. Elsevier.

Liu, Y., Liu, Z. Z., & Liu, M. D. (2014). Decomposition process of rare earth rough concentrate by low temperature sulfation. *Chinese Journal of Nonferrous Metals*, *24*(12), 3147.

Lucas, J., Lucas, P., Le Mercier, T., Rollat, A., & Davenport, W. G. (2014). *Rare earths: science, technology, production, and use*. Elsevier.

Ma, E. (2019). Recovery of Waste Printed Circuit Boards Through Pyrometallurgy. *Electronic Waste Management and Treatment Technology*, 247-267

Malaysia, A. S., & Negara, M. P. (2011). Rare Earth Industries: Moving Malaysia's Green Economy Forward. *Akademi Sains Malaysia, Academy of Sciences. Malaysia: Kuala Ltunptu·, Malaysia.*

Matinde, E., & Hino, M. (2011). Dephosphorization treatment of high phosphorus iron ore by pre-reduction, mechanical crushing, and screening methods. *ISIJ international*, *51*(2), 220-227.

Moodley, S. (2011). *A study of the chlorination behaviour of various titania feedstocks* (Doctoral dissertation).

Morris, A. E. (2001). Iron Resources and Direct Iron Production.

Norgate, T., & Jahanshahi, S. (2011). Assessing the energy and greenhouse gas footprints of nickel laterite processing. *Minerals Engineering, 24 (7),* 698-707.

Pell, M. (2012). *Gas fluidization*. Elsevier.

Poston Jr, J. A., Siriwardane, R. V., Fisher, E. P., & Miltz, A. L. (2003). Thermal decomposition of the rare earth sulfates of cerium (III), cerium (IV), lanthanum (III) and samarium (III). *Applied surface science*, *214*(1-4), 83-102.

Pozo-Gonzalo, C. (2021). Demand for rare-earth metals is skyrocketing, so we're creating a safer, cleaner way to recover them from old phones and laptops. *The Conversation, Academic rigour, journalistic flair.* Retrieved from URL https://theconversation.com/demand-for-rare-earth-metals-is-skyrocketing-so-were-creating-a-safer-cleaner-way-to-recover-them-from-old-phones-and-laptops-141360.

Qi, D. (2018). *Hydrometallurgy of Rare Earths: Extraction and Separation*. Elsevier.

Reuter, M. A., Krüger, J., Dong, Y., & Yang, T. (1994). Direct reduction during the production of ferroniobium in an electric furnace. *Minerals Engineering*, *7*(2-3), 279-292.

Rhodes, M. J. (Ed.). (2008). *Introduction to particle technology*. John Wiley & Sons.

Ross, H. U. (1973). The fundamental aspects of iron ore reduction.

Sadri, F., Nazari, A.M. and Ghahreman, A. (2017). A Review on the Cracking, Baking and Leaching Processes of Rare Earth Element *Concentrates. Journal of Rare Earths, 35 (8),* 739–752.

Schulz, K. J., DeYoung, J. H., Seal, R. R., & Bradley, D. C. (Eds.). (2018). *Critical Mineral Resources of the United States: Economic and Environmental Geology and Prospects for Future Supply*. Geological Survey.

Schwartz, D., Gadiou, R., Brilhac, J. F., Prado, G., & Martinez, G. (2000). A kinetic study of the decomposition of spent sulfuric acids at high temperature. *Industrial & engineering chemistry research*, *39*(7), 2183-2189.

Shamsuddin, M., & TMS. (2016). *Physical chemistry of metallurgical processes* (p. 71). Wiley, TMS.

Sithole, P., Goso, X.C., and Lagendijk, H. (2017). Laboratory-scale sulphation roasting testwork for copper and cobalt production. *The Southern African Institute of Mining and Metallurgy.* 485-496.

Sohn, H. Y., & Goel, R. P. (1979). Principles of roasting. *Min. Sci. Eng.*, 11(3), 137-153.

Soltani, F., Abdollahy, M., Petersen, J., Ram, R., Becker, M., Koleini, S. J., & Moradkhani, D. (2018). Leaching and recovery of phosphate and rare earth elements from an iron-rich fluorapatite concentrate: Part I: Direct baking of the concentrate. *Hydrometallurgy*, *177*, 66-78.

Tagawa, H. (1984). Thermal decomposition temperatures of metal sulfates. *Thermochimica acta*, *80*(1), 23-33.

Takagi, T., (2012). The modes of occurrence of rare-earths ores and the issues on their beneficiation processes. In *EGU General Assembly Conference Abstracts* (Vol. 14, p.9271).

Takeno, N. (2005). Atlas of Eh-pH diagrams, Intercomparison of thermodynamic databases, Geological Survey of Japan Open File Report No. 419, National Institute of Advanced Industrial Science and Technology. *Research Center for Deep Geological Environments*, *219*.

Tan, Q., Li, J., & Zeng, X. (2015). Rare earth elements recovery from waste fluorescent lamps: a review. *Critical Reviews in Environmental Science and Technology*, *45*(7), 749-776.

Teixeira, L. A. V., Silva, R. G., Avelar, A., Majuste, D., & Ciminelli, V. S. (2019). Selective extraction of rare earth elements from monazite ores with high iron content. *Mining, Metallurgy & Exploration*, *36*(1), 235-244.

Thomas, K. G., & Cole, A. P. (2016). Roasting developments–Especially oxygenated roasting. *In Gold Ore Processing* (pp. 373-392). Elsevier.

UNCTAD, W. (2014). United nations conference on trade and development. *Commodities at a glance. Special issue on rare earths*. (6).

Uwadiale, G. G. O. O. (1992). Magnetizing reduction of iron ores. *Mineral Processing and Extractive Metullargy Review*, *11*(1-2), 1-19.

Verbaan, N., Bradley, K., Brown, J., & Mackie, S. (2015). A review of hydrometallurgical flowsheets considered in current REE projects. In *Symposium on Critical and Strategic Materials* (pp. 147-162). British Columbia Ministry of Energy and Mines, Victoria, British Columbia.

Xie, F., Zhang, T. A., Dreisinger, D., & Doyle, F. (2014). A critical review on solvent extraction of rare earths from aqueous solutions. *Minerals Engineering*, *56*, 10-28.

Yang, H., Rong, Y., Tang, R., Xue, X. X., & Li, Y. (2013). Recovery of iron from Baotou rare earth tailings by magnetizing roast. *Rare Metals*, *32*(6), 616-621.

Yokogowa. (n.d). *Technical Information: Overview Rotameter* (Report No. TI 1R1A0-E-H). Retrieved from https://web-material3.yokogawa.com/product_TIRotameterEnged4.us.pdf

You, Z., Li, G., Zhang, Y., Peng, Z., & Jiang, T. (2015). Extraction of manganese from iron rich MnO2 ores via selective sulfation roasting with SO2 followed by water leaching. *Hydrometallurgy*, *156*, 225-231.

Yuan, S., Yang, H., Xue, X. X., & Zhou, Y. (2017). Kinetics of roasting decomposition of the rare earth elements by CaO and coal. *Metals*, *7*(6), 213.

Zhang, J., & Edwards, C. (2012, January). A review of rare earth mineral processing technology. *In 44th Annual Meeting of The Canadian Mineral Processors. Ottawa* (Vol. 1101, pp. 79-102).

Zhang, Z., Jia, Q., & Liao, W. (2015). Progress in the separation processes for rare earth resources. In *Handbook on the physics and chemistry of rare earths* (Vol. 48, pp. 287-376). Elsevier.

Zhang, B., Liu, C., Li, C., & Jiang, M. (2016). Separation and recovery of valuable metals from low-grade REE–Nb–Fe ore. *International Journal of Mineral Processing*, *150*, 16-23.

Zhang, J., Zhao, B., & Schreiner, B. (2016). *Separation hydrometallurgy of rare earth elements* (p. 259). Switzerland: Springer International Publishing.

Zhao, L., Wang, L., Shuai, G., Long, Z., Cui, D., & Huang, X. (2018). Thermal decomposition and oxidation of bastnaesite concentrate in inert and oxidative atmosphere. *Journal of Rare Earths*, *36*(7), 758-764.

Zheng, X. P., & Lin, H. K. (1994). Mineralogy and flotation of rare-earth-bearing barium fluorophlogopite. *Minerals engineering*, *7*(12), 1495-1503.

APPENDICES

APPENDIX A: EQUIPMENT USED FOR SAMPLE PREPARATION

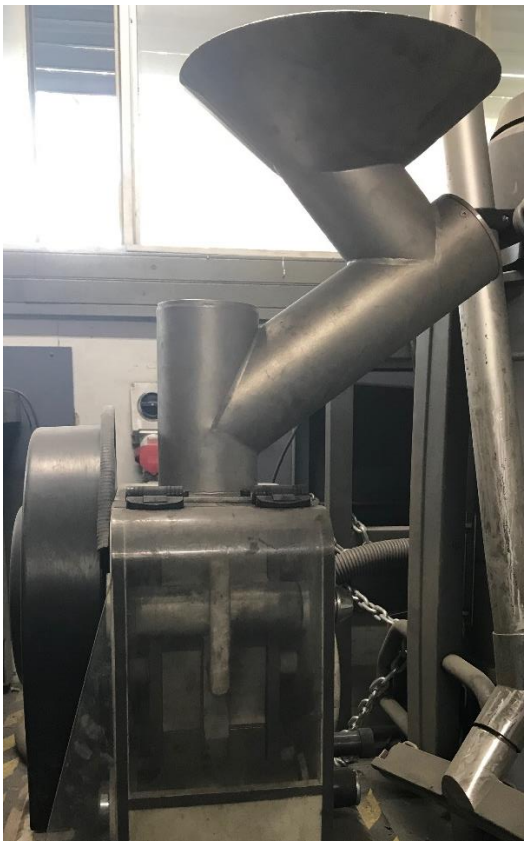


Figure 0.1. Picture of the jaw crusher used in the test work.



Figure 0.2. Picture of the Sieb Technik Mill and a sample bowl with the ZKD ore.



Figure 0.3. A picture of the riffle splitter used for sampling the materials.



Figure 0.4. A picture of the vibrating sieve shaker and woven wire sieves used for the sizing of the samples.

The bulk density of the head samples was determined by weighing 50 g sample from the head samples into a volumetric cylinder. The volume that each material occupied was recorded and used to calculate the density using **equation (0.1)**.

$$\rho = \frac{\text{mass of material (g)}}{\text{volume occupied (cm}^3\text{)}} \qquad (0.1)$$

APPENDIX B: ROTAMETER MEASUREMENT PRINCIPLE

Rotameters are used to measure the flow of liquids and gases in pipes and sheathed lines. These devices are attractive as they have:

- simple measurement principle,
- an uncomplicated design and are low maintenance,
- are suitable for continuous processes,
- are cost effective, have a high efficiency and accuracy,
- allow for the visual evaluation of the measured fluid.

The rotameter consists of a float that is installed in a vertical tube whose diameter gradually widens towards the top. The measured fluid flows vertically around the fluid. The float is raised according to the flowrate, leaving a certain gap between it and the walls of the tube. The position of the float stabilizes under a constant flowrate of the fluid. At this point the sum of the forces operating on the float are zero and the flow rate can be determined from the height of the float. Due to prevailing physical relationships the measurement technique is dependent on the density, viscosity, and temperature of the medium. Exact results can be assumed only if the characteristics of the fluid medium remain constant (Yokogawa, n.d).

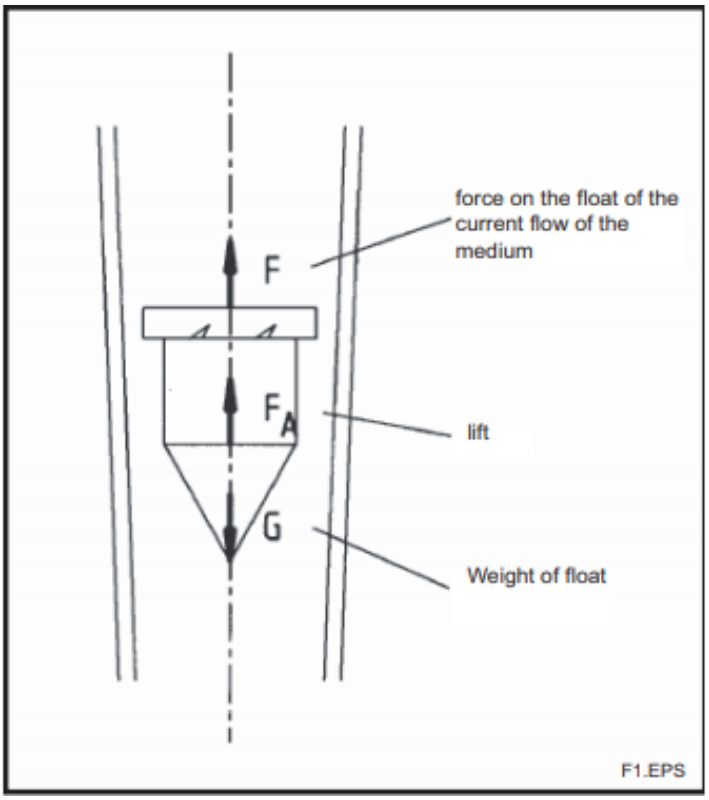


Figure 0.5. Rotameter measurement principle (Yokogawa, n.d).

APPENDIX C: EXPERIMENTAL SETUP FOR FLUIDIZED SULFATION ROASTING STUDIES



Figure 0.6. Extraction system utilised during the sulfation roasting experiments.



Figure 0.7. Data logger used to monitor the sample bed temperature through the K-type thermocouple.

APPENDIX D: SAFETY, HEALTH AND ENVIRONMENTAL

CeO_2 and $Ce_2(SO_4)_3$, ZKD ore and PyEarth slag

CeO_2 is an acutely toxic material. Exposure to CeO_2 can cause respiratory tract, skin, and eye irritation. Exposure to $Ce_2(SO_4)_3$ can cause skin and respiratory irritation as well as serious eye irritations. The REE bearing resources (ZKD ore and PyEarth slag) contained minimal amounts of radioactive metals (Th and U) and were therefore grouped as non-radioactive materials.

- Dust masks, goggles, gloves, and PPE were utilised when handling these powders.
- Labs had adequate ventilation for dust formation and fume hoods were used when handling the material.
- All staff handling the REE-bearing resources were expected to wear a TLD radiation badge, where the amount of radiation exposure was measured monthly.

$Fe_2(SO_4)_3$

$Fe_2(SO_4)_3$ is a corrosive chemical which is harmful or fatal if swallowed. The chemical is toxic by ingestion; may cause irritation to the mouth and stomach. Higher doses may lead to abnormal liver function. $Fe_2(SO_4)_3$ inhalation may cause irritation of the upper respiratory tract, mucous membrane, and lung tissues, resulting in difficulty in breathing. Exposure to the skin and eyes may result in severe burns.

Safety measures:

- Appropriate PPE: including a respirator, gloves, safety glasses and boots were worn by personnel throughout the study.
- The lab area had adequate ventilation; and a fume hood was used while handling the material.

Sulfur dioxide (SO_2)

Exposure to SO_2 either by inhalation, swallowing or skin contact is dangerous and precautions were taken to reduce the risk of contact during the study. Inhalation of the gas is the most harmful route of exposure. The severity of the gas on health effects is dependent on the dosage and duration of exposure. The common symptoms of exposure are throat irritation, coughing, constriction of the chest and smarting of the eyes.

Safety measures:

- The pipes and connections were tested for leaks prior to the start of every experiment.

- The labs were equipped with detectors for detection of any leaks. When unsafe levels of the gas were detected, the gas supply was immediately shut down.
- All staff working in the facility were equipped with mini gas detectors attached to their PPE for early detection of any leaks.
- All staff handling the gas were equipped with a respirator and PPE, which includes chemical safety goggles and a face shield, boots, imperious gloves, and coveralls.

N_2 and O_2

Nitrogen and oxygen are gas invisible. N_2 gas becomes more reactive at elevated temperatures. Inhalation the gas in excessive concentrations can result in dizziness, nausea, vomiting, loss of consciousness and death. Exposure to O_2 gas can cause toxicity to the central nervous system shown by dizziness, convulsions, and loss of consciousness. Heating of these gases will cause their pressure to rise which can result in bursting.

- Suitable PPE including safety goggles, boots, imperious gloves, coveralls, and respiratory protection were worn throughout the study.

The labs were equipped with detectors for detection of any leaks. When unsafe levels of the gas were detected, the gas supply was immediately shut down.

APPENDIX E: PREDOMINANCE PHASE DIAGRAMS

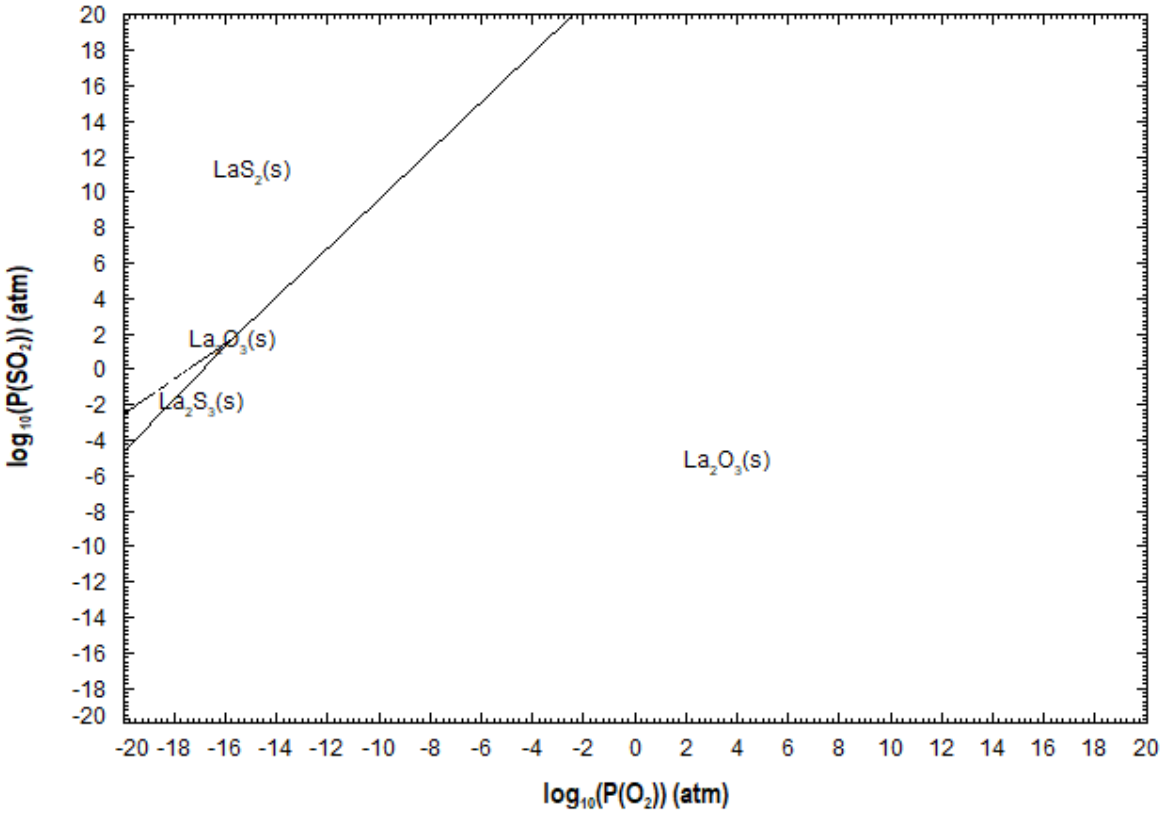


Figure 0.8. Predominance diagram for La–O–S system at 600°C.

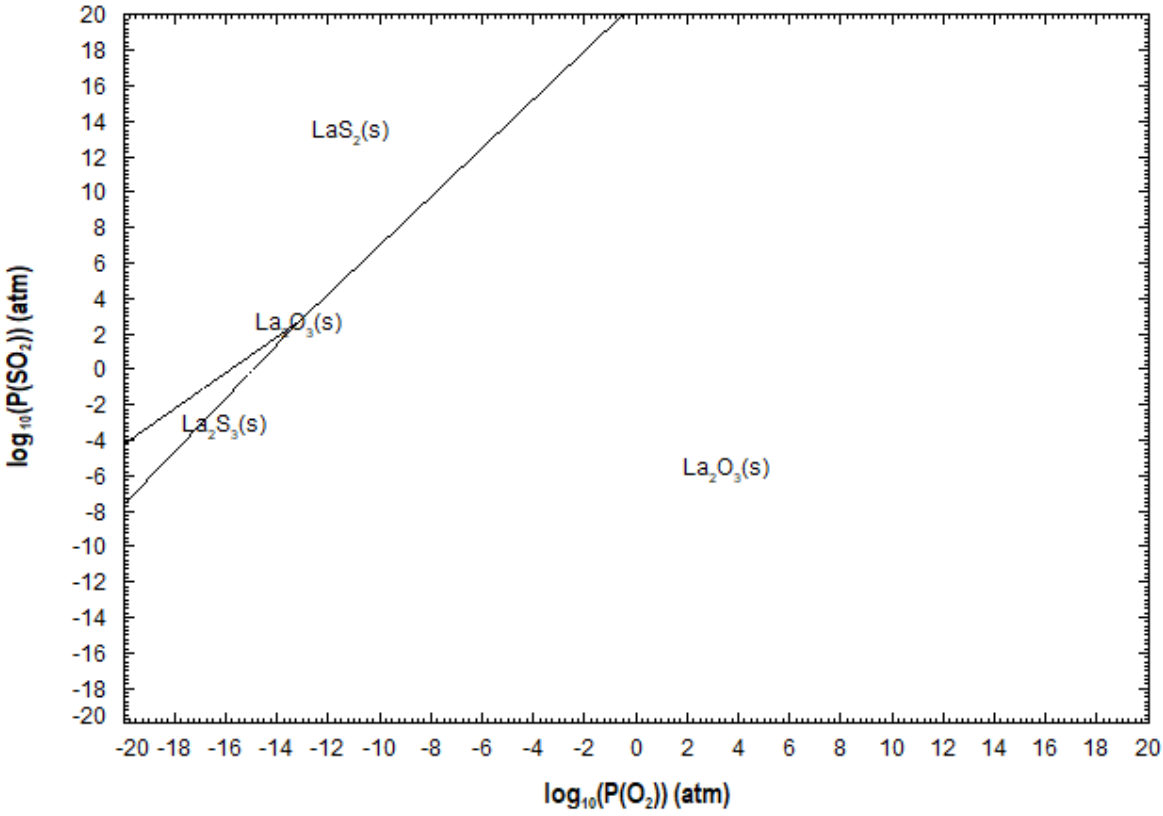


Figure 0.9. Predominance diagram for La–O–S system at 700°C.

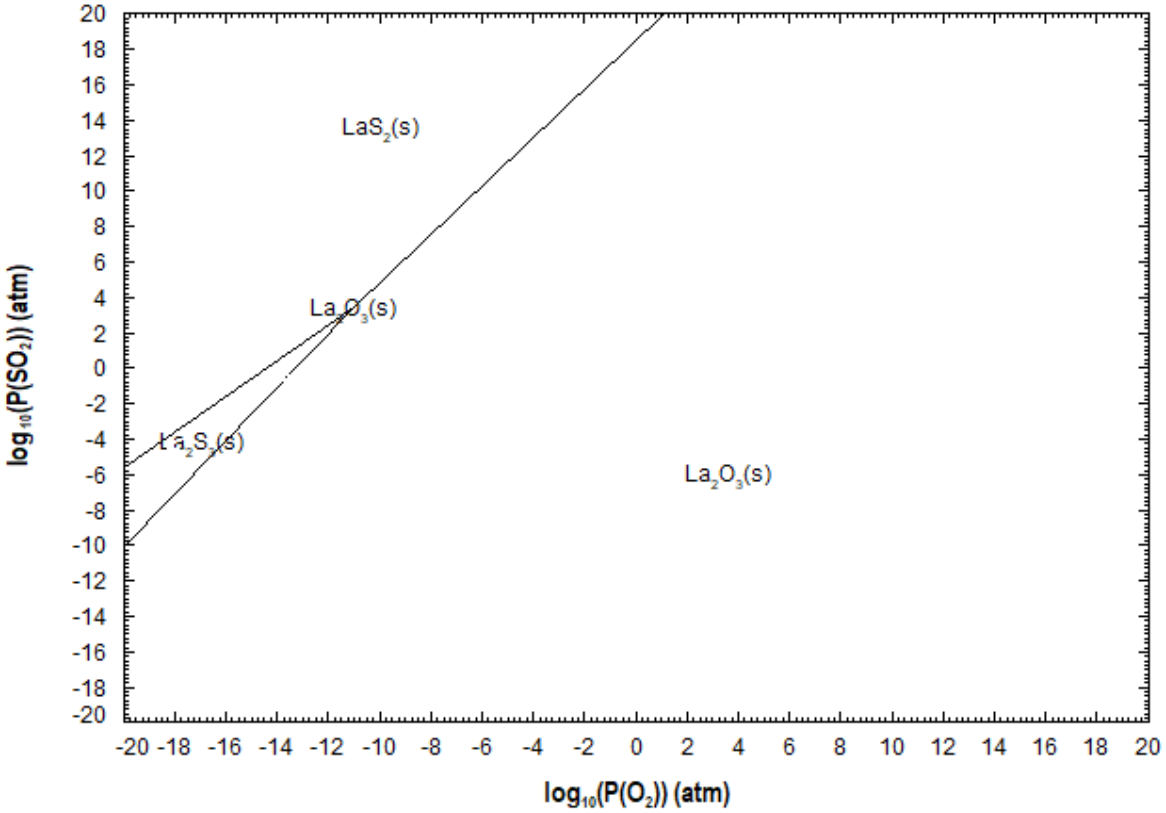


Figure 0.10. Predominance diagram for La–O–S system at 800°C.

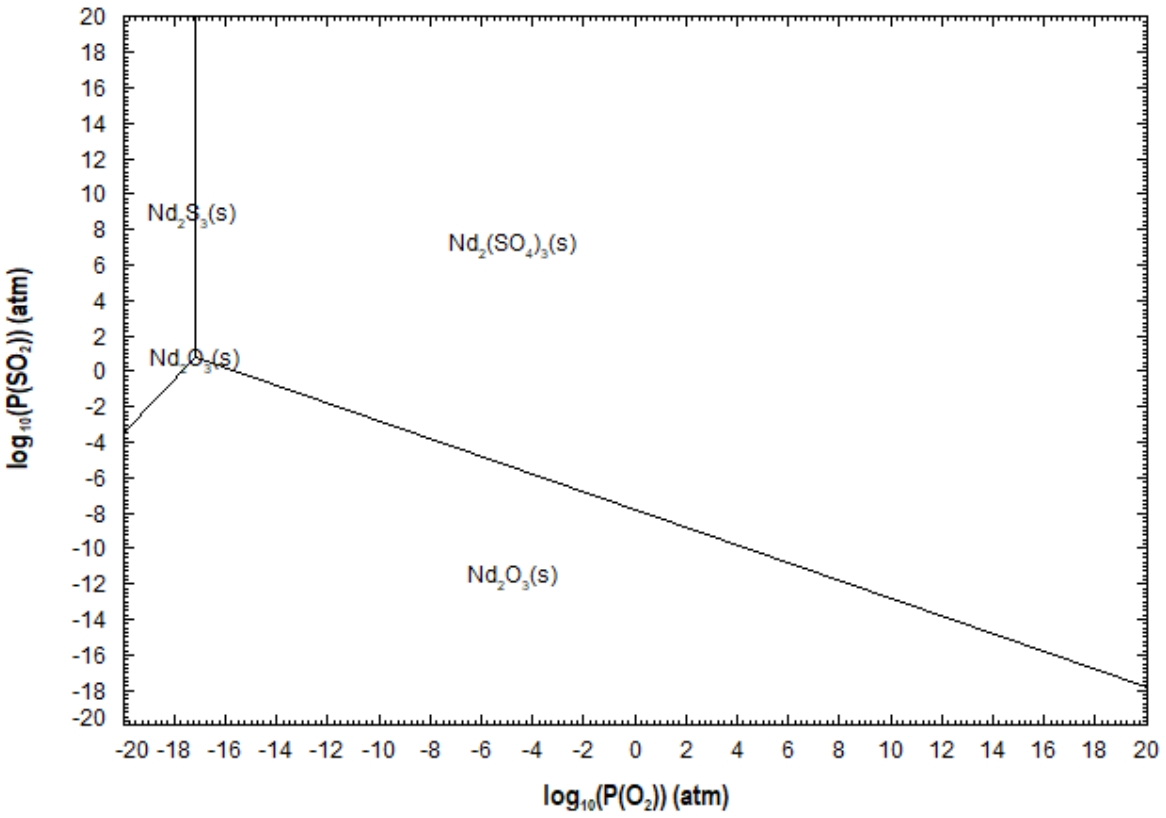


Figure 0.11. Predominance diagram for Nd–O–S system at 600°C.

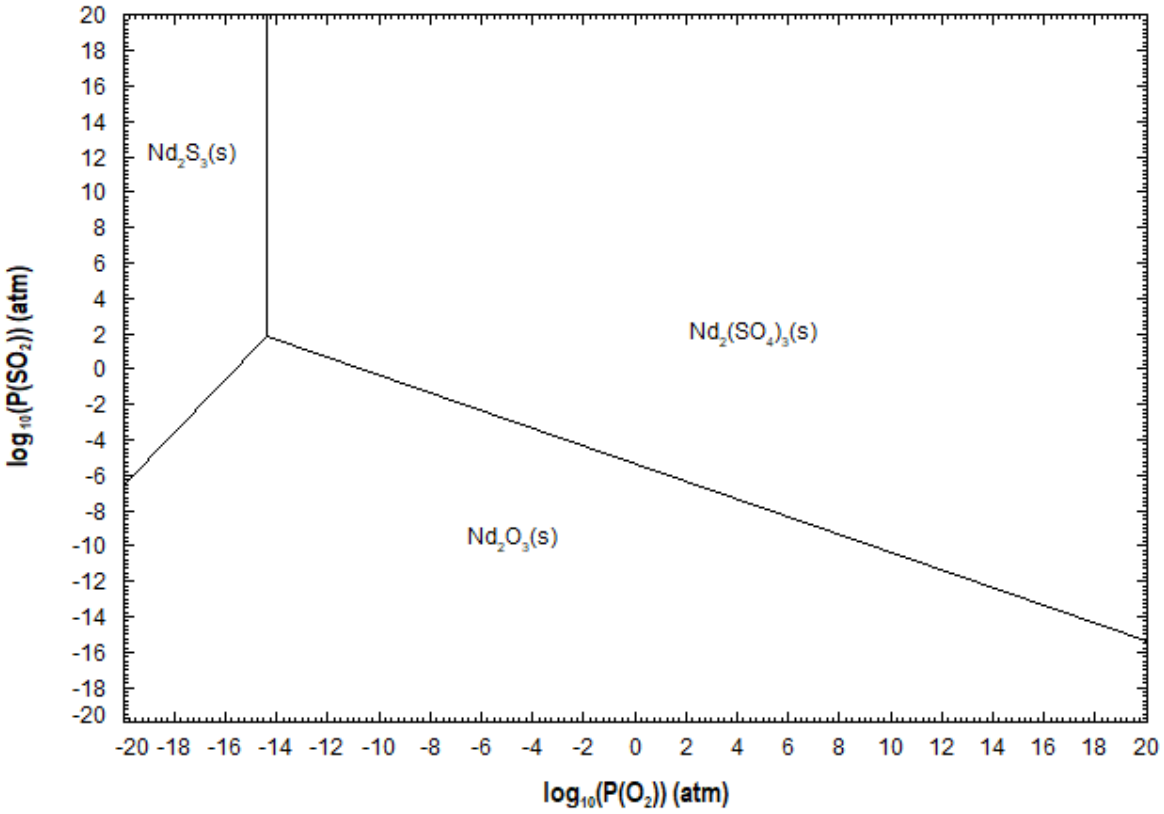


Figure 0.12. Predominance diagram for Nd–O–S system at 700°C.

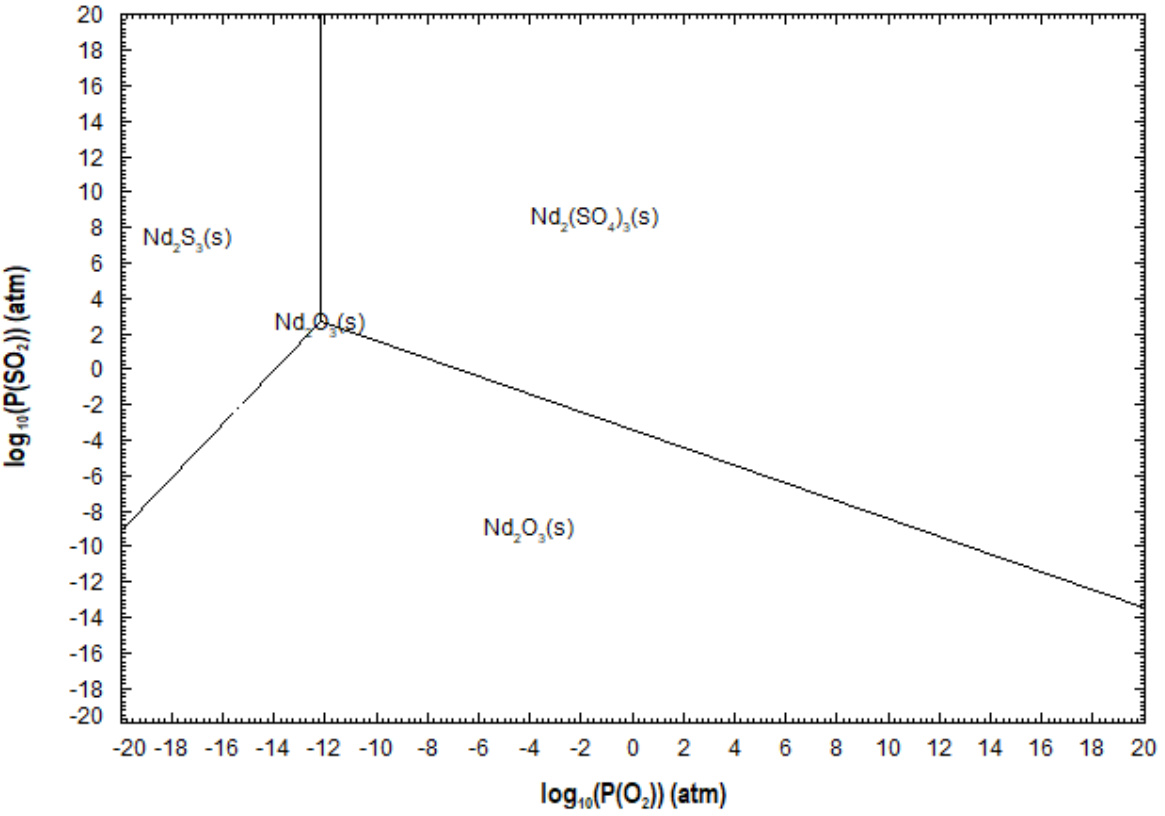


Figure 0.13. Predominance diagram for Nd–O–S system at 800°C.

APPENDIX F: PRELIMINARY SULFATION ROASTING-LEACHING MASS BALANCES

Table 0.1. Mass Balance for Preliminary Sulfation Roasting studies.

Test No.	Test Material	Sample Description	Mass of Feed (g)	pH (initial)	pH (end)	Ce in Feed (g)	Ce in Leach Liquor (g)	Leaching efficiency (solution based)
1	CeO_2	24 h, 630°C	5.13	3.90	3.48	2.38	1.34	56
2		48 h, 630°C	5.90	3.59	3.47	2.78	1.32	47
3		24 h, 700°C	6.53	3.18	3.36	3.03	2.69	89
4		48 h, 700°C	7.53	3.67	3.48	3.93	3.04	77
5		24 h, 750°C	8.06	3.76	3.40	3.71	2.23	60
6		48 h, 750°C	7.35	4.01	3.97	3.26	1.47	45
7		24 h, 800°C	8.54	4.36	3.83	4.03	2.26	56
8		48 h, 800°C	6.32	4.36	3.83	3.06	1.79	59

Table 0.2. Mass Balance for the Stability Tests.

Test No.	Test Material	Sample Description	Mass of Feed (g)	pH (initial)	pH (end)	Feed		Leach liquor		Leaching efficiency	
						Ce (g)	Fe (g)	Ce (g)	Fe (g)	Ce (%)	Fe (%)
9	$Ce_2(SO4)_3$-$Fe_2(SO_4)_3$ (1:1 mass ratio)	24 h, 750°C	2.31	1.78	1.83	0.99	0.508	0.742	0.004	75	1

APPENDIX G: FLUIDIZATION PARAMETERS

Terminal velocity

Terminal velocity (or free-fall velocity) of a particle in a fluid bed is the maximum allowable velocity of a particle moving through a fluid. The terminal velocity (U_t) is important in fluidization because it helps select the suitable gas velocity utilised during fluidization. The terminal velocity (U_t) for the various size fractions in the head samples were determined using Equation 6.2 and the results are summarized in **Table 0.3**. Operating at gas velocities that are higher than the terminal velocity will result in the particles being carried upward with the gas stream.

The gas velocity used in the fluidized sulfation roasting studies should be a value above the minimum fluidization velocity but below the terminal velocity of the smallest particles (Moodley., 2011). The minimum fluidization velocity was utilised for the fluidized sulfation roasting studies. The U_{mf} utilised for the ZKD ore, 9.94 cm/s, was higher than the U_t of all the particles except for the 600 µm particles. The U_{mf} utilised for the PyEarth ™, 23.88 cm/s, was higher than the U_t of all the particle sizes. The effect of the U_{mf} on the particles was further investigated in the elutriation section.

$$u_t = g{d_p}^2 \frac{(\rho_s - \rho_g)}{18\mu} \quad (0.1)$$

u_t = terminal velocity (cm/s)

g = gravitational constant ($cm^3.g^{-1}.s^{-2}$)

d_p = average particle diameter (cm)

ρ_s = solid density (g/cm^3)

ρ_g = gas density (g/cm^3)

μ = gas viscocity (g/cm. s)

Table 0.3. Terminal Velocity of the head samples.

Particle size (µm)	ZKD Ore (cm/s)	PyEarth ™ Slag (cm/s)
600	16.47	19.25
425	8.26	9.66
300	4.12	4.81
212	2.06	2.40
150	1.03	1.20
106	0.51	0.60

Elutriation Rate Constants

When particles with a wide size distribution are fluidized, the fine particles are carried over from the fluidized bed with the gas stream if the gas velocity exceeds the terminal velocities of the particles. Elutriation from a fluidized bed is the ejection of particles from the bed surface due to the bursting of the bubbles (KATO et al., 1987). The elutriation constant ($kg/m^2.s$) gives an indication of the tendency of a particular material/ size fraction to be blown out of the reactor. The values presented in **Table 0.4 and 0.5** were obtained for the initial PSD and the PSD after 1 hour of fluidization at ambient temperatures using N_2 gas as the fluid.

Table 0.4. Experimental data for the ZKD ore elutriation calculation.

Initial mass of sample = 51.04 grams		**Blow over = 6.05 grams**	
Particle size distribution			
Size (µm)	**Mass (grams)**	**Size (µm)**	**Mass (grams)**
-600+425	4.40	-600+425	-
-425+300	6.63	-425+300	-
-300+212	5.49	-300+212	-
-212+150	5.42	-212+150	0.28
-150+106	4.68	-150+106	1.28
-106	24.42	-106	4.25

Table 0.5. Experimental data for the PyEarth ™ slag elutriation calculation.

Initial mass of sample = 50.71 grams		**Blow over = 3.49 grams**	
Particle size distribution			
Size (µm)	**Mass (grams)**	**Size (µm)**	**Mass (grams)**
-600+425	19.46	-600+425	-
-425+300	16.55	-425+300	-
-300+212	8.26	-300+212	-
-212+150	4.52	-212+150	1.42
-150+106	0.81	-150+106	0.73
-106	1.38	-106	1.34

From the elutriation studies of the two materials the highest blow-over was experienced for the ZKD ore. This was expected as the ZKD ore had the highest mass fraction of fine material, i.e. <212 µm, at the beginning of the elutriation studies. Finer particles, i.e. -106 µm, have the highest tendency to be elutriated and this trend is seen in both materials. Small fractions of the ZKD ore and PyEarth ™ slag particles in -212 +150 µm size range were also elutriated while larger particles (>300 µm) were not elutriated.

From literature, it was found that the particle size and fines content influence fluidization mechanisms and behaviours. Although this is the case, the effect of fines content is not easy to explain as it is dependent on several factors, such as the type of material, fraction of the fines, and particle size of the fines to name a few . Sun & Grace., (1990), investigated the effect of particle size distribution on fluidization using materials that had similar d_{50} and a varying PSD (i.e. narrow, wide, and bimodal) within the same size range (-130 + 20µm). It was found that the wide particle distribution, like the size distribution utilised in this study, resulted in the highest conversion rate, smallest voids and largest bed expansion. Meanwhile, Baeyans et al., (1992) and George and Grace (1978), found that the entrainment of particles is a result of bubbles bursting at the bed surface.

Elutriation constants were determined using Equation 6.3 and the calculated values are summarized in **Table 0.6**.

$$\frac{W_i}{W_{io}} = exp\left(-\frac{k_i^* At}{W}\right) \quad (0.2)$$

W_{io} = Initial weight of mass fraction i

W_i = Final weight of mass fraction i

W = Total weight of sample before fluidization

A = Area of reactor (m^2)

t = Time (s)

K_i^* = elutriation constant ($kg/m^2.s$)

Elutriation constants are proportional to the weight of the material that is being removed from the fluidized bed. Smaller size fractions are more likely to be elutriated than larger particles. Although this is the case, this trend was not observed for the two head sample materials because they had higher elutriation rates associated with the larger particle size range. The ZKD ore had higher elutriation constants at all the particle size ranges than the PyEarth ™ slag, which is a result of the high fine contents in the material as well as its density.

Table 0.6. Elutriation Constants.

Elutriation Constants (kg/m.s)		
Size Fraction	**ZKD Ore**	**PyEarth ™ Slag**
-212+150	0.04	0.02
-150+106	0.02	1.44×10^{-3}
-106	0.02	4.01×10^{-3}

APPENDIX H: SULFATION ROASTING BED SAMPLES XRD ANALYSIS

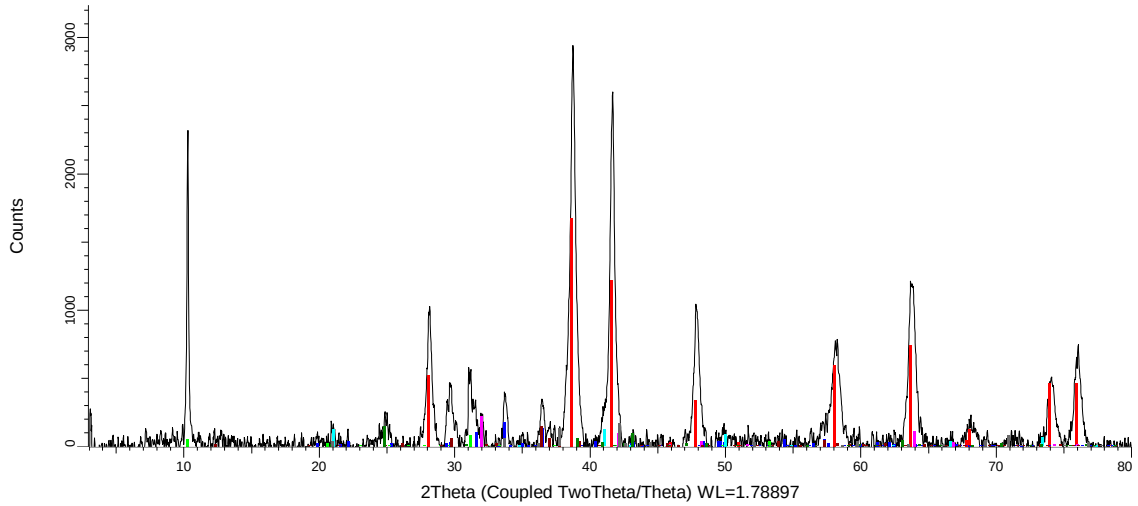


Figure 0.14. X-ray diffraction pattern for the ZKD ore sulfated in a O_2 depleted atmosphere at 600°C.

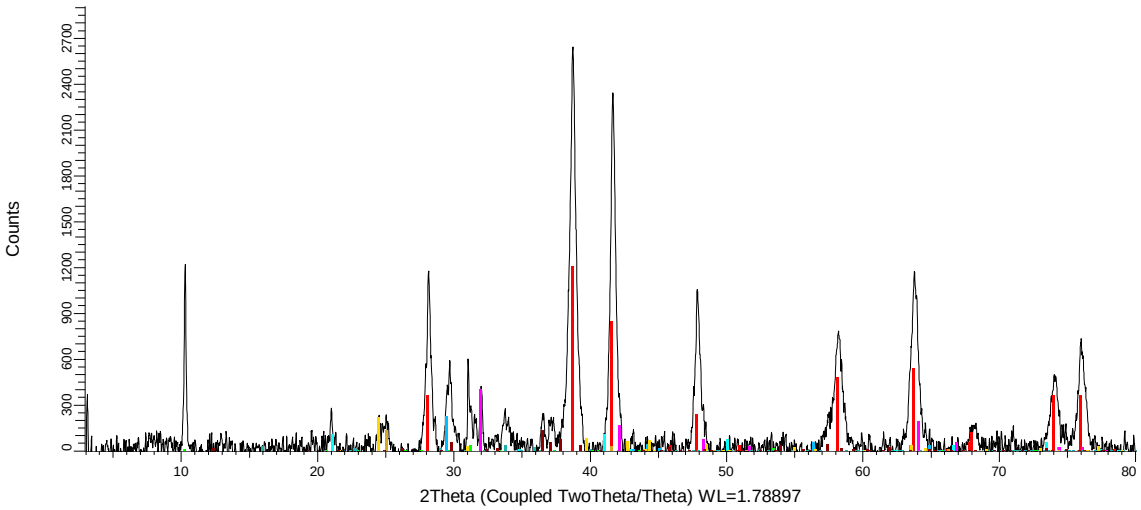


Figure 0.15. X-ray diffraction pattern for the ZKD ore sulfated in a O_2 depleted atmosphere at 700°C.

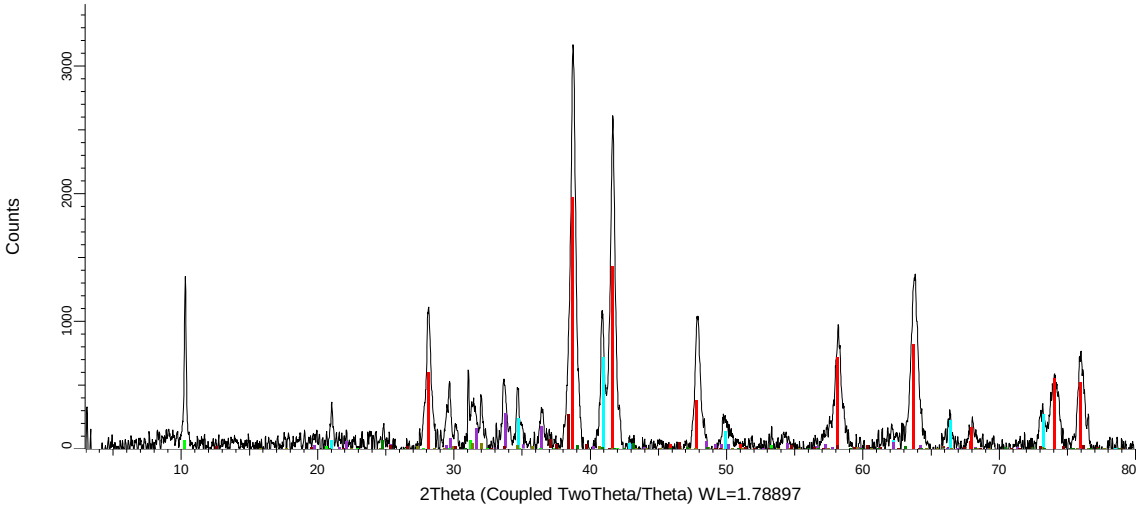


Figure 0.16. X-ray diffraction pattern for the ZKD ore sulfated in a O_2 depleted at 800°C.

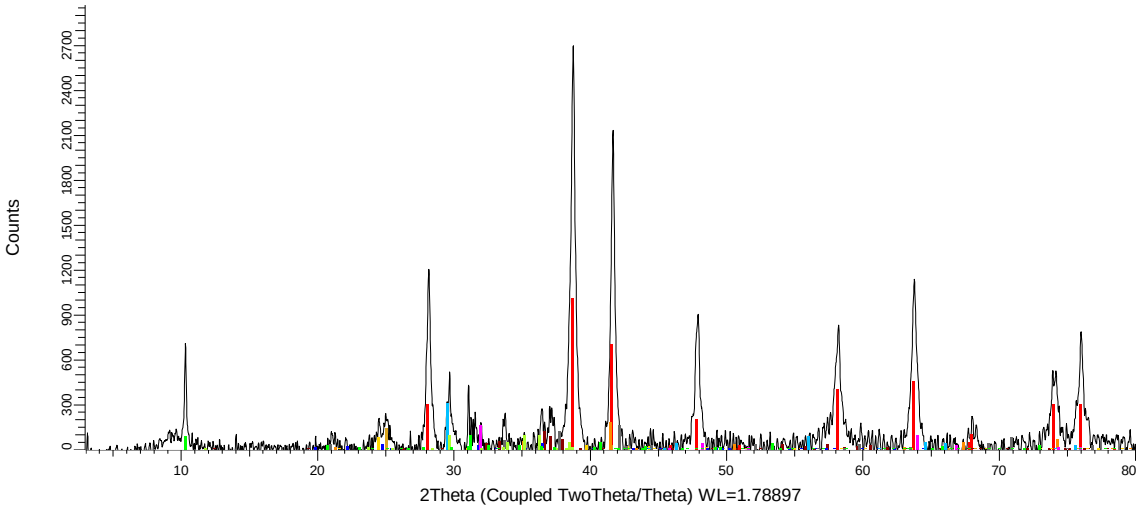


Figure 0.17. X-ray diffraction pattern for the ZKD ore sulfated in a O_2-rich atmosphere at 600°C.

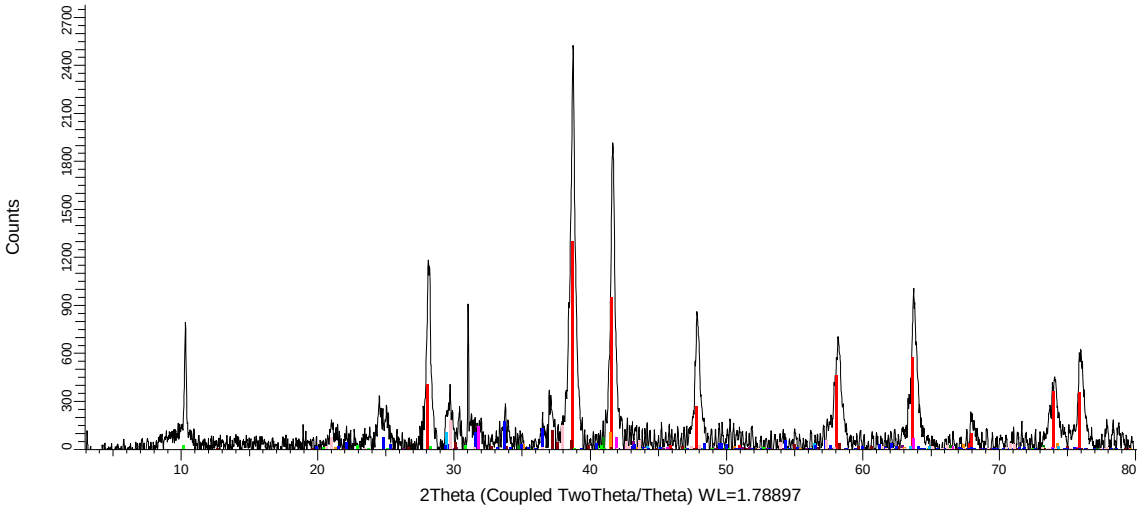


Figure 0.18. X-ray diffraction pattern for the ZKD ore sulfated in a O_2-rich atmosphere at 700°C.

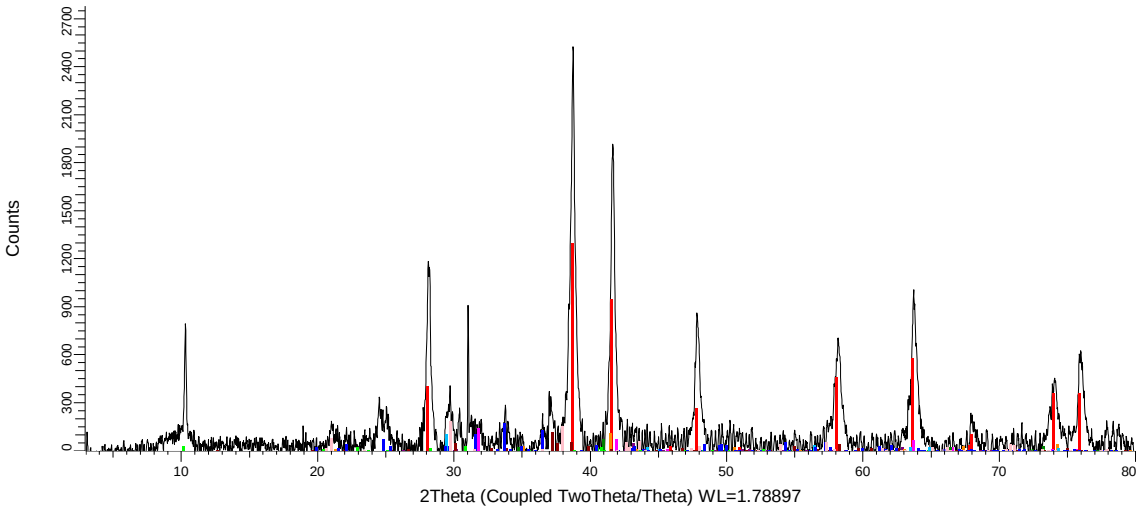


Figure 0.19. X-ray diffraction pattern for the ZKD ore sulfated in a O_2-rich atmosphere at 800°C.

Table 0.7. Summary sulfation roasting consitions for the PyEarth ™ slag.

Test No.	Gas Composition	Time (h)
19	32% SO_2 + 68% N_2	1
20		4
21		8
22	32% SO_2 + 16% O_2 + 52% N_2	1
23		4
24		8

Table 0.8. Detailed XRD analysis for the sulfation of the PyEarth slag.

Compound Name	Formula	Test No.					
		19	20	21	22	23	24
Perovskite	$(Ce, La, Nd, Pr)_{0.5}$ $(Ca_{0.75}$ $Sr_{0.25})$ (TiO_3)	5,3	5,7	5,3	5,0	4,6	4,3
Grossular	$Al_{1.89}Ca_{2.869}$ $Fe_{0.241}$ O_{12} Si_3	0	0,6	0	0	0,4	0,4
Gypsum	H_4CaO_6S	0,1	0,1	0,3	0,3	0,2	0
Zeolite	$Al_2Ba_{0.995}O_8Si_2Yb_{0.005}$	6,6	6,9	7,7	7,4	5,8	5,2
Spinel	$Al_{1.844}Fe_{0.142}Mg_{1.012}O_4$	13,8	17,6	17,6	15,4	13,4	13,4
Magnetite	Fe_3O_4	0,6	0,9	0,6	0,5	1,4	0,6
Amorphous		73,5	68,3	68,6	71,4	74,1	76,1

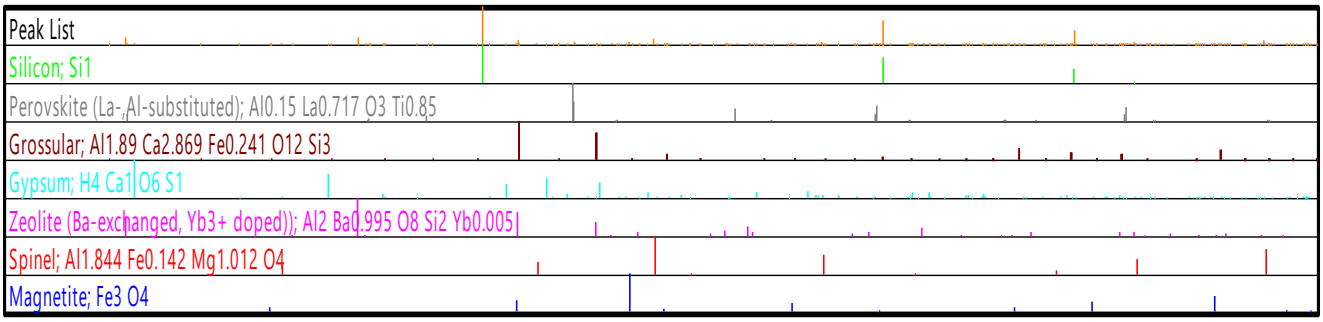


Figure 0.20. X-ray diffraction pattern for the PyEarth ™ slag samples after sulfation roasting.

APPENDIX I: POURBIAX DIAGRAMS

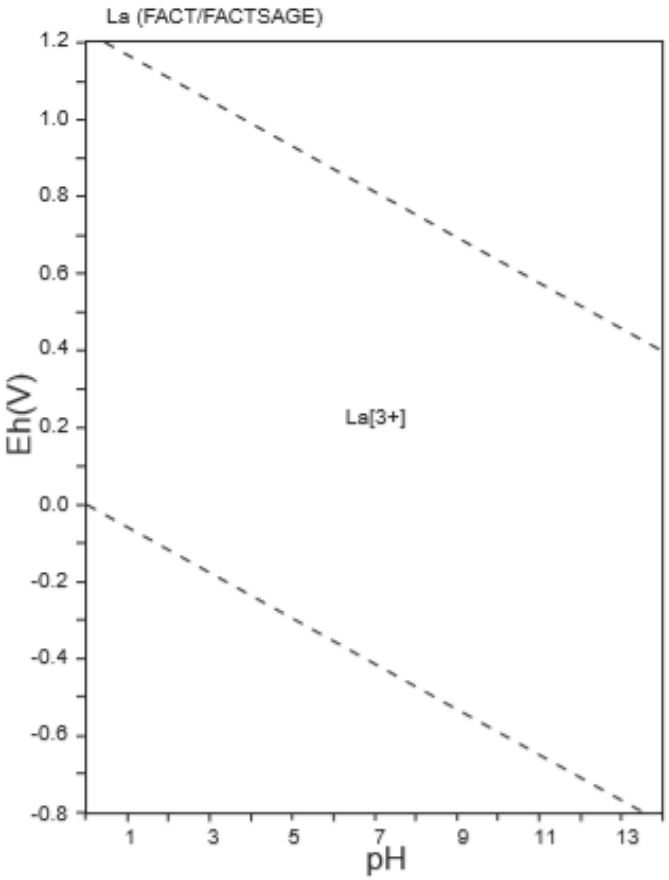


Figure 0.21. Eh-pH diagram of the system La-O-H (1). Fe = 10−10, 298.15K, 105 Pa (Takeno., 2005).

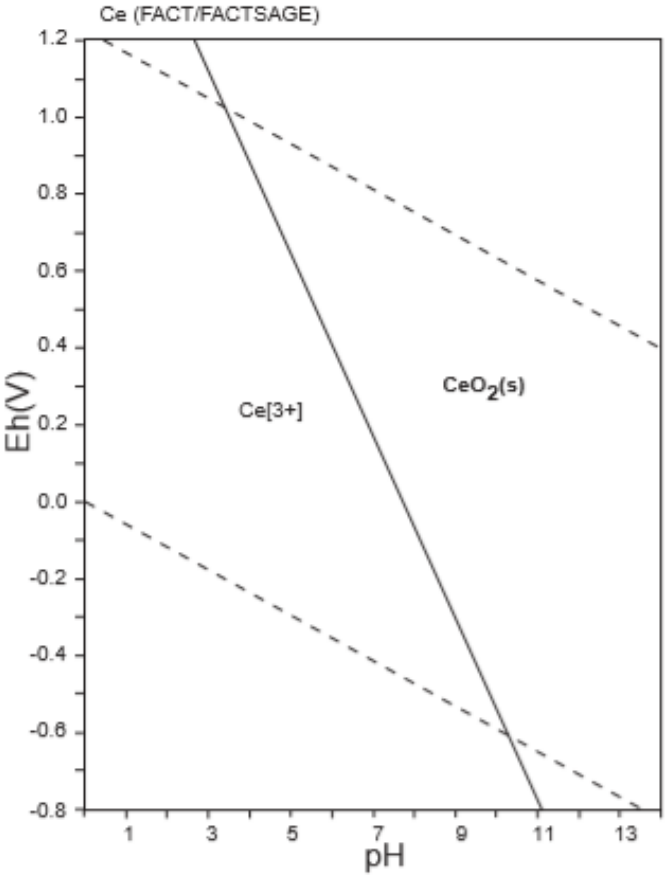


Figure 0.22. Eh-pH diagram of the system Ce-O-H (1). Fe = 10−10, 298.15K, 105 Pa (Takeno., 2005).

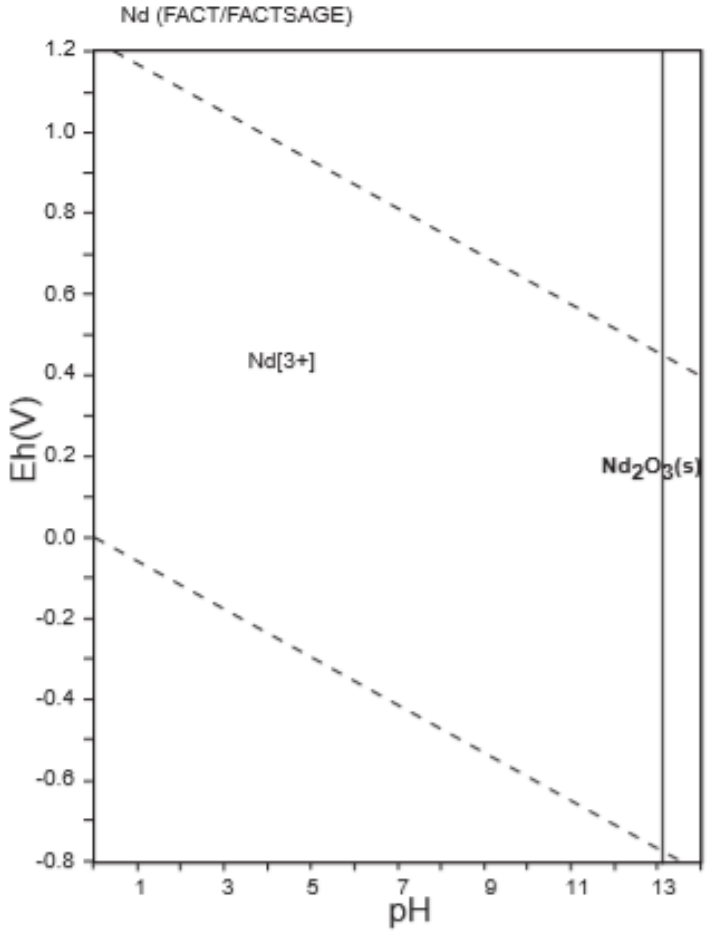


Figure 0.23. Figure 0.20. Eh-pH diagram of the system Nd-O-H (1). Fe = 10−10, 298.15K, 105 Pa (Takeno., 2005).

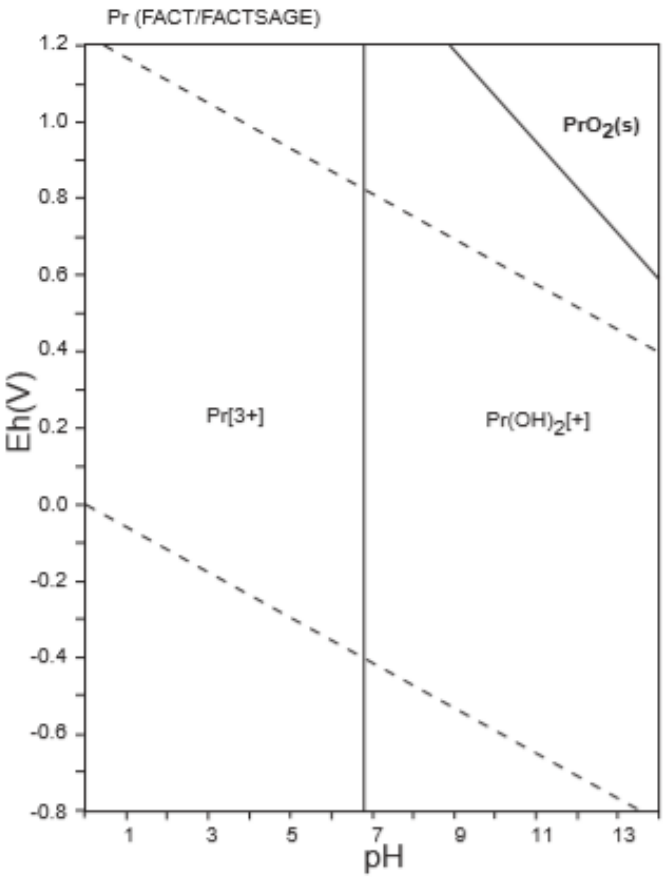


Figure 0.24. Figure 0.20. Eh-pH diagram of the system Pr-O-H (1). Fe = 10−10, 298.15K, 105 Pa (Takeno., 2005).

APPENDIX J: MASS BALANCES

Table 0.9. Mass Balance for The ZKD Ore Sulfation Roasting Studies (Ce and La).

Test No.	Sample Description			Total Feed (g)	Ce				La			
	Temperature (°C)	Time (h)	Gas atmosphere		Feed (g)	Residue (g)	Solution (g)	% Extraction	Feed (g)	Residue (g)	Solution (g)	% Extraction
1	600	1	32% SO_2+68% N_2	8,04	0,08	0,07	0,00	6,07	0,05	0,04	0,01	25,53
2	700			8,04	0,08	0,07	0,01	10,15	0,05	0,03	0,02	33,44
3	800			8,01	0,08	0,07	0,01	9,84	0,05	0,03	0,02	34,47
4	600		32% SO_2+16% O_2+52% N_2	8,06	0,08	0,06	0,02	24,35	0,05	0,04	0,01	19,80
5	700			8,05	0,08	0,06	0,02	28,76	0,05	0,04	0,02	30,09
6	800			8,08	0,08	0,07	0,01	10,70	0,05	0,04	0,01	29,11
7	600	4	32% SO_2+68% N_2	8,04	0,08	0,06	0,01	18,97	0,05	0,04	0,01	25,64
8	700			8,02	0,08	0,07	0,00	4,40	0,05	0,03	0,02	36,35
9	800			8,09	0,08	0,08	0,00	3,62	0,05	0,04	0,01	27,20
10	600		32% SO_2+16% O_2+52% N2	8,09	0,08	0,06	0,02	23,49	0,05	0,03	0,02	30,87
11	700			8,05	0,08	0,06	0,02	27,84	0,05	0,03	0,02	36,91
12	800			8,08	0,08	0,06	0,02	23,52	0,05	0,03	0,02	33,26
13	600	8	32% SO_2+68% N_2	8,02	0,08	0,07	0,01	15,66	0,05	0,03	0,02	32,87
14	700			8,03	0,08	0,07	0,01	12,01	0,05	0,03	0,02	34,78
15	800			8,06	0,08	0,07	0,01	12,22	0,05	0,04	0,01	21,27
16	600		32% SO2+16% O2+52% N2	8,08	0,08	0,05	0,03	38,04	0,05	0,01	0,04	77,32
17	700			8,07	0,08	0,03	0,05	60,53	0,05	0,01	0,04	87,79
18	800			8,06	0,08	0,06	0,02	28,80	0,05	0,01	0,04	77,40

Table 0.10. Mass Balance for The ZKD Ore Sulfation Roasting Studies (Nd and Pr).

Test No.	Sample Description				Nd				Pr			
	Temperature (°C)	Time (h)	Gas atmosphere	Total Feed (g)	Feed (g)	Residue (g)	Solution (g)	% Extraction	Feed (g)	Residue (g)	Solution (g)	% Extraction
1	600	1	32% SO_2+68% N_2	8,04	0,03	0,02	0,00	11,62	0,01	0,01	0,00	15,89
2	700			8,04	0,03	0,02	0,01	20,29	0,01	0,01	0,00	24,20
3	800			8,01	0,03	0,02	0,01	21,31	0,01	0,01	0,00	25,31
4	600		32% SO_2+16% O_2+52% N_2	8,06	0,03	0,03	0,00	4,42	0,01	0,01	0,00	9,26
5	700			8,05	0,03	0,02	0,01	21,71	0,01	0,01	0,00	24,91
6	800			8,08	0,03	0,02	0,00	16,21	0,01	0,01	0,00	19,00
7	600	4	32% SO_2+68% N_2	8,04	0,03	0,02	0,00	10,00	0,01	0,01	0,00	14,93
8	700			8,02	0,03	0,02	0,01	22,07	0,01	0,01	0,00	26,27
9	800			8,09	0,03	0,02	0,00	12,97	0,01	0,01	0,00	17,17
10	600		32% SO_2+16% O_2+52% N2	8,09	0,03	0,02	0,00	18,19	0,01	0,01	0,00	22,12
11	700			8,05	0,03	0,02	0,01	23,60	0,01	0,01	0,00	27,23
12	800			8,08	0,03	0,02	0,00	18,57	0,01	0,01	0,00	23,00
13	600	8	32% SO_2+68% N_2	8,02	0,03	0,02	0,00	18,19	0,01	0,01	0,00	22,52
14	700			8,03	0,03	0,02	0,01	21,33	0,01	0,01	0,00	25,39
15	800			8,06	0,03	0,03	0,00	4,69	0,01	0,01	0,00	9,98
16	600		32% SO2+16% O2+52% N2	8,08	0,03	0,01	0,02	73,16	0,01	0,00	0,01	74,52
17	700			8,07	0,03	0,00	0,02	85,81	0,01	0,00	0,01	86,66
18	800			8,06	0,03	0,01	0,02	72,11	0,01	0,00	0,01	73,80

Table 0.11. Mass Balance for The ZKD Ore Sulfation Roasting Studies (Fe).

Test No.	Sample Description			Fe				
	Temperature (°C)	Time (h)	Gas atmosphere	Total Feed (g)	Feed	Residue	Solution	% Recovery
1	600	1	32% SO2+68% N2	8,04	2,84	2,62	0,21	7,57
2	700			8,04	2,84	2,62	0,21	7,57
3	800			8,01	2,83	2,61	0,21	7,57
4	600		32% SO2+16% O2+52% N2	8,06	2,85	2,63	0,22	7,57
5	700			8,05	2,84	2,63	0,22	7,57
6	800			8,08	2,85	2,64	0,22	7,57
7	600	4	32% SO2+68% N2	8,04	2,84	2,62	0,21	7,57
8	700			8,02	2,83	2,62	0,21	7,57
9	800			8,09	2,86	2,64	0,22	7,57
10	600		32% SO2+16% O2+52% N2	8,09	2,86	2,64	0,22	7,57
11	700			8,05	2,84	2,63	0,22	7,57
12	800			8,08	2,85	2,64	0,22	7,57
13	600	8	32% SO2+68% N2	8,02	2,83	2,62	0,21	7,57
14	700			8,03	2,83	2,62	0,21	7,57
15	800			8,06	2,85	2,63	0,22	7,57
16	600		32% SO2+16% O2+52% N2	8,08	2,85	2,64	0,22	7,57
17	700			8,07	2,85	2,63	0,22	7,57
18	800			8,06	2,85	2,63	0,22	7,57

Table 0.12. Mass Balance for The PyEarth ™ Slag Sulfation Roasting Studies (Fe).

Test No.	Sample Description			Mass Feed(g)	Fe			
	Temperature (°C)	Time (h)	Gas atmosphere		Feed (g)	Residue (g)	Solution (g)	% Extraction
19	700	1	32% SO2+68% N2	3,02	0,35	0,20	0,14	41,75
20		4		3,45	0,40	0,12	0,28	69,50
21		8		3,15	0,36	0,10	0,26	72,87
22		1	32% SO2+16% O2+52% N2	3,5	0,40	0,18	0,22	54,59
23		4		3,35	0,39	0,19	0,19	49,44
24		8		3,35	0,39	0,23	0,15	39,96

Table 0.13. Mass Balance for The PyEarth ™ Slag Sulfation Roasting Studies (Ce and La).

Test No.	Sample Description			Mass Feed(g)	Ce				La			
	Temperature (°C)	Time (h)	Gas atmosphere		Feed (g)	Residue (g)	Solution (g)	% Extraction	Feed (g)	Residue (g)	Solution (g)	% Extraction
19	700	1	32% SO2+68% N2	3,02	0,10	0,08	0,02	15,66	0,05	0,05	0,01	14,72
20		4		3,45	0,11	0,10	0,01	11,09	0,06	0,06	0,01	9,78
21		8		3,15	0,10	0,09	0,01	11,63	0,06	0,05	0,01	11,46
22		1	32% SO2+16% O2+52% N2	3,5	0,11	0,10	0,02	13,96	0,06	0,06	0,01	13,22
23		4		3,35	0,11	0,09	0,02	20,96	0,06	0,05	0,01	20,81
24		8		3,35	0,11	0,09	0,02	19,49	0,06	0,05	0,01	20,05

Table 0.14. Mass Balance for The PyEarth ™ Slag Sulfation Roasting Studies (Fe).

Test No.	Sample Description			Mass Feed(g)	Nd				Pr			
	Temperature (°C)	Time (h)	Gas atmosphere		Feed (g)	Residue (g)	Solution (g)	% Extraction	Feed (g)	Residue (g)	Solution (g)	% Extraction
19	700	1	32% SO2+68% N2	3,02	0,04	0,03	0,01	23,15	0,01	0,01	0,00	19,12
20		4		3,45	0,05	0,04	0,01	18,84	0,01	0,01	0,00	14,11
21		8		3,15	0,04	0,03	0,01	19,62	0,01	0,01	0,00	15,94
22		1	32% SO2+16% O2+52% N2	3,5	0,05	0,04	0,01	21,32	0,01	0,01	0,00	17,38
23		4		3,35	0,04	0,03	0,01	24,28	0,01	0,01	0,00	21,14
24		8		3,35	0,04	0,03	0,01	22,81	0,01	0,01	0,00	19,93

Table 0.15. pH readings for the fluidized sulfation roasting bed samples leaching tests.

Test No.	Temperature (°C)	Time (h)	Gas atmosphere	pH Initial	pH adjusted	pH final
1	600	1	32% SO_2+68% N_2	3,85	3,61	4,21
2	700			4,95	3,20	5,17
3	800			4,94	3,45	5,49
4	600		32% SO_2+16% O_2+52% N_2	3,35	-	3,60
5	700			2,96	-	3,85
6	800			3,88	3,12	3,76
7	600	4	32% SO_2+68% N_2	4,22	3,42	4,43
8	700			4,98	3,50	5,40
9	800			4,38	3,07	4,94
10	600		32% SO_2+16% O_2+52% N2	3,86	3,42	3,89
11	700			4,17	3,06	4,17
12	800			4,83	3,46	5,41
13	600	8	32% SO_2+68% N_2	5,29	3,28	5,73
14	700			5,26	3,24	5,86
15	800			5,01	2,90	5,67
16	600		32% SO2+16% O2+52% N2	3,06	-	3,67
17	700			3,31	-	3,73
18	800			3,87	3,53	4,55
19	700	1	32% SO2+68% N2	7,49	4,98	5,86
20		4		5,89	3,95	5,23
21		8		7,62	4,89	6,33
22		1	32% SO2+16% O2+52% N2	6,96	4,48	5,72
23		4		7,77	4,79	6,39
24		8		7,19	4,35	5,35

Table 0.16. Mass Balance over the fluidized bed setup.

Test No.	Temperature (°C)	Time (h)	Gas atmosphere	Feed (g)	Products (g)	Tailings (g)	% Mass loss
1	600	1	32% SO2+68% N2	51,66	48,06	3,6	6,97
2	700			50,93	45,94	4,99	9,80
3	800			51,26	43,5	7,76	15,14
4	600		32% SO2+16% O2+52% N2	51,76	47,74	4,02	7,77
5	700			51,22	48,28	2,94	5,74
6	800			51,09	46,6	4,49	8,79
7	600	4	32% SO2+68% N2	51,98	45,6	6,38	12,27
8	700			51,06	41,87	9,19	18,00
9	800			51,76	43,05	8,71	16,83
10	600		32% SO2+16% O2+52% N2	51,85	46,42	5,43	10,47
11	700			51,8	45,37	6,43	12,41
12	800			51,46	42,13	9,33	18,13
13	600	8	32% SO2+68% N2	51,71	44,33	7,38	14,27
14	700			51,37	42,82	8,55	16,64
15	800			50,96	42,31	8,65	16,97
16	600		32% SO2+16% O2+52% N2	50,56	45,15	5,41	10,70
17	700			50,86	48,16	2,7	5,31
18	800			51,59	46,87	4,72	9,15
19	700	1	32% SO2+68% N2	50,33	49,27	1,06	2,11
20		4		50,55	45,74	4,81	9,52
21		8		52,04	38,84	13,2	25,37
22		1	32% SO2+16% O2+52% N2	49,98	41,039	8,941	17,89
23		4		51,93	37,76	14,17	27,29
24		8		51,51	43,92	7,59	14,74